AD-772 503

SYNTHESIS OF COMPOUND SEMICONDUCTING MATERIALS AND DEVICE APPLICATIONS: GALLIUM NITRIDE LIGHT EMITTING DIODES

D.A. Stevenson, et al

Stanford University

Prepared for:

Advanced Research Projects Agency

December 1973

DISTRIBUTED BY:

NTIS

National Technical Information Service
U. S. DEPARTMENT OF COMMERCE
5285 Port Royal Road, Springfield Va. 22151

AD772503

SPECIAL TECHNICAL REPORT

SYNTHESIS OF COMPOUND SEMICONDUCTING MATERIALS AND DEVICE APPLICATIONS; GALLIUM NITRIDE LIGHT EMITTING DIODES

December 1973

DDC
RECEIVED
JAN 16 1974
C

Grant No. DAHC15 72-G-6

DISTRIBUTION STATEMENT A
Approved for public release;
Distribution Unlimited

The views and conclusions contained in this document are those of the authors and should not be interpreted as necessarily representing the official policies, either expressed or implied, of the Advanced Research Projects Agency or the U. S. Government.

CMR-73-17

CENTER FOR MATERIALS RESEARCH

STANFORD UNIVERSITY • STANFORD, CALIFORNIA

Special Technical Report

Sponsored by
Advanced Research Projects Agency
ARPA Order No. 1644/2

Program Code Number: P2D10

Contractor: Stanford University

Grant No. DAHC15 72-G-6

Principal Investigator: D. A. Stevenson

Date: December 1973

Grant Title: Synthesis of Compound Semiconducting Materials and Device Applications

Report Title: Gallium Nitride Light Emitting Diodes

Author: H. P. Maruska

Reproduced by
NATIONAL TECHNICAL
INFORMATION SERVICE
U S Department of Commerce
Springfield VA 22151

Center for Materials Research
Stanford University
Stanford, California 94305
(415) 321-2300, Ext. 4118

DISTRIBUTION STATEMENT A
Approved for public release;
Distribution Unlimited

CMR 73-17

TABLE OF CONTENTS

Chapter		Page
1.	LIGHT-EMITTING DIODES	1
	1.1 Introduction	1
	1.2 Classification and Basis of Operation of LED's	2
	1.3 LED Efficiencies	7
	1.4 Examples of LED Materials	10
	1.5 Purpose of This Work	23
2.	SYNTHESIS TECHNIQUES AND PROPERTIES OF GALLIUM NITRIDE	25
	2.1 Synthesis and Growth Techniques	25
	2.2 Doping	31
	2.3 Optical Properties	32
	2.4 Electrical Properties	36
	2.5 Electroluminescence	39
3.	EXPERIMENTAL TECHNIQUES	41
	3.1 Open-Flow Vapor Growth System	41
	3.2 Doping Procedure	47
	3.3 Point-Contact LED's	53
	3.4 Improved Large-Area Metal Contacts	54
	3.5 Measurement of Wavelength and Intensity of Luminescence	57
	3.6 Electrical Characteristics	63
	3.7 Scanning Electron Microscope	67
	3.8 Transmission Electron Microscope	70
	3.9 Proton Bombardment and Proton-Assisted Diffusion	71

Pages Korean #2-5 blank

TABLE OF CONTENTS (Contd)

Chapter		Page
4.	EXPERIMENTAL RESULTS	73
	4.1 Growth and Fabrication of GaN Light-Emitting Diodes	74
	4.2 Emission Spectra of GaN:Mg Light-Emitting Diodes	75
	4.3 Electrical Characteristics	84
	4.4 Temperature Dependence of Luminescence and Electrical Characteristics	89
	4.5 Growth and Surface Morphology of GaN	96
	4.6 Pattern of Light Emission	103
	4.7 Characteristics of the Insulating (Mg-doped) Region	117
	4.8 Electrical Potential Distribution	130
	4.9 Diode Capacitance	134
	4.10 Proton Bombardment and Proton-Assisted Diffusion	141
5.	DISCUSSION	143
	5.1 Basic Mechanisms for Diode Operation	143
	5.2 Mechanism for GaN m-i-n Diode Electrical Characteristics	154
	5.3 Mechanisms for Electroluminescence	160
	5.4 Impact Ionization in GaN m-i-n Diodes	171
	5.5 Nature of the Potential Barrier	180
	5.6 Model for GaN Light-Emitting Diodes	185
6.	CONCLUSIONS	193

LIST OF FIGURES

Number		Page
Figure 1.1	Spectral sensitivity of the human eye.	11
Figure 1.2	Best reported values of luminous power conversion for light-emitting diodes.	15
Figure 1.3	Chromaticity diagram.	17
Figure 1.4	The color matching functions V(x), V(y), and V(z), (red, green, and blue).	18
Figure 2.1	Equilibrium vapor pressure of N_2 over GaN(s)-Ga(ℓ).	30
Figure 3.1	Open-Flow Vapor Growth System for preparing gallium nitride.	43
Figure 3.2	Quartz sample holder.	46
Figure 3.3	System for positioning dopant crucible in sidearm of vapor growth apparatus.	49
Figure 3.4	Graphite dopant crucible.	52
Figure 3.5	Gallium nitride light-emitting diode attached to a glass slide.	56
Figure 3.6	Schematic diagram of a gallium nitride light-emitting diode on a TO-5 transistor header.	58
Figure 3.7a	Experimental arrangement for measuring the wavelength and intensity of electroluminescence (schematic).	59
Figure 3.7b	Experimental arrangement for measuring the wavelength and intensity of photoluminescence (schematic).	60
Figure 3.8	Spectral response of the S-20 photocathode.	62
Figure 3.9	System for measuring I-V characteristics (schematic).	64
Figure 3.10	System for simultaneous measurement of power efficiency and I-V characteristics of a light-emitting diode (schematic).	66

LIST OF FIGURES (Contd)

Number		Page
Figure 3.11	Schematic diagram of the scanning electron microscope.	68
Figure 4.1	Electroluminescence spectrum of point-contact GaN:Mg light-emitting diode (sample #6·8·72).	76
Figure 4.2	Electroluminescence spectrum of GaN:Mg m-i-n diode, sample #6·28·72 (forward bias).	78
Figure 4.3	Electroluminescence spectrum of typical GaN:Mg m-i-n diode (forward bias).	79
Figure 4.4	Dependence of the peak wavelength of the emission on applied voltage (forward bias).	81
Figure 4.5	Typical reverse-bias electroluminescence spectrum for GaN:Mg m-i-n diodes.	82
Figure 4.6	Dependence of the peak wavelength of the emission on applied voltage (reverse bias).	83
Figure 4.7	Photoluminescence spectrum of Mg-doped GaN.	85
Figure 4.8	Dependence of light power output on electrical power input for GaN:Mg light-emitting diodes.	86
Figure 4.9	External quantum efficiency of GaN:Mg light-emitting diodes.	87
Figure 4.10	Typical diode I-V characteristic.	88
Figure 4.11	Log-log plot of diode I-V characteristic (sample #7·7·72).	90
Figure 4.12	Luminous intensity as a function of applied voltage.	91
Figure 4.13	Temperature dependencies of diode current and luminous intensity at constant voltage.	93
Figure 4.14	Temperature dependencies of diode current and luminous intensity at various constant voltages.	94
Figure 4.15	Temperature dependence of photoluminescence intensity.	95

LIST OF FIGURES (Contd)

Number		Page
Figure 4.16	Hexagonal islands of GaN nucleated on (0001)-sapphire.	97
Figure 4.17	Hexagonal islands of GaN, which have coalesced to form a continuous film on the left side of the picture. (0001)-orientation.	99
Figure 4.18	Surface of gallium nitride sample #5·19·72, grown on $(1\bar{1}02)$-sapphire.	100
Figure 4.19	Typical facetted surface developed in GaN grown on $(1\bar{1}02)$-sapphire.	101
Figure 4.19A	Gallium nitride films on quartz substrates, showing crystallite size at various distances downstream from the ammonia inlet: (a) 2"; (b) 3"; (c) 4". Magnification 200X.	102
Figure 4.20	Laue pattern of $(10\bar{1}3)$-GaN (grown in $(1\bar{1}02)$-sapphire substrate).	104
Figure 4.21	Gallium nitride light-emitting diode with external illumination. The $(1\bar{1}02)$ sapphire substrate is removed, exposing the n-GaN layer. Magnification 28X.	105
Figure 4.22	Light spot pattern observed during forward biasing of the diode shown in Figure 4.21. Magnification 28X.	107
Figure 4.23	Light spot pattern of forward-biased diode at 200X magnification.	108
Figure 4.24	Same diodes as in Figure 4.23 with external illumination and light spot pattern superimposed (200X). $(10\bar{1}3)$-orientation.	109
Figure 4.25	Gallium nitride light-emitting diode #12·7·72 with external illumination. $(10\bar{1}3)$-orientation.	111
Figure 4.26	Gallium nitride light-emitting diode #12·7·72 (cf. Figure 4.25) with forward bias, illustrating light spot pattern.	112

LIST OF FIGURES (Contd)

Number		Page
Figure 4.27	Diode #12·7·72 (cf. Figure 4.25) with reverse bias, illustrating different set of light spots appearing with reverse bias than forward bias.	113
Figure 4.28	Diode mounted perpendicular to a glass slide showing sapphire substrate, GaN, and metal contact.	115
Figure 4.29	Light spots observed when diode shown in Figure 4.28 was forward biased. The light spots occur within the GaN region. Magnification 500X.	116
Figure 4.30	Perpendicular view of diode #12·13·72, as seen in the scanning electron microscope. The entire device (including the $(1\bar{1}02)$-sapphire substrate) and the two metal contacts (to the n- and i-layers) are visible. Magnification 25X.	120
Figure 4.31	Scanning electron micrograph of diode #12·13·72 at 100X magnification--no bias. $(1\bar{1}02)$-oriented sapphire substrate.	121
Figure 4.32	Scanning electron micrograph of diode #12·13·72 at 100X magnification with forward bias (+22 volts).	122
Figure 4.33	Scanning electron micrograph of diode #12·13·72 at 100X magnification with reverse bias (-22 volts).	123
Figure 4.34	Scanning electron micrograph of diode #12·13·72 at 500X magnification with reverse bias. The insulating (Mg-doped) GaN layer can be clearly distinguished. $(1\bar{1}02)$-oriented sapphire substrate.	124
Figure 4.35	Scanning electron micrograph of diode #12·13·72 at 1000X magnification with no bias.	126

LIST OF FIGURES (Contd)

Number		Page
Figure 4.36	Scanning electron micrograph of diode #12·13·72 at 1000X magnification with forward bias. The bias was removed during part of the scan, as indicated.	127
Figure 4.37	Scanning electron micrograph of diode #12·13·72 at 1000X magnification with reverse bias. The bias was removed during part of the scan, as indicated.	128
Figure 4.38	Transmission electron micrograph of insulating (Mg-doped) region of a GaN LED. Notice no evidence of precipitates or dislocations. Magnification 240,000X.	129
Figure 4.39	Superimposed zero bias and forward bias line scan traces and SEM photograph of a gallium nitride light-emitting diode. Magnification 1000X.	131
Figure 4.40	Superimposed zero bias and forward bias line scan traces and SEM photograph of a gallium nitride light-emitting diode. Magnification 2500X.	132
Figure 4.41	Superimposed zero bias and reverse bias (-6, -12, and -18 volts) line scan traces and SEM photograph of a gallium nitride light-emitting diode. Magnification 2500X.	133
Figure 4.42	Electric potential distribution across a gallium nitride light-emitting diode when forward bias is applied.	135
Figure 4.43	Electric potential distribution across a gallium nitride light-emitting diode when reverse bias is applied.	136
Figure 4.44	The capacitance and conductance as functions of applied voltage for a typical GaN diode. Also included is the quantity, $1/C^2$, as a function of voltage.	138
Figure 4.45	Current-voltage characteristic of a GaN m-i-n diode prepared by proton bombardment.	140

Number		Page
Figure 5.1	Fowler-Nordheim plot of GaN:Mg light-emitting diode current-voltage characteristic. Cf. Figure 4.11.	155
Figure 5.2	Fowler-Nordheim plot of GaN:Mg light-emitting diode current-voltage characteristics at various temperatures. Cf. Figure 4.14.	156
Figure 5.3	Plot of log I versus log V for GaN:Zn light-emitting diode (after PANKOVE, 1972, Figure 8).	157
Figure 5.4	The I-V characteristic of the GaN:Zn light-emitting diode shown in Figure 5.3, replotted to the Fowler-Nordheim Equation.	158
Figure 5.5	Log of electroluminescence intensity versus $(\text{voltage})^{-1/2}$. Cf. Figure 4.12.	163
Figure 5.6	Log of forward and reverse bias electroluminescence intensity versus $(\text{voltage})^{-1/2}$.	164
Figure 5.7	Log of electroluminescence intensity versus $(\text{voltage})^{-1/2}$ at various temperatures. Cf. Figure 4.14.	165
Figure 5.8	Log of luminous intensity versus log of diode current at various temperatures. Cf. Figure 4.14.	166
Figure 5.9	Carrier multiplication factor M as a function of applied voltage for a GaN light-emitting diode.	176
Figure 5.10	Plot of (external quantum efficiency) x $(\text{voltage})^{-1/2}$ versus $(\text{voltage})^{-1/2}$.	179
Figure 5.11	Charge concentrations, electric fields, and electric potentials at a p-n junction. N_A, N_D are respectively the concentrations of acceptors and donors; F_A, F_D, and F are respectively the electric field due to the	

Number		Page
	ionized acceptors, electric field due to the ionized donors, and total electric field; Φ_A, Φ_D, and Φ are respectively the potential due to the ionized acceptors, potential due to the ionized donors, and total potential; and Φ_B is the barrier potential.	182
Figure 5.12	Schematic of processes responsible for electroluminescence in GaN m-i-n diodes. The situation for forward bias is illustrated.	187
Figure 5.13	Growth and device operation of a gallium nitride light-emitting diode: (a) Nucleation of GaN islands on a $(1\bar{1}02)$ sapphire substrate; (b) Growth of GaN islands, until they meet; (c) Growth of continuous GaN film after the islands have met, indicating the position of the sub-grain boundaries; (d) Complete GaN m-i-n diode, showing the structural origin of the electroluminescence with forward bias.	189

LIST OF SYMBOLS

a	constant; lattice parameter (Å); activity
A	area (cm^2); constant
b	constant
B	barrier height (eV)
c	constant; lattice parameter (Å)
C	capacitance (pF)
d	thickness of insulator (cm)
E	energy (eV)
E_a	activation energy (eV)
E_g	band gap energy (eV)
E_m	minimum energy for impact ionization (eV)
F	electric field (volts/cm)
F_L	luminous power (lumens)
G	Gibbs free energy (Kcal)
$G°$	standard Gibbs free energy (Kcal)
h	Planck's constant (4.14×10^{-15} eV-sec)
i	insulating
I	current (amps)
J	current density (amp/cm^2)
k	Boltzmann constant (0.864×10^{-4} eV/°K)
K	equilibrium constant
ℓ	length (cm); free path (cm); dimensionless parameter characterizing trap distribution
$\overline{\ell}$	mean free path (cm)
m	metal

LIST OF SYMBOLS (Contd)

m	mass of electron (9.1×10^{-31} Kg)
m^*	effective mass of electron (Kg)
n	electron carrier density (cm^{-3}); numerical constant
N	effective charge density in depletion region (cm^{-3})
N_A	acceptor density (cm^{-3})
N_D	donor density (cm^{-3})
N_L	luminescent center density (cm^{-3})
p	hole carrier density (cm^{-3})
P	light power output (watts); ionization probability; pressure
q	electronic charge (1.60×10^{-19} coul)
R	resistance (Ω); gas constant (1.987 cal/°K-mole)
T	temperature (°C, °K)
T_e	effective electron temperature (°K)
V	bias voltage (volts)
$V(\lambda)$	eye sensitivity functior
$[V_N^{\cdot}]$	concentration of positively charged vacancies on the nitrogen lattice
w	width of depletion region (cm)
x	distance (cm)
α	absorption coefficient (cm^{-1})
ε	permittivity (farads/m)
ε_o	permittivity of free space (8.85×10^{-12} farads/m)
η	efficiency
η_{EQ}	external quantum efficiency
η_{rad}	radiative efficiency of recombination

λ	wavelength ($\mathring{A}$)
μ	mobility ($cm^2/V\text{-}sec$)
ν	frequency (sec^{-1})
σ	conductivity ($\Omega\text{-}cm^{-1}$); cross-section (cm^2)
τ	lifetime
Φ	electric potential (volts)
Φ_B	barrier potential (volts)

ABSTRACT

The synthesis and characterization of hetero-epitaxial gallium nitride (GaN) films were undertaken with particular reference to the phenomenon of light emission. Gallium nitride was grown by the chemical vapor deposition technique using sapphire substrates. Techniques for characterization included optical, scanning electron, and transmission electron microscopy and measurements of various electrical and optical properties of the films. The thin films of GaN were doped during growth with zinc and magnesium to form n-i junctions. Such material provided the basis for the fabrication of m-i-n light-emitting diodes, which emitted light in the high-energy violet region of the visible spectrum with Mg doping and green light with Zn doping.

Undoped GaN layers were ordinarily n-type with carrier concentrations in excess of 10^{18} cm^{-3}. Insulating GaN was produced through compensation by doping with the acceptor impurities Zn and Mg. Light-emitting diodes were prepared by growing onto a sapphire substrate a film of highly conducting undoped GaN (n-layer), followed by a film of insulating GaN (i-layer), and then placing a metal contact over the surface (m-layer). Such a structure forms an m-i-n diode, which contains two electrical junctions, m-i and i-n. Most of the diodes studied had a Mg-doped i-layer, and such diodes exhibited violet electroluminescence which peaked at 2.9 eV with a 400 meV halfwidth. External quantum efficiencies of about 0.005% were obtained in these diodes with a bias of 20 volts.

The light is emitted from the diodes in the form of small (<10 μ

diameter), discrete spots. These light spots are generated at the junction in the diode which forms the cathode. Although Laue patterns indicate that the GaN films are single-crystalline, the surfaces of the layers show a strongly facetted structure, and the positions of the light spots correspond to these facets. Gallium nitride is nucleated in the form of a large number of individual islands which subsequently coalesce to form a continuous film. The coalesced islands are slightly misaligned, resulting in the formation of subgrain boundaries. No evidence for precipitates or dislocations within the individual cells was found.

The electric potential distribution across the m-i-n diodes was obtained through the voltage-contrast capability of the scanning electron microscope. Potential gradients and electric fields of about 10^5 volts/cm are developed at the m-i and i-n junctions, but not throughout the bulk of the i-layer. These observations, coupled with a study of the diode current-voltage characteristics, including their temperature dependence, lead to a model of current control in GaN diodes by tunnelling through a potential barrier. The I-V characteristics follow the Fowler-Nordheim field-emission equation.

It is proposed that impact ionization, occurring at the subgrain boundaries in the GaN films, is responsible for the electroluminescence. High-energy electrons empty the luminescent centers by collisions, and the subsequent recombination of electrons in thermal equilibrium in the conduction band with these centers results in the generation of light. This model is consistent with photomultiplication measurements and with the voltage dependence of the external quantum efficiency. The models

developed for the diode electrical properties and for the electroluminescence are useful in understanding the characteristics of m-i-n junctions.

"God said, 'Let there be light,' and there was light. God saw that the light was good, and God divided light from darkness."

Gn 1: 3, 4

Chapter 1

LIGHT-EMITTING DIODES

1.1 Introduction

Light-emitting diodes (LED's) are devices that emit electromagnetic radiation in response to an applied electric field. Light emission from a material due to an electric field is termed electroluminescence. The light involved with the process of electroluminescence is not determined simply by the temperature of the material, as is the case with incandescence (black body radiation). Applications for LED's are found in the areas of indicator lights, alpha-numeric displays, picture displays (solid-state color television) and IR sources. Commercially available red LED's are now being used as numerals in calculators and wristwatches, and in place of panel meters in various types of electronic equipment. For most application, then, it is necessary that the emitted light fall in the visible portion of the electromagnetic spectrum (4000 Å to 7000 Å), since the purpose of the devices is to transmit information from instruments to people.

Solid-state semiconductor materials are used for the manufacture of various light-emitting diodes. They feature many attractive qualities in contrast to incandescent light sources: reliability, long life, low cost, small size, and low power requirements and operating voltages. The last three items are particularly important for compact battery operated equipment. The operating characteristics of semiconductor LED's are compatible with silicon integrated circuits, which makes them especially suitable for visual displays in computer systems.

1.2 Classification and Basis of Operation of LED's

It is possible to distinguish five classes of semiconductor light-emitting diodes. These are,

(1) p-n homojunction diodes

(2) p-n heterojunction diodes

(3) Schottky barrier and m-i-s diodes

(4) electroluminescent cells (powders dispersed in organic binders)

(5) infrared emitting diodes coated with phosphors that emit visible light ("up-converters").

The first class of diodes involves a single material, part of which is doped p-type and the other part of which is doped n-type to form a p-n junction. The n-type side of the diode is prepared so as to contain an excess of electrons, while the p-type side has a deficit of electrons (that is, an excess of holes). Excess electrons are introduced into a semiconductor by substituting in place of a normal lattice constituent an element (dopant) which contains one more than the proper number of bonding electrons. Holes occur when the substituted dopant lacks one from the proper number of bonding electrons. When a potential difference is applied to such a diode, electrons are injected from the n-type region across the junction into the p-type region, where they can recombine with holes. Conversely, holes can be injected into the n-side with subsequent recombination with electrons; usually one process is dominant in a given semiconductor. The carriers which have been injected into a region in which they were originally scarce are called minority carriers. The carriers present in excess are the majority

carriers.

The excess electrons are situated in the semiconductor's conduction band in the n-type region, while the holes reside in the valence band in the p-type region. The valence and conduction bands are separated by a forbidden energy region, called the "energy gap" or "band gap" of the material. This is just the energy required to move an electron from the valence band (where a hole is left behind) to the conduction band. Thus, for example, if electrons are injected from the conduction band on the n-side to the conduction band on the p-side, under the influence of an applied potential difference, and they recombine with holes in the valence band, the total energy difference involved is just the "band gap" energy. This energy of recombination can be released from the diode in the form of photons. All of the photons emitted by a light-emitting diode will not possess exactly the same energy because the electrons and holes which recombine are distributed in energy in their respective bands. The energy distributions of the electrons and holes are governed by Fermi-Dirac statistics, but if the semiconductor is not degenerately doped, the distributions in the valence and conduction bands may be approximated by Maxwell-Boltzmann statistics. Since the carriers are distributed in energy in this way, a plot of number of photons emitted vs. energy has the form of a bell-shaped curve.

In many cases the electrons and holes recombine at a localized energy state within the forbidden energy gap. Such recombination sites are due to imperfections in the crystal, including the purposely introduced dopant atoms. In such a case the photon energy will be the

energy separation between this level and one of the bands. Notice that two photons of different energies adding up to the band gap energy could be emitted, but in many situations of interest the localized state is quite close (a few tenths of an electron-volt) from either the valence or the conduction band, so that the energy released is approximately the band gap energy of the semiconductor. In any case the band gap determines the highest frequency range of light which may be emitted. In order for the light to be visible to the human eye, a minimum band gap of 1.8 eV is required. The largest band gap that will produce visible light is about 3.1 eV, although materials with still larger band gaps may contain appropriate recombination centers to provide visible light.

In this first class of light-emitting diodes, then, the crystal is homogeneous throughout except for the change in dopant. The problems associated with joining dissimilar materials, such as interface states acting as electronic traps, dislocations, and lattice strains, are avoided. Various disruptions of the crystalline perfection usually decrease the number of photons emitted rather than just providing recombination centers, and the recombination energy is dissipated non-radiatively at the imperfections.

However, it is not possible to form p-n junctions in all materials. There are substances which exhibit excellent luminescence when stimulated with external light sources (photoluminescence) or when bombarded with electron beams (cathodoluminescence), and therefore appear to be attractive candidates for electroluminescence. This is especially true if their band gaps fall in the visible region of the spectrum. However,

only one conductivity type, which, depending on the compound, is either n or p, but not both, can be achieved by doping. In the absence of a p-n homojunction, other schemes must be devised for creating the minority carriers necessary for recombination. Such approaches are involved in diodes of classes 2, 3, and 4. In class 2 diodes, different materials are used on the two sides of a p-n junction, forming a heterojunction. The semiconductors involved in such an arrangement are one which can only be doped p-type joined to another which can only be doped n-type. In most cases, the energy gaps are not the same in the two substances, leading to a further complication beyond the lattice strains involved: the potential barriers that must be surmounted at the junction will be different for electrons and holes. Few sets of materials fit into this heterojunction scheme, because the two compounds selected should be completely mutually soluble. If they are not, a two phase region with poor electrical properties can result in the junction area.

It is also sometimes possible to obtain electroluminescence from materials in which one cannot form p-n junctions by the use of Schottky barriers or m-i-s structures (type 3 didoes). A Schottky barrier is formed at a non-ohmic (i.e., rectifying) metal contact to a semiconductor, and light can be generated in the high-field region occurring at this contact. In the m-i-s (metal-insulator-semiconductor) structure, an insulating layer, either of the semiconductor itself or some other substance, is interposed between the metal contact and the semiconductor. Often such an insulating layer is inadvertantly formed when fabricating a Schottky barrier if the metal used for the contact diffuses into the

semiconductor, rendering it insulating (by compensating the dopant already in it).

In some cases it is possible to inject minority carriers from the metal (which contains large quantities of both electrons and holes near its Fermi level) into the high-field barrier or insulating region in the semiconductor, whereupon recombination can occur with majority carriers. But some materials resist injection of minority carriers even by this process, and then one must resort to the creation of the minority carriers within the material. There are two possible mechanisms for this: impact ionization and internal field emission. Impact ionization occurs when majority carriers are accelerated by the applied electric field to such high energies they can remove other carriers from a filled band by colliding with them. In this way minority carriers appear in the formerly filled band. Alternatively, it is possible to remove majority carriers from trap levels within the forbidden energy gap by this collision process, so that empty states are formed for recombination. With the internal field emission process, carriers are directly removed from a filled band or from filled localized levels by the action of the electric field (quantum mechanical tunneling). For materials where the band separation (or separation between a level and a band) is of sufficiently large energy so that visible light may be emitted during recombination, the calculated field strengths required for internal field emission appear to be prohibitively large.

A device which also operates without minority carrier injection is the electroluminescent cell. Here a fine powder of a luminescent material is dispersed in an insulating plastic binder and placed between

two flat, transparent electrodes, forming a capacitor. This assemblage is not conducting to a direct current, and so it is operated a-c. The subject of a-c electroluminescent cells has been the topic of a prodigious amount of study, but will not be considered in detail in the present work, where we are only concerned with d-c operated LED's.

The fifth class of diode (the "up-converter") is a two stage device, involving a p-n homojunction diode which emits infrared light coupled directly to a phosphor material which is capable of visible light emission through photoluminescence. The phosphor is painted onto the diode's surface and emits the visible light after absorbing simultaneously two or three infrared photons from the LED. These infrared photons must all be absorbed at the same instant by the rare-earth atoms in the phosphor, in order to give sufficient energy to raise these atoms directly from their ground state to an excited state. A visible photon is emitted when the atom returns to its ground state.

1.3 LED Efficiencies

The various types of diodes that have now been described differ in the quality of their performances, and these differences may be made quantitative by discussing the efficiency of the devices. There are a number of efficiencies which may be measured. It must be noted that some authors only choose to quote the efficiency which makes their devices look the best, and this can lead to difficulties in comparisons with other diodes. The basic efficiency of an LED is the internal quantum efficiency. This is simply the ratio of photons created inside the device in the high field region to carriers introduced into it. In

a p-n junction, it will be the ratio of photons produced to minority carriers injected, and at low temperatures (typically below 200°K) this efficiency can approach 100%. At room temperature there is a drop off by at least an order of magnitude due to the onset of non-radiative transitions. It is appropriate to comment briefly at this point concerning "non-radiative transitions," because no one is exactly sure just what they are. One possibility is that the energy is dissipated through the creation of a number of phonons. Since the energy of a phonon is much smaller than the recombination energy to be dissipated, a very large number of phonons would have to be emitted simultaneously, which is highly unlikely. Another process is Auger recombination, whereby the energy produced when a hole and electron recombine is transferred to another carrier, which then becomes quite "hot" (at a high energy state in the conduction band or deep in the valence band). This "hot" carrier afterwards emits a series of phonons which need not be emitted simultaneously since there is a continuum of states within the band. Therefore this process is reasonable. A third process which is also sometimes appropriate involves recombination at a conducting inclusion (precipitate) in the material which happens to have little or no band gap. This again affords a continuum of states so that a series of phonons may be emitted. Of course not every material has inclusions. All that is known with certainty is that non-radiative recombination does occur, and it unfortunately serves to reduce diode efficiencies.

Although it is important that the internal quantum efficiency be as high as possible, this efficiency cannot be directly measured and by itself does not show just how much light can be extracted from a device.

This value is given by the external quantum efficiency, which is the ratio of the number of photons that are actually emitted from the diode to the number of carriers introduced. Since the indices of refraction of semiconductors of interest are larger (in the range of two to three) than that of air (one), only photons which strike the surface of a diode within a small solid angle (of about 15°) are not reflected. The photons which are reflected can be internally absorbed in various ways: at imperfections, in the metal contacts, or they may produce new hole-electron pairs which then recombine non-radiatively. Any of these processes will cause the external quantum efficiency to be smaller than the internal quantum efficiency.

The power efficiency is the ratio of light output power (in watts) to electrical input power (in watts). It is related to the quantum efficiency by a factor of the photon energy ($h\nu$) divided by qV (where V is the applied voltage). This efficiency is especially important in applications where power consumption is critical, such as battery operated systems.

Then there is the luminous efficiency, which is the ratio of luminous power (in lumens) to the electrical input power. The luminous power F_L is defined as

$$F_L = 680 \int \frac{dP}{d\lambda} V(\lambda) d\lambda \qquad (1.3.1)$$

where P is the light output power in watts, λ is the wavelength of the emitted light (recall that the photons emitted by an LED are distributed over a small range of energy and hence wavelength) and $V(\lambda)$ is a factor relating to the sensitivity of the human eye. The response

curve of the average eye is shown in Figure 1.1. It is apparent that the eye is most sensitive to green light, and that its response falls off rapidly in the red and violet regions of the spectrum. Thus while the quantum or power efficiency is important as far as the general electronic characteristics of a device are concerned, it is the luminous efficiency which indicates the actual impact an LED will have on a human observer. For example, the highest quantum efficiencies are found in GaAs diodes which emit in the infrared, where the human eye has no response, and so the actual luminous efficiency of these LED's is zero.

The most efficient electroluminescence by any standard is obtained from p-n homojunction diodes operated with forward bias (minority carrier injection). This type of device yields the highest photon/carrier ratio of any of the possible light emission schemes previously described. However, it has not been possible to obtain all of the visible colors with this arrangement, and it has been necessary to work with some of the other methods to get the colors desired. A trade-off between efficiency and wavelength of emission can be made. Various examples of electroluminescent materials are described below.

1.4 Examples of LED Materials

Silicon carbide was the first material in which electroluminescence was reported [LOSSEV, 1923]. Diodes used in early studies were made from commerical material which had been manufactured for use as an abrasive, and no care had been taken to control impurities present. The samples had unintentional p-n junctions grown in. Yellow, green and blue light has been observed in more carefully prepared SiC diodes

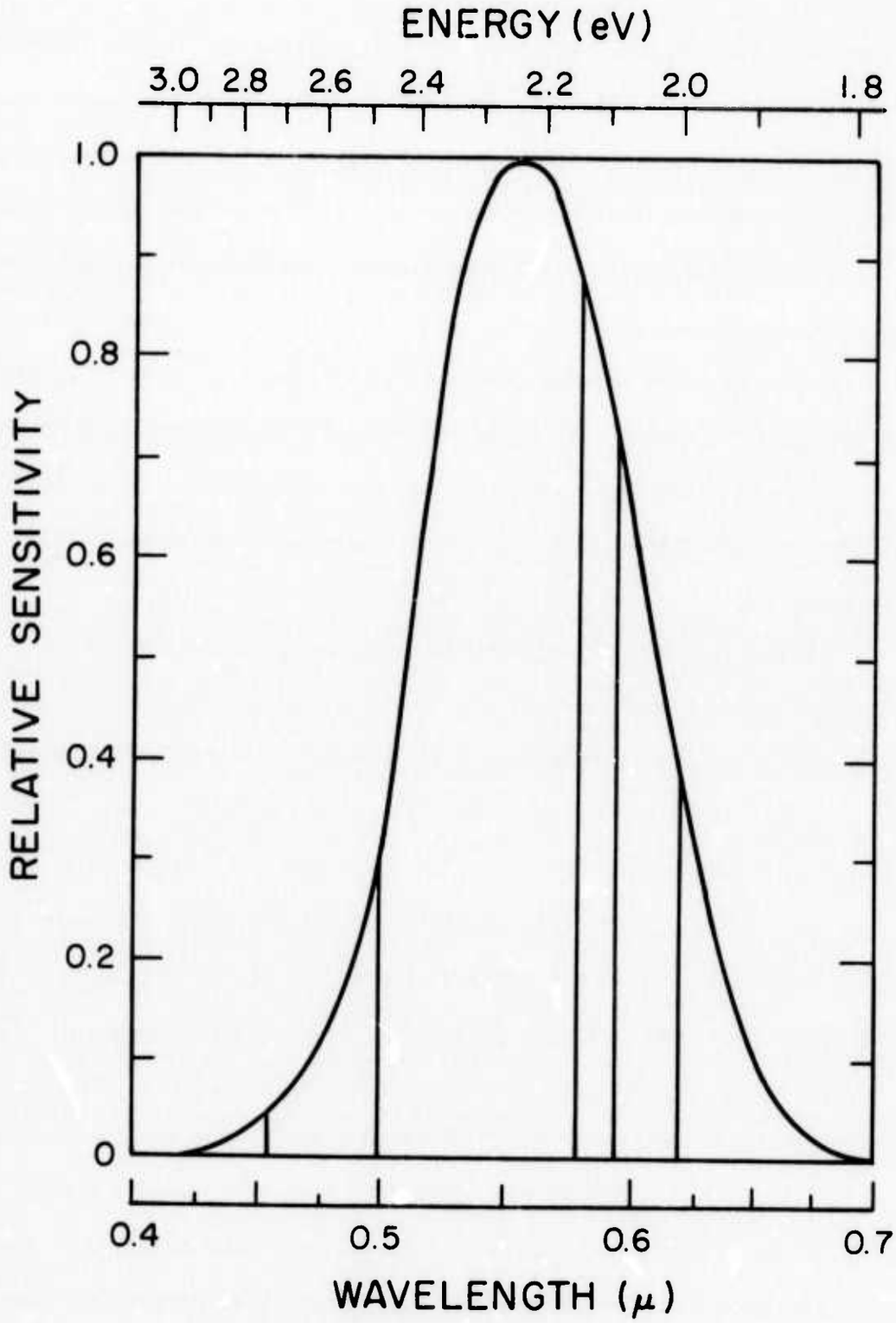

Figure 1.1 Spectral sensitivity of the human eye.

[PATRICK, 1957; VIOLIN, KAL'NIN, PASYNKOV, TAIROV and YASKOV, 1969] but it is a difficult material to grow and control. It occurs in both a cubic and many hexagonal polytypes. Hexagonal polytypes correspond to variations in the size of the unit cell due to rotations in the bonding, and they can all occur in the same sample. The most common polytype, 6H, has an attractively large band gap of 2.8 eV. But most reported SiC growth requires furnace temperatures in excess of 2000°C, and so do techniques for doping with N, B, and Al. The best value of external quantum efficiency (η_{EQ}) reported for this material is 0.005% [POTTER, BLANK, and ADDAMIANO, 1969] and there has been no improvement in recent years.

Materials such as Ge (forbidden energy gap, E_g, = 0.66 eV), Si (E_g = 1.1 eV) and GaAs (E_g = 1.4 eV), for which the technology for preparing good p-n junctions is quite advanced, cannot be used for the generation of visible light. The only materials other than SiC in which p-n junctions have been fabricated and which have suitable band gaps are the III-V compound semiconductor GaP, and certain solid solutions of the III-V compounds GaAs, GaP, InP and AlAs (viz., $GaAs_{1-x}P_x$, $In_{1-x}Ga_xP$ and $Ga_{1-x}Al_xAs$), as well as the II-VI ternary compound $ZnSe_xTe_{1-x}$. Of these compounds, GaP is the most efficient light emitter [SAUL, ARMSTRONG, and HACKET, JR., 1969], even though it is an indirect band gap semiconductor. In materials with indirect band gaps, the lowest minimum of energy in the conduction band does not occur at the same value of crystal momentum (wave-number, k) as the maximum of energy in the valence band. When a hole and electron recombine, both energy and momentum must be conserved. The recombination process in an indirect band gap semiconductor is

therefore a two step (inefficient) process requiring phonon participation to conserve momentum, since the momentum of the photon created is negligibly small. This requirement of momentum conservation can be avoided in some cases by utilizing isoelectronic traps. In GaP the two commonly used isoelectronic traps are Zn-O (Zn substituted for Ga and O substituted for P, on nearby sites) and N (substituted for P). Notice that these substitutions do not change the number of bonding electrons and so do not produce excess electrons or holes. However, they introduce perturbations in the lattice which are localized in x-space and therefore not localized in k-space. Thus the recombination may occur at these sites.

The band gap of GaP is 2.2 eV, so that the shortest wavelength possible for the emitted light is 5530 Å, which is in the green portion of the spectrum. This is obtained using the shallow isoelectronic trap N, and external quantum efficiencies as high as 0.6% are reported [LOGAN, WHITE, and WIEGMANN, 1971]. The Zn-O trap is much deeper, and red light (6980 Å) is emitted from GaP:Zn,O diodes with efficiencies as high as 7% [SAUL, ARMSTRONG, and HACKET, JR., 1969]. Yellow light can be obtained by combining both of these traps in the same LED [ROSENZWEIG, LOGAN, and WIEGMANN, 1971].

$GaAs_{1-x}P_x$ is a solid solution of GaAs and GaP. GaAs has a direct band gap and infrared (8900 Å) light-emitting diodes with efficiencies of more than 20% at 300°K have been produced [HILL, 1965]. The addition of phosphorus moves the band gap of GaAs towards the visible, and red LED's are produced from material with a P concentration of about 40%. With more than 44% phosphorus present, the band gap becomes indirect

and the efficiency drops off by several orders of magnitude (isoelectronic traps are currently being studied). Up to the vicinity of the breakpoint η_{EQ} remains at levels commonly seen in GaAs [MARUSKA and PANKOVE, 1967].

$Ga_{1-x}Al_xAs$ is a solid solution of GaAs and AlAs (E_g = 2.16 eV, indirect) and this system affords red LED's which have efficiencies as high as 6% at 300°K [WOODALL, LYNCH, and SHANG, 1970]. $In_{1-x}Ga_xP$ is a solution of InP (E_g = 1.29 eV direct) and GaP which can emit red light with the same efficiency as $GaAs_{1-x}P_x$. It is also possible to obtain yellow (5900 Å) luminescence, but a new problem is encountered. It is necessary to grow ternary solid solution crystals on a substrate, which is usually one of the binary compounds, and this gives rise to lattice parameter mismatches with strains and dislocations. The ternary compound $In_{0.50}Ga_{0.50}P$ has an excellent lattice match to GaAs, and such (red emitting) diodes work well, but the composition required for yellow light is so badly mismatched to the substrate that efficiencies of only 0.01% are found [HAKKI, 1970]. $ZnSe_xTe_{1-x}$ will be discussed with the other II-VI compounds below.

Green GaP:N LED's show the highest luminous efficiency, even though they do not have the highest quantum efficiency. The luminous power obtained for various p-n junction LED's as a function of input power is shown in Figure 1.2. Also included in this figure are some representative phosphor up-converters, to be discussed below. A thorough review of p-n junction electroluminescence in the III-V compounds has recently been presented [BERGH and DEAN, 1972].

There are a number of other III-V compound semiconductors which

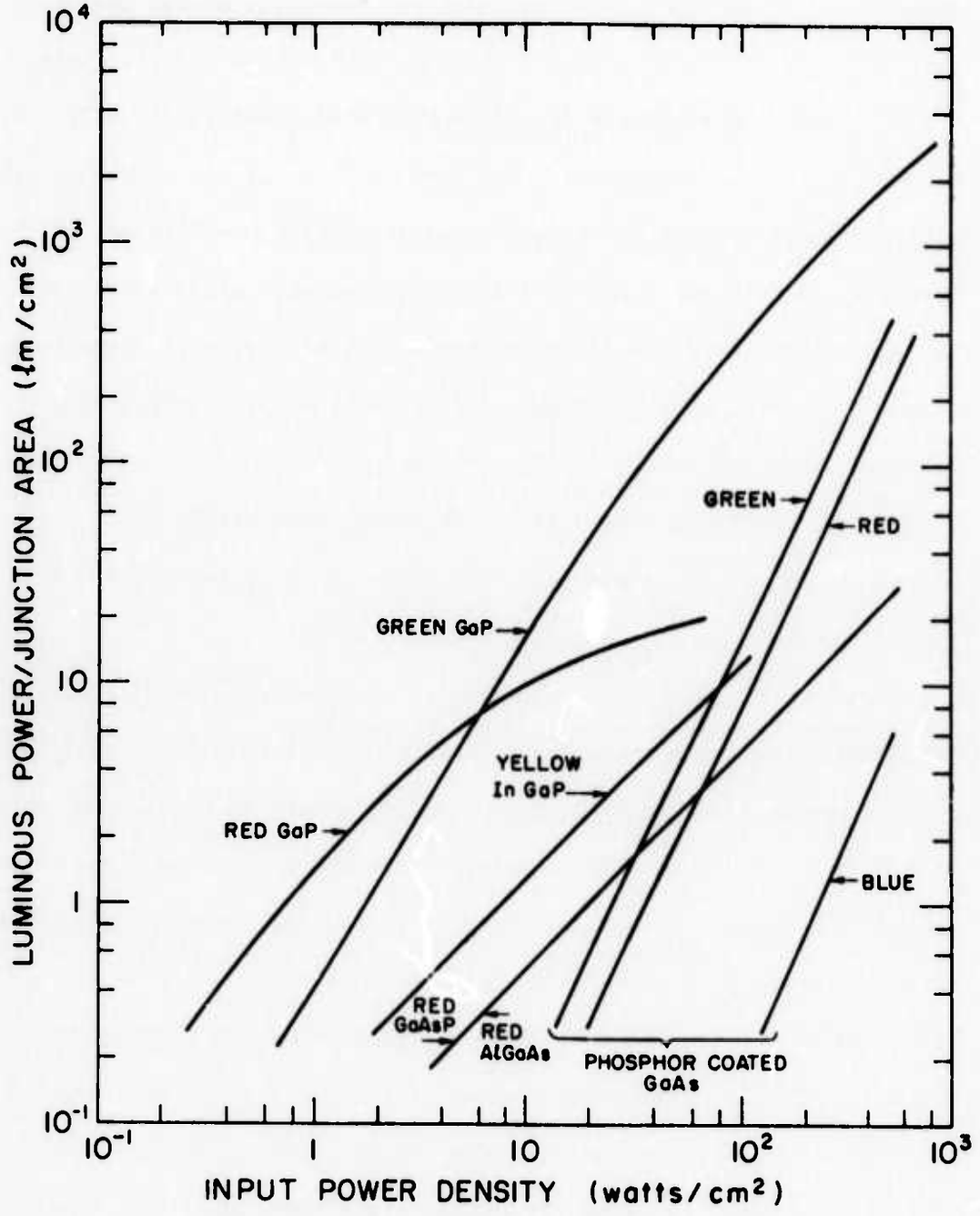

Figure 1.2 Best reported values of luminous power conversion for light-emitting diodes.

were not discussed above. These remaining compounds either have band gaps that are too small to allow visible light emission (InSb, InAs, and GaSb), or are difficult to grow (boron compounds) or are deliquescent (aluminum compounds). The last group to be considered are the nitrogen compounds, which have only recently been investigated, and more will be said about one of them in particular, GaN, a little later in this section. In the II-VI compounds with sufficiently large band gaps, p-n junctions have not been formed, because self-compensation prevents them from being doped both n- and p-type [MANDEL, 1964; TITLE, MANDEL, and MOREHEAD, 1964; MANDEL, MOREHEAD, and WAGNER, 1964]. Therefore efficient p-n homojunction LED's have only been obtained in the red to green portion of the visible spectrum.

However, it is desirable to also obtain blue and violet LED's. These would add two more colors for single lamp indicator lights, and blue is required for color picture displays, where it is also necessary in admixture with the other colors to produce skin tones and the color white. The mixing of colors to produce shades and hues can be presented on a chromaticity diagram, shown in Figure 1.3. This diagram is developed as follows [WRIGHT, 1964]. It has been observed that combinations of only three primary colors are necessary to match every one of the myriad of colors that occur in the world. That is, beams of the three primary colors can be focussed on a spot, and their relative intensities varied, until the average person will agree that this spot exactly matches in hue a test spot (of some unknown color) next to it. These primary colors, red, green, and blue, can be indicated by three eye-sensitivity curves, V(x), V(y), and V(z), as shown in Figure 1.4.

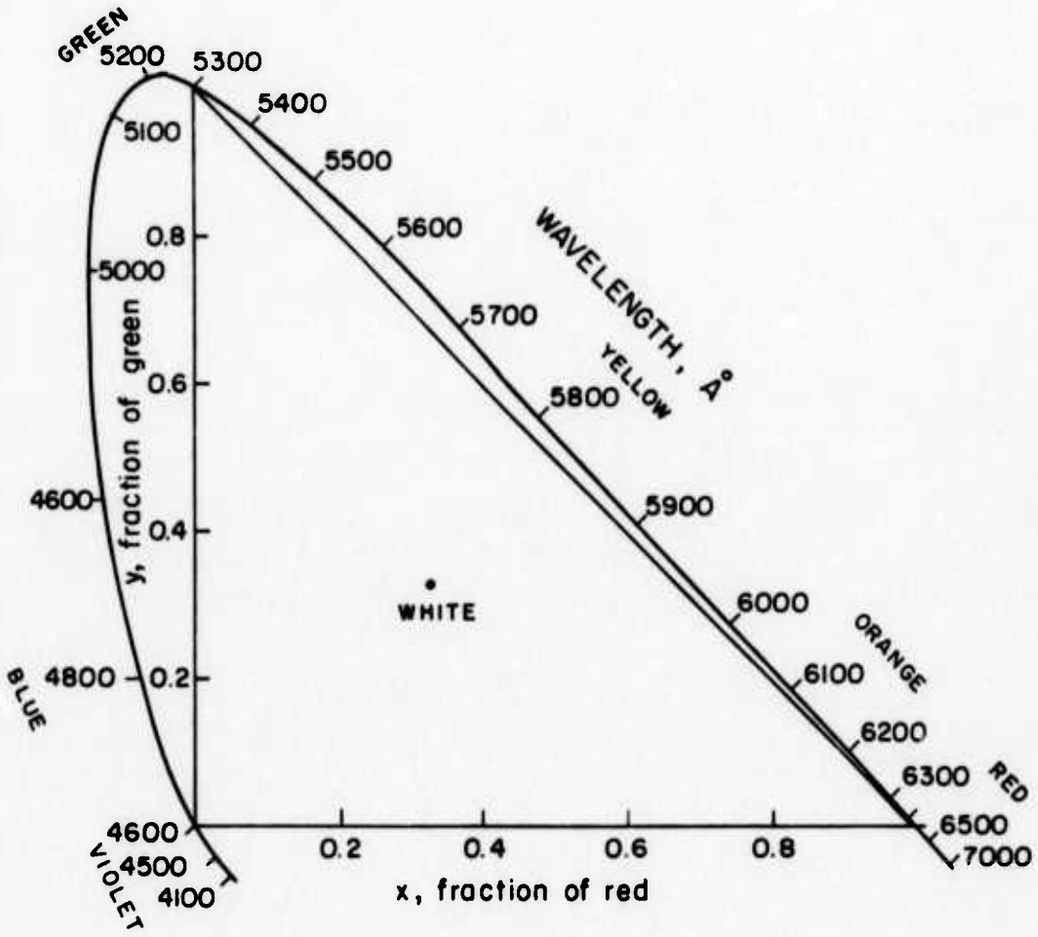

Figure 1.3 Chromaticity diagram.

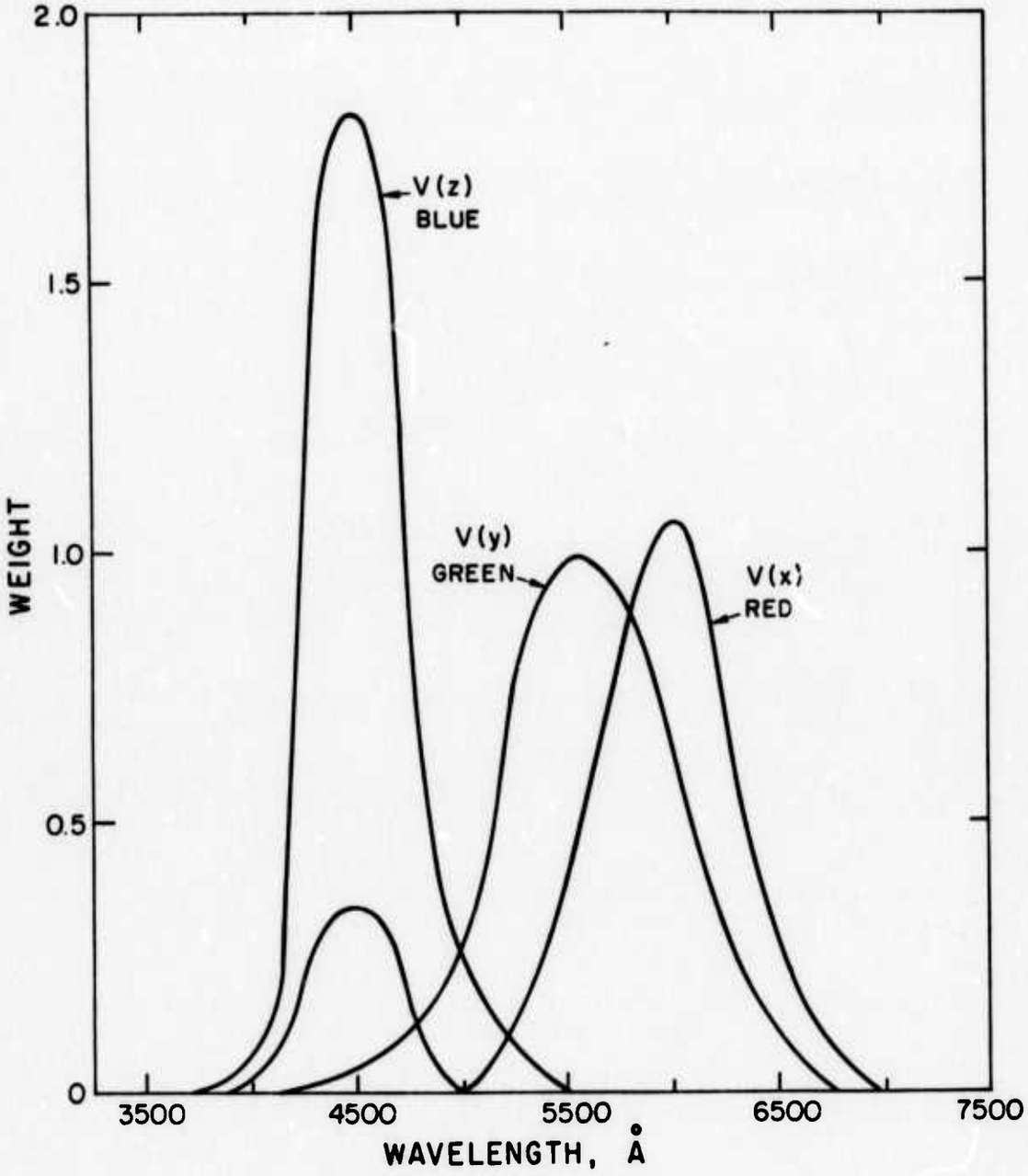

Figure 1.4 The color matching functions V(x), V(y), and V(z), (red, green, and blue).

Notice that V(y) is the same curve as V(λ) in Figure 1.1. To determine the color of a light source, three integrations are performed:

$$X = \int \frac{dP}{d\lambda} V(x)d\lambda; \tag{1.4.1}$$

$$Y = \int \frac{dP}{d\lambda} V(y)d\lambda; \tag{1.4.2}$$

$$Z = \int \frac{dP}{d\lambda} V(z)d\lambda. \tag{1.4.3}$$

These results can be reduced to two dimensions as follows:

$$x = \frac{X}{X + Y + Z}; \tag{1.4.4}$$

$$y = \frac{Y}{X + Y + Z}; \tag{1.4.5}$$

$$z = \frac{Z}{X + Y + Z}; \tag{1.4.6}$$

$$x + y + z = 1. \tag{1.4.7}$$

This gives the chromaticity diagram. The locus of pure spectral radiation is given on the horseshoe curve. The point W represents white light. Yellow and orange colors can be formed by mixing red and green, but it can be seen why blue is necessary to obtain colors throughout the diagram. Actually, red, green, and violet are the three most valuable colors to have, since with them all hues can be covered.

In order to obtain light emission in the high energy end of the visible spectrum, a number of the other kinds of device structures (diodes of classes 2-5) have been attempted. These have usually been applied to the II-VI compounds [FISCHER, 1966], most of which possess band gaps greater than 2 eV. Of these compounds, ZnTe (E_g = 2.1 eV) always occurs p-type, while ZnSe (2.6 eV), CdS (2.4 eV), and ZnS (3.7 eV) only occur n-type. Notice that with the band gaps involved light emission should occur throughout the visible region. Indeed, light corresponding to most of the region has been reported in these materials, but with efficiencies at least an order of magnitude lower than efficiencies found in $GaAs_{1-x}P_x$ and GaP.

It is possible to obtain p-n junctions in solid solutions of ZnSe and ZnTe, $ZnSe_xTe_{1-x}$, in the composition region 40 to 60% [AVEN and GARWACKI, 1964], because material in this range can be doped both n- and p-type. Red-orange light emission is afforded by these devices, which is highly efficient (η_{EQ} = 13%) at liquid nitrogen temperature (78°K) but which falls off to only 0.001% efficiency at room temperature [AVEN, 1965; AVEN and GARWACKI, 1967]. Thus these diodes cannot compete with red diodes in the III-V compounds. It is possible to form p-n heterojunctions by growing ZnTe on ZnSe [FISCHER, 1966] but these yellow-orange LED's also do not prove very efficient.

Devices involving Schottky barriers or m-i-s structures have yielded red and yellow-green luminescence in ZnTe. The yellow-green lights never have efficiencies greater than 0.01% [BORFELD and KLEINKNECHT, 1968; EASTMAN, HAERING, and BARNES, 1964], but red luminescence, due to deep levels such as oxygen, is an order of magnitude better

[KENNEDY and RUSS, 1967; DONNELLY, FOYT, LINDLEY, and ISELER, 1970]. Still, the red LED's are not as efficient as $GaAs_{1-x}P_x$.

Various colors of light emission have been seen in ZnSe. Early work on a number of device structures involving metal contacts to this material, some of which rely on minority carrier injection and others of which involve impact ionization, has been reviewed by Fischer [FISCHER, 1965]. Much better results have been achieved more recently. Red and green d-c electroluminescence has been observed in hot-pressed ZnSe diodes [CHIN and BOYER, 1973]. Park et al. [PARK, GEESNER, and SHIN, 1972] have achieved efficiencies of 0.1% in yellow-orange ZnSe LED's and Allen et al. [ALLEN, LIVINGSTONE, and TURVEY, 1972] have obtained 0.5% efficiencies in reverse-biased Schottky barriers on Mn-doped ZnSe. Such diodes show the characteristic yellow Mn color. These workers have also prepared ZnSe m-i-s diodes where the i-region consisted of a thin layer of ZnO and the ZnSe was doped with aluminum [LIVINGSTONE, TURVEY, and ALLEN, 1973]. These diodes emitted blue light (4650 Å) but the efficiency was only 10^{-4}%, which is a little low, even for a spectral range where few devices are available.

Cadmium sulfide devices of this type have not proved particularly successful either, although the material is interesting because it exhibits the phenomenon of double-injection (injection of electrons at the cathode and holes at the anode, simultaneously). Red and green lights have been reported [SMITH, 1957; KEATING, 1963]. Zinc sulfide is the most widely studied II-VI compound, but typical efficiencies are also about 0.01% for d-c electroluminescence, except in Mn-doped ZnS where efficiencies are comparable to the ZnSe:Mn diodes described

above. Zinc sulfide electroluminescent cells, operated with an alternating field, are more efficient: power efficiencies as high as 5% have been obtained [LEHMANN, 1958]. In these cells the ZnS is typically activated with copper and chlorine, and the light emission is green. Unfortunately the efficiency of such cells deteriorates in a matter of hours. Although people once hoped to light rooms with panels of ZnS electroluminescent cells attached to the ceiling, the actual light output of these devices has never become nearly great enough, and all that has been done with them is to make the common "night lights" used for indicating obstacles such as stairways in a dark house at night. Considering once again d-c electroluminescence in ZnS, it will be noticed that this semiconductor has an attractively wide band gap (3.7 eV) and should be able to show luminescence throughout the visible spectrum. But it is difficult to obtain useful n-type conductivity in it, let alone p-type conductivity. Blue light (4475 Å) has been observed in undoped samples (impurity concentration less than 10 ppm) with extremely low efficiencies of 10^{-7}% [BITER, INDRADEV, and WILLIAMS, 1969]. Samples doped with Cu and Cl show the efficiencies of 0.01% noted earlier, with green and blue light emission. Manganese doping leads to much better efficiencies, but the emitted light is yellow. Power efficiencies of 0.33% are reported for ZnS:Mn [VECHT, WERRING, ELLIS, and SMITH, 1969]. The topic of d-c electroluminescence in ZnS has recently been reviewed [VECHT and WERRING, 1970].

Another possible scheme for producing visible light involves the "up-converter" device, which combines electroluminescence and photoluminescence. Since very efficient infrared light-emitting diodes can

be produced with p-n junctions in GaAs, it has been found possible to generate the visible light by coating such diodes with rare-earth phosphors [GALGINAITIS, 1971]. The phosphor then absorbs two or three of the infrared photons simultaneously, raising it to an excited state from which it returns to the ground state with the emission of a visible photon. Red, green, and blue LED's are available, as shown in Figure 1.2. For example in order to produce blue luminescence at 4800 Å, a $BaY_{0.5}Yb_{0.499}Tm_{0.001}F_5$ phosphor must absorb three 8900 Å photons from the GaAs LED [JOHNSON, GUGGENHEIM, RICH, and OSTERMAYER, 1971]. The best power efficiency is only 0.03% because this is a three step process which is bound to lack efficiency. The process also involves long luminescent time constants (which is not good for animated displays).

It may also be noted that light can be generated in reverse-biased p-n junction due to intraband relaxation of hot carriers [CHYNOWETH and McKAY, 1956]. Such luminescence shows a very broad spectrum, bears no relationship to the band gap of the material, and is not an efficient source of light.

1.5 Purpose of This Work

Throughout the years a good source of blue electroluminescence has not been found, and no source of violet light has been reported at all. Recently a new semiconductor, the III-V compound GaN, has become the object of a number of studies. Gallium nitride has a larger band gap (3.4 eV) than GaP, but apparently cannot be doped both n- and p-type. This makes GaN similar to the II-VI compounds. The large band gap makes it an attractive material for luminescence throughout the visible

spectrum, like ZnS, but unlike ZnS it is a good n-type conductor. Quite recently green and blue light emission has been reported from m-i-s structures in GaN [PANKOVE, MILLER, and BERKEYHEISER, 1971; PANKOVE, MILLER, and BERKEYHEISER, 1972]. The insulating (i) region was produced by doping with Zn. Since we have learned from an early report on GaN [MARUSKA and TIETJEN, 1969] that Mg doping will also cause the material to become insulating, and that Mg may form a shallower acceptor level than Zn (it is to this dopant level to which the luminescent recombination evidently occurs), we have undertaken the following study of GaN light-emitting diodes, with special emphasis on Mg doping. It is expected that the results obtained should be applicable to GaN:Zn LED's, as well as LED's in other materials. It is hoped that the Mg-doped m-i-s diodes will give violet electroluminescence. Although we cannot expect as high efficiencies as found in p-n homojunction diodes, we still think the LED's will be of great interest, because no other violet lights are available. If such violet lights can be made, it should then be possible to obtain various other colors by down-converting with phosphors which will only be a one step process. Thus it should be possible to produce all the colors with one material, GaN. The major reason for working with GaN rather than a more established luminescent material such as ZnS is that almost no work has been done on GaN and so this should be a fruitful topic of research.

Chapter 2

SYNTHESIS TECHNIQUES AND PROPERTIES OF GALLIUM NITRIDE

Gallium nitride, one of the lesser-studied members of the family of III-V Compound Semiconductors, has recently become the object of a number of investigations because of its potential for opto-electronic devices. While most of the III-V compounds crystallize with the diamond-cubic zincblende structure, GaN has the hexagonal wurtzite structure. It has a larger band gap than any of the Ga and In compounds of Sb, As, or P; the fundamental absorption edge of GaN occurs in the near ultraviolet at 3.4 eV. It behaves electrically like the II-VI compounds, since it apparently exhibits only one conductivity type (n-type). The most successful synthesis techniques for GaN involve the reaction of Ga or a gallium halide with ammonia. Semi-insulating GaN has been produced by doping with Zn, and the resulting m-i-n structures which can then be fabricated from a metal contact (m), a zinc-doped GaN layer (i), and an undoped n-type GaN layer (n) have shown d-c electroluminescence.

2.1 Synthesis and Growth Techniques

The first report of the preparation of GaN was made in 1932 [JOHNSON, PARSONS, and CREW, 1932]. Metallic gallium was held in a quartz boat at 1000°C while ammonia gas was passed over it. The result was a grey powder which was formed by the reaction,

$$2Ga(s) + 2NH_3(g) \rightarrow 2GaN(s) + 3H_2(g). \qquad (2.1.1)$$

These workers found that gallium metal did not react with nitrogen (N_2)

gas, even when the system was held at elevated temperatures for long periods of time. This is consistent with the common observation that nitrogen behaves as if it were an "inert gas" such as argon or helium, and is therefore often used to provide "inert" atmospheres for chemical reactions. The "inertness" of nitrogen is a result of a great stability of the N-N bond, which has a bonding enthalpy of 226 Kcal. To form GaN is is necessary to provide a source of atomic nitrogen, either by directly decomposing N_2 or by using NH_3 to provide a high N activity.

We may divide the efforts in preparing GaN into two categories, namely,

(1) those involving the reaction of Ga or a gallium compound with atomic nitrogen N (so-called "activated nitrogen");

(2) those involving the use of ammonia with gallium or its compounds.

There are only three reports of the first type of synthesis. In the first of these [PASTRNAK and SOUCKOVA, 1963], atomic nitrogen was created in an electric discharge, and the samples were contaminated from the electrodes. In the second report [KOSICKI and KAHNG, 1969], a Y-shaped tube was utilized, such that in one arm, atomic nitrogen was created in an rf gas discharge, while Ga metal was vaporized in the second arm. The gases reacted in the third arm to form thin films of GaN on heated substrates. Since the vapor pressure of Ga at the temperatures used is quite low, very thin layers, only about 1000 Å thick, were formed. This technique deserves further study, using a better source of Ga. The third report involved reactive rf sputtering [HOVEL and CUOMO, 1972], a technique which also needs to be further

pursued.

A number of reports have been made of the growth of GaN by the reaction involving ammonia. As was noted previously, the first GaN was grown this way. Early variations in the technique involved starting with gallium compounds instead of elemental gallium. These compounds included $(NH_4)_3GaF_6$ [HAHN and JUZA, 1940], Li_3GaN_2 [JUZA and HUND, 1948], $GaCl_3$ [RENNER, 1959], GaAs or GaP [ADDAMIANO, 1961], and Ga_2O_3 [LORENZ and BINKOWSKI, 1962]. Ammonia was directly reacted with these starting materials. The products were powders or tiny crystallites, usually contaminated with impurities from the starting materials.

Work on GaN is so much less advanced than most of the other III-V compounds (save those involving boron) because it was not until 1969 that the first large area single-crystals, suitable for detailed investigations of material properties, were grown. Layers up to 100 μ thick and 1 cm^2 in area were produced on heterogeneous substrates (Al_2O_3 and SiC) by the open-flow vapor growth process [MARUSKA and TIETJEN, 1969]. This process was originally developed for the growth of GaAs and $GaAs_{1-x}P_x$ [TIETJEN and AMICK, 1966] and involves the simultaneous transport of both GaCl (formed by the reaction of HCl with Ga upstream) and NH_3 separately to the furnace region where the substrate is held. This avoids the formation of a polycrystalline surface layer of GaN on the Ga or Ga-compound source. This skin occurred in all the previously employed crystal growth processes and impeded further reaction. The open-flow vapor growth process will be fully described in Section 3.1.

A similar type of growth apparatus involving flowing GaCl and NH_3,

with the GaN deposited on sapphire substrates, has been described by Ilegems [ILEGEMS, 1972]. A small variation of the technique, in which trimethylgallium was substituted for GaCl, was described by Manasevit et al. [MANASEVIT, ERDMAN, and SIMPSON, 1971]. These investigators also used Al_2O_3 and SiC substrates.

Quite recently, GaN has been grown on sapphire substrates from a Ga-Bi melt in an ammonia atmosphere [LOGAN and THURMOND, 1972]. A thermal gradient was used, and the rate limiting step was the transport of N through the melt because of its low solubility.

The lack of single-crystal substrates of this material is a great impediment to its further development. The commonly used sapphire substrates have neither lattice nor thermal matching to GaN. Sapphire is rhombohedral, but may be referred to the hexagonal system. It has lattice parameters a = 4.75 Å and c = 13.00 Å. GaN has the hexagonal wurtzite structure, with a = 3.19 Å and c = 5.19 Å [MARUSKA and TIETJEN, 1969; ILEGEMS and MONTGOMERY, 1973]. The thermal expansion coefficients for the a parameter are 6×10^{-6} $°K^{-1}$ for GaN and 9×10^{-6} $°K^{-1}$ for sapphire [WACHTMAN, 1962]. SiC has a better lattice parameter match, but equally bad thermal expansion match. In addition, SiC is much more difficult to obtain and the surface is very difficult to prepare for growth. No other substrate material has been shown to be particularly useful.

The synthesis techniques described above lead either to powder or single crystals on heterogeneous substrates, while no mention has been made of the preparation of large crystals from the melt. The reason for this is the thermal instability of GaN at elevated temperatures.

LORENZ and BINKOWSKI [1962] observed the evolution of N_2 gas from GaN heated to temperatures as low as 600°C. It has recently been shown [THURMOND and LOGAN, 1972] that for temperatures above 800°C, the equilibrium pressure of N_2 over GaN(s)-Ga(ℓ) is greater than one atm, and rises to 100,000 atm at 1700°C, as displayed in Figure 2.1. The standard Gibbs free energy change, $\Delta G°$, for the reaction,

$$GaN(s) = Ga(\ell) + \frac{1}{2} N_2(g), \qquad (2.1.2)$$

is negative for temperatures in excess of 800°C. Since the solubility of GaN in Ga is negligible, one may assume that the species in the condensed phases in the above reaction (GaN(s) and Ga(ℓ)) are at unit activity. As a consequence, GaN will decompose above 800°C in an open system maintaining a nitrogen pressure of one atm (which is the standard state for nitrogen). However, in the open-flow vapor growth system using ammonia, the pressure of N_2 is not one atm. MARUSKA and TIETJEN [1969] reported growing GaN in this system at 825°C with an ammonia partial pressure of 0.14 atm (and a hydrogen partial pressure of 0.86 atm). The equilibrium among N_2, NH_3 and H_2 is described by the equation,

$$NH_3(g) = \frac{1}{2} N_2(g) + \frac{3}{2} H_2(g), \qquad (2.1.3)$$

which leads to the following relationship among the partial pressures:

$$P_{N_2}^{1/2} = K \frac{P_{NH_3}}{P_{H_2}^{3/2}} . \qquad (2.1.4)$$

At 825°C, the equilibrium constant K, found from the JANAF Tables [STULL, 1967], is equal to 3×10^3, so that the pressure of N_2 is

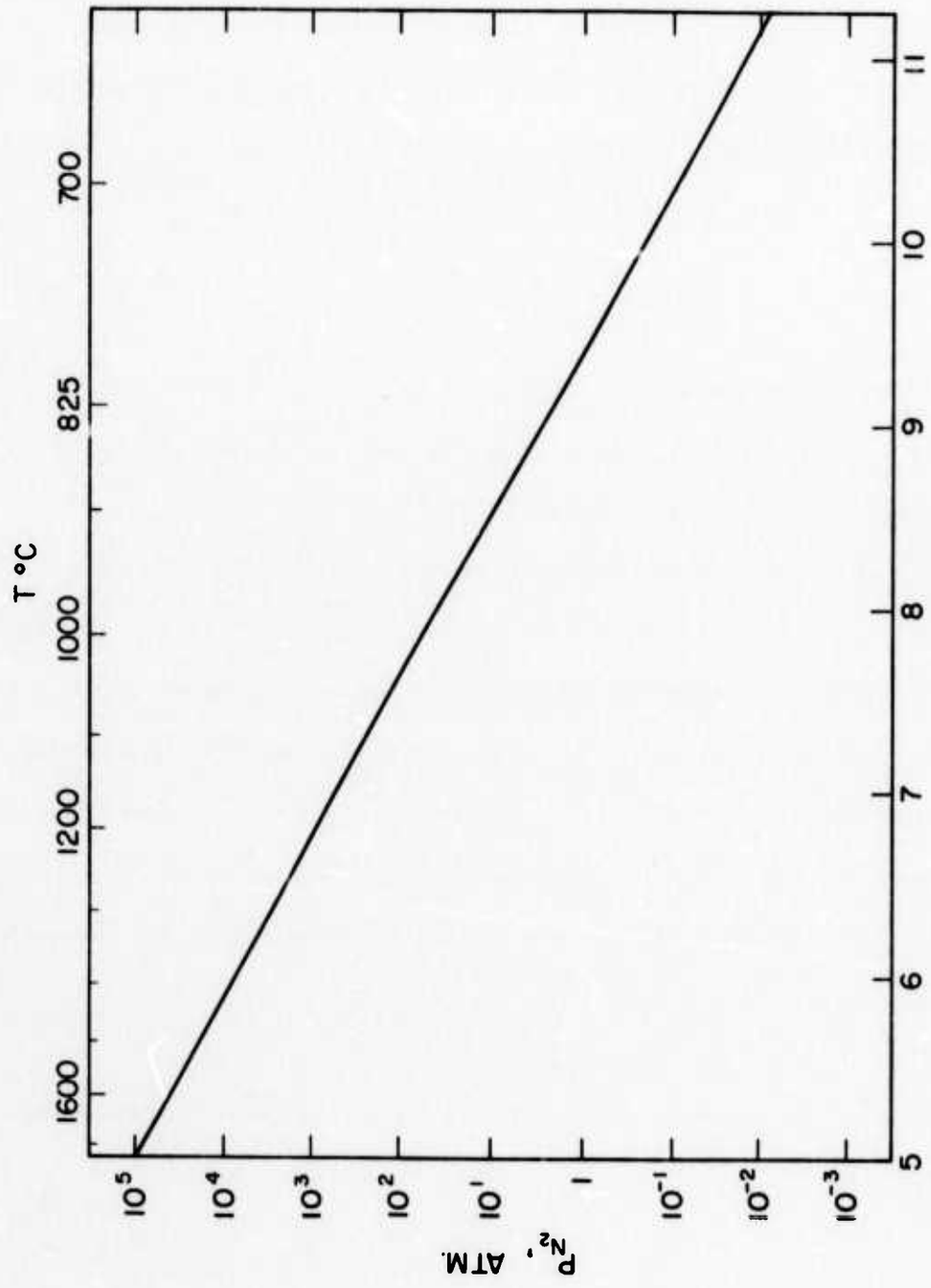

Figure 2.1 Equilibrium vapor pressure of N_2 over GaN(s)-Ga(ℓ).

2.8×10^5 atm, corresponding to a nitrogen activity of 2.8×10^5. The Gibbs free energy change, ΔG, involved in the reaction of Equation 2.1.2 is expressed as,

$$\Delta G = \Delta G^\circ + RT\ell n \frac{a_{Ga}\, a_{N_2}^{1/2}}{a_{GaN}} . \qquad (2.1.5)$$

The activities of Ga and GaN are unity, and the activity of N_2 was calculated above. The value of ΔG° may be obtained from Figure 2.1 and is -1 Kcal; therefore, ΔG = +12.7 K cal. Since ΔG is the driving force for the chemical reaction, and the value of ΔG is positive, then the reaction represented by Equation 2.1.2 will proceed to the left and GaN will grow rather than decompose under the conditions present in the open-flow vapor growth system.

It would be useful to grow large area single crystal boules of GaN from a melt, perhaps by the Czochralski crystal-pulling technique, as is used for GaAs and GaP. The substrates of high crystalline quality could be cut from the boule for further work. However, not surprisingly, no one has ever succeeded in melting GaN. Decomposition occurred even under 700 atm of N_2 pressure at 1600°C [MacCHESNEY, BRIDENBAUGH, and O'CONNER, 1970]. It does not seem reasonable to expect this method to ever work out. Vapor growth and solution growth on heterogeneous substrates seem much more practical.

2.2 Doping

The first studies of intentional doping of GaN were carried out on powders by Grimmeiss et al. [GRIMMEISS and KOELMANS, 1959, and GRIMMEISS, GROTH, and MAAK, 1960]. They discovered that it was not possible to

diffuse dopants into their samples at the temperatures where GaN is stable. This observation has been confirmed by other workers [NUESE and HAWRYLO, 1970; and ILEGEMS, 1972]. Grimmeiss et al. found that they could readily dope their samples by adding the dopant materials directly to the gallium boat before the run (Ga + NH_3 process). They introduced a wide variety of elements, including Zn, Li, Cd, Hg, Mg, Cu, Au, and Ag, and measured emission spectra (see Section 2.3).

Dopants are introduced in the open-flow vapor growth process by either adding an extra tube with furnace in which the element is vaporized [MARUSKA and TIETJEN, 1969] or else by placing a second boat containing the dopant next to the gallium reservoir [ILEGEMS, DINGLE, and LOGAN, 1972]. The dopants Zn, Cd and Mg have been introduced in this manner. Dopants with insufficient vapor pressures may be transported into the reaction zone in the form of their chlorides, in the same manner as Ga. Silicon and Ge are introduced in the form of their gaseous hydrides, silane and germane. The effects of these dopants on optical and electrical properties are discussed in Sections 2.3 and 2.4.

2.3 Optical Properties

The band gap of GaN is larger than the band gap of any of the pnictides of Ga or In. The first measurement of its value was made on a powder formed by the Ga + NH_3 technique, and the value reported was 3.25 eV at room temperature [KAUER and RABENAU, 1957]. This value was estimated from optical absorption measurements. Absorption measurements were made on large crystals of GaN (~1 cm^2) formed by the open-flow growth GaCl + NH_3 technique on sapphire substrates in 1969, and a value

of E_g = 3.39 was found [MARUSKA and TIETJEN, 1969]. These authors fit their absorption data to the expression

$$\alpha = \alpha_o(E - E_g)^n \qquad (2.3.1)$$

which yielded a value of n = 0.62. A value of n = 0.5 is expected for a direct band gap material, while n = 2 for an indirect one, so they concluded that GaN is direct. Further study on the same kind of samples [PANKOVE, MARUSKA and BERKEYHEISER, 1970] suggested that E_g = 3.5 eV at room temperature. These workers also obtained a photoluminescent peak at 3.477 eV at low temperature which shifted to 3.36 eV at 300°K [PANKOVE, BERKEYHEISER, MARUSKA and WITTKE, 1970]. In addition they determined the temperature dependence of the luminescence to be 6.0×10^{-4} eV/°K, which they stated was likely to be the temperature dependence of the band gap as well.

A similar result was obtained at 4.2°K for powder samples (NH_3 + Ga method) by measuring photoluminescence, and the band gap at this temperature was estimated to be 3.48 eV [GRIMMEISS and MONEMAR, 1970]. They also obtained a peak at 3.43 eV which they ascribed to recombinations involving shallow impurity levels. In the energy region 3.0-3.3 eV they located four peaks each separated by 90 meV, which they attributed to phonon replicas.

A somewhat larger value of E_g was reported for the thin samples grown on sapphire substrates by the microwave discharge technique of Kosicki and Kahng. A "knee" was found in the optical absorption data at 3.8 eV and was interpreted as the fundamental direct energy gap [KOSICKI, POWELL, and BURGIEL, 1970]. Other members of this group of

researchers then made measurements of optical absorption on thin hexagonal needles of GaN, and proposed that E_g = 3.65 eV at 2°K [DINGLE, SELL, STOKOWSKI, DEAN, and ZETTERSTROM, 1971]. However, they then obtained photoluminescence at 3.50 eV at 1.6°K [DINGLE and ILEGEMS, 1971], and laser action at 3.45 eV at 2°K [DINGLE, SHAKLEE, LEHENY, and ZETTERSTROM, 1971]. By combining the results of absorption, reflectance and luminescence studies on epitaxial layers of GaN grown on sapphire substrates (open-flow GaCl + NH_3 technique) they ultimately concluded that GaN is a direct band gap semiconductor with its lowest exciton state at 3.474 eV at 2°K, so that if one assumes an exciton binding energy of 28-31 meV, then E_g = 3.50 eV [DINGLE, SELL, STOKOWSKI, and ILEGEMS, 1971]. At room temperature, therefore, E_g = 3.4 eV (see also CHU, 1971). Thus there is now good agreement on the band gap of GaN.

In addition to determining the band gap, various optical studies have been concerned with elucidating the phonon structure, dielectric constants, electron effective mass, and impurity binding energies in undoped GaN. It should be noted that undoped GaN contains a large number of free carriers, probably due to native defects. It is these "impurity binding energies" which are referred to above. It should also be noted that these free carriers have caused much confusion in the interpretation of optical results, in particular, in the determination of the band gap [this is discussed in DINGLE, SELL, STOKOWSKI, and ILEGEMS, 1971].

Optical phonons, dielectric constants, optical electron mass (0.4 m) and relaxation time, and Born effective charge were reported by Manchon et al. [MANCHON, JR., BARKER, JR., DEAN, and ZETTERSTROM,

1971]. A donor energy of 42 meV and an acceptor energy of 200 meV, along with an electron effective mass m* = 0.25 m were found by Dingle and Ilegems [DINGLE and ILEGEMS, 1971]. The refractive index was studied by Ejder [EJDER, 1971]. A more complete study of the lattice dispersion has recently been reported [BARKER, JR. and ILEGEMS, 1973].

There have also been a number of studies on intentionally doped material. It was noted in the previous section that the photoluminescent spectra due to a large number of dopants in powder samples was first discussed by Grimmeiss et al. [GRIMMEISS and KOELMANS, 1959, and GRIMMEISS, GROTH, and MAAK, 1960]. These workers found that Li introduced a band at 5600 Å, Zn introduced a peak at 4300 Å, while Mg served only to increase the intensity of the "satellite emissions." The satellite emissions have been more recently associated with phonons coupled to a recombination between shallow donor and acceptor levels [GRIMMEISS and MONEMAR, 1971, and DINGLE and ILEGEMS, 1971]. The Zn band did not shift with temperature, while the Li band did. Various other peaks in the region of 5000-5800 Å were seen in samples doped with Cd, Hg, Cu, Au, and Ag. An energy level scheme was postulated with the following assignments: Zn, 0.4 eV; Cd, 0.6 eV; Li, 0.87 eV; Hg, 0.6 eV (measured from the valence band).

The presence of oxygen was said to cause an absorption band at 5200 Å and color GaN yellow [LORENZ and BINKOWSKI, 1962].

Several dopants have been introduced into vapor grown material. Zn colors normally clear GaN orange-brown, Mg makes it light yellow, while Si and Ge do not alter its color, and Hg appears to be relatively insoluble [MARUSKA and TIETJEN, 1969]. In low concentrations,

Zn is reported to form a shallow acceptor level (~200 meV) while at high concentrations (~10^{20} atoms/cm^3) an emission band at 2.85 eV appears [ILEGEMS, DINGLE, and LOGAN, 1972]. The same applies to Cd. These authors feel that Zn and Cd in large concentrations form some type of complex with the numerous native donors present.

There have been three attempts to calculate the band structure of GaN [BLOOM, 1971; JONES and LETTINGTON, 1972; and BOURNE and JACOBS, 1972]. The results are similar. However, in view of the dearth of good experimentally determined properties, there is some question as to how accurate these calculations are.

2.4 Electrical Properties

Undoped GaN samples are always high-conductivity n-type, with electron concentrations usually in excess of 10^{19} cm^{-3} and mobilities of about 100 cm^2/V-sec reported [MARUSKA and TIETJEN, 1969; DINGLE, SELL, STOKOWSKI, DEAN, and ZETTERSTROM, 1971; DINGLE and ILEGEMS, 1971; HSIEH, 1971; MANASEVIT, ERDMANN, and SIMPSON, 1971]. There have been two reports of the growth of high resistivity "undoped" GaN. CHU [1971] reported films on silicon substrates which showed a resistivity of 10^6 Ω-cm. He claimed that his growth process (which involved $GaBr_3$ instead of GaCl) prevented "decomposition of GaN" which leads to the large electron concentration found in samples of other workers. However, his electrical data indicated a deep level (1.1 eV) which controlled the conductivity, and as will be seen below, deep levels can profoundly affect the electrical properties. HOVEL and CUOMO [1972] used reactive rf sputtering (to form the N species) and

reported resistivities of 10^8 Ω-cm in yellow-colored material. The color makes one suspicious of the purity of the layers.

A reduction in carrier concentration with an increase in mobility ($n \approx 10^{17}$ cm^{-3}, $\mu > 300$ cm^2/V-sec) has been reported for vapor grown material [DINGLE, SELL, STOKOWSKI, and ILEGEMS, 1971]. These workers found that material grown very close to the position in the tube where the GaCl and NH_3 first mix and react show these properties, while the carrier concentration was found to increase (up into the 10^{19} cm^{-3} range) in GaN grown on substrates placed further downstream. This is consistent with the viewpoint that the carriers are due to native donors which are nitrogen vacancies, rather than introduced impurities. This hypothesis of nitrogen vacancies in GaN has been expressed by many workers in the field [RABENAU, 1962; MARUSKA and TIETJEN, 1969; HSIEH, 1971; ILEGEMS and MONTGOMERY, 1973]. The various authors have used mass spectrographic techniques and found no impurities in excess of 10^{17} atoms/cm^3. The elements found were ones such as Fe and Mg, which are unlikely to form shallow donors in a III-V compound. If nitrogen vacancies are responsible for the high electron concentration so that

$$n = [V_N^{\bullet}] \qquad (2.4.1)$$

then it is reasonable that the lowest n will be found in material grown in the region where the nitrogen activity is highest, i.e., directly at the opening of the ammonia inlet tube.

More indirect evidence for the nitrogen vacancy hypothesis has recently been found in solution-grown GaN layers [LOGAN and THURMOND, 1972]. Here the solvent was a Ga-Bi solution, and it was possible to

vary the Ga activity by varying the Bi atom fraction in the melt. If Equation 2.4.1 holds, then $n \sim a_{ga}^{1/2}$. Due to the large experimental uncertainty in the measured n, the results of Logan and Thurmond support but do not confirm the dependence. One cannot readily rule out the possibility of Ga interstitials rather than N vacancies. A controversy of this kind has existed in the case of ZnO for more than a hundred years [HEILAND, MOLLWO and STOCKMAN, 1959]. Interestingly, ZnO is isoelectronic with GaN. It should be noted that Logan and Thurmond's material contained about 10^{19} electrons/cm^3, so it is no improvement over vapor grown GaN.

GaN has never been made conducting p-type. The one report in the literature of p-type conductivity with Ge doping [MARUSKA and TIETJEN] is erroneous and due to overzealousness on the part of the first author. Therefore it behaves very much like the wide band gap II-VI compounds. Semi-insulating material has been produced by heavy doping with Zn in the open-flow vapor growth technique. Zn apparently first substitutes for Ga and forms a normal shallow acceptor level [ILEGEMS, DINGLE, and LOGAN, 1972]. However, at these small concentrations of Zn doping, it is not possible to compensate the native donors and the material remains n-type (although with reduced mobility values). With large concentrations of Zn additions, an acceptor level about 0.7 eV deep is formed (which becomes even deeper with more Zn additions) [PANKOVE, MILLER, and BERKEYHEISER, 1971; PANKOVE, MILLER, and BERKEYHEISER, 1972; also ILEGEMS, DINGLE, and LOGAN, 1972]. It has also been reported that Mg has a similar effect, also producing high-resistivity material [MARUSKA and TIETJEN, 1969]. The actual electrically active concentrations of

these dopants have never been measured.

2.5 Electroluminescence

GaN has been shown to be an efficient phosphor. In a recent study, photoluminescence with external quantum efficiencies of 5% at 77°K and 0.5% at room temperature was reported for vapor grown material [PANKOVE, BERKEYHEISER, MARUSKA, and WITTKE, 1970]. The calculated internal quantum efficiency was 100% at low temperatures. Thus the material seems very attractive for making light-emitting diodes. The most efficient LED's require p-n junctions. Unforunately, all attempts to produce conducting p-type material have been unsuccessful (Section 2.4). However, it has been possible to compensate the native donors by heavy Zn doping. Once this insulating (i) GaN became available, it was possible to produce m-i-n structures which exhibited electroluminescence. Green [PANKOVE, MILLER and BERKEYHEISER, 1971], blue [PANKOVE, MILLER, and BERKEYHEISER, 1972], and both yellow and red light [PANKOVE, MILLER, and BERKEYHEISER, 1973] has been reported, in each case with a Zn-doped i-layer. The light emission occurs with either polarity of bias, although it was found that blue light only occurs when the metal (m) contact is made negative with respect to the n-region (negative bias), while green and yellow light occur with either polarity, and red also requires negative bias. The spectral position of the peak is said to be determined by growth conditions, such as the Zn vapor pressure, the rate of growth, and the duration of the growth. However, details have not been given. The peaks obtained are rather broad, at least 350 meV at half maximum. The emission intensity increases with

increasing current through the diodes, but does not shift in position. External power efficiencies as high as 0.1% have been found with some diodes but values in the range of 0.001 to 0.01% are reported to be more common. The work of these investigators is presently continuing. The mechanisms responsible for the operating characteristics of the diodes have not been elucidated. Since the current has been found to be proportional to the square of the applied voltage, it is felt that space charge limited current flow is occurring in the diodes, but this question requires much further study.

Chapter 3

EXPERIMENTAL TECHNIQUES

The methods used for the growth and doping of GaN, for fabricating LED's, and for studying the structural characteristics of the material and the properties and operating characteristics of the diodes are described in this chapter. The gallium nitride prepared for this study was grown by the open-flow vapor growth method of chemical vapor deposition, which has been shown to be the most successful method available (Section 2.1). Material used for the fabrication of light-emitting diodes was doped either with Zn or Mg, or else bombarded with high-energy protons, with major emphasis on Mg doping. The relationship between growth conditions and structural characteristics of the GaN was investigated. These studies included scanning electron and transmission electron microscopy, as well as optical microscopy. Procedures for the fabrication of LED's, such as mounting and contacting techniques, were developed, and properties of these diodes were investigated. These properties included the intensity and spectral distribution of the electroluminescence, and such diode electrical characteristics as the voltage and temperature dependence of the current, and the luminescence efficiency.

3.1 Open-Flow Vapor Growth System

The open-flow vapor growth system was originally developed for the synthesis of $GaAs_{1-x}P_x$ [TIETJEN and AMICK, 1966] and has since been used to produce a number of other III-V compounds, including GaN [MARUSKA and TIETJEN, 1969]. In all of these cases the starting materials are

the metallic form of the Group III element and the gaseous hydride of the Group V element. Anhydrous HCl gas is used to transport the Group III element. A diagram of the apparatus is shown in Figure 3.1. The heart of the system is a single 2.8 cm ID straight quartz tube 80 cm long. This tube is separated from another quartz tube having the same ID by a large bore (35 mm) pyrex stopcock, so that two chambers are formed, a forechamber and a growth chamber. The growth chamber tube has three heated zones (respectively eight, six, and eight inches in length) surrounded by conventional temperature controlled resistance heated furnaces. The appropriate gases are introduced into the growth tube at one end (the right end in Figure 3.1) and the substrate is introduced into the growth tube from the other end, through the forechamber and stopcock. Substrates are mounted at the end of a precision ground (Trubore) quartz rod, which slides through a ground Trubore bearing. The two chambers and stopcock allow samples to be inserted into and removed from the growth zone without shutting down the system. The substrate on the end of the Trubore rod is initially placed in the forechamber, with the stopcock closed. Hydrogen gas is passed through both chambers, each of which is provided with an exit tube which terminates in a trap and bubbler. The bubbler is filled with low vapor pressure halocarbon oil. In this way air is purged from the system. Since the exhaust tubes are open to the atmosphere, the pressure in the system is maintained at 1 atm. After the chambers are cleared of air, the stopcock is opened and the substrate is pushed into the growth zone, and the furnaces are then brought up to operating temperature. When a run is over, the Trubore rod is retracted into the forechamber, the

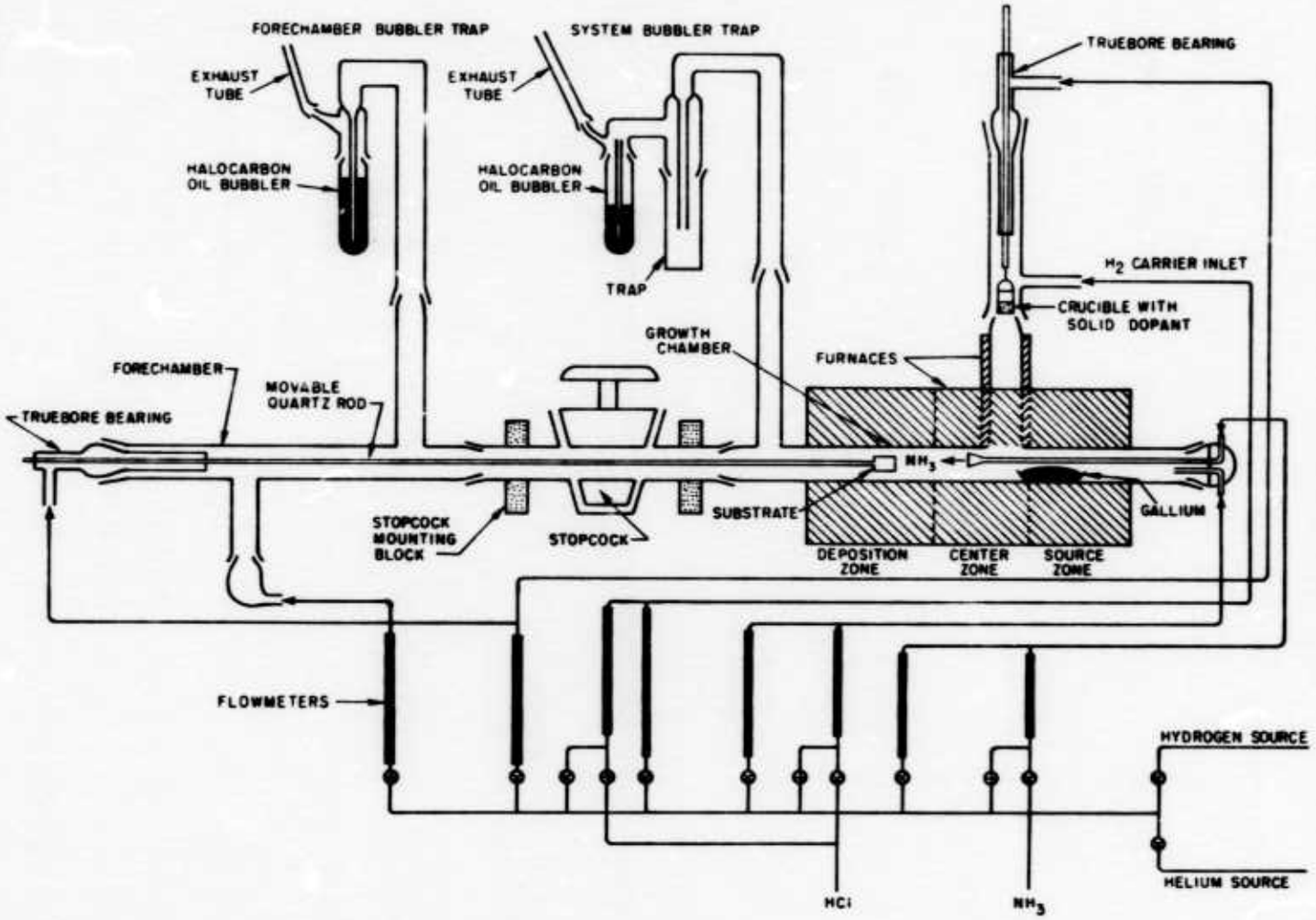

Figure 3.1 Open-Flow Vapor Growth System for preparing gallium nitride.

stopcock is closed, and the sample is removed after it has cooled. The furnaces and flows of gases in the growth tube need not be adjusted at this time, because this tube is sealed off from the air by the closed stopcock. A new substrate can immediately be positioned on the Trubore rod and a new run is ready to begin. As many as eight separate samples have been grown this way in an eight hour day.

The basic reaction involved in the preparation of GaN by the open-flow vapor growth technique is [BAN, 1972],

$$GaCl(g) + NH_3(g) \rightarrow GaN(s) + HCl(g) + H_2(g). \qquad (3.1.1)$$

GaCl is formed by the reaction of elemental Ga with HCl. As shown in Figure 3.1, the Ga is placed in a 4" long quartz boat in the first (most upstream) temperature zone in the growth tube. The HCl gas is admitted to the tube at the far right, and passes over the Ga. If thermodynamic equilibrium were attained in this zone, the $GaCl_3$ would form in addition to (and in greater quantities than) GaCl. However, very high flow rates are used in the process, and no evidence for $GaCl_3$ formation was seen when a mass spectrometer was directly connected to a typical apparatus [BAN, 1972]. The ammonia is introduced into the reaction zone through a long 1/4" OD quartz tube inside the growth tube which bypasses the Ga boat. If the ammonia came into contact with the Ga, a skin of GaN would form on it and further reaction would cease. Upstream diffusion of gases is negligible, as evidence by the fact that no GaN skin was found on the Ga surface after any of the runs made in the present study. The ammonia is introduced into the main gas stream in the center furnace zone. The ammonia and GaCl mix and react,

forming GaN in the deposition zone. The deposition zone and center zone were maintained at 900°C, while the source zone was held at 950°C. Thermocouples placed in contact with the quartz reaction tube were positioned at the center of each furnace zone.

A hydrogen atmosphere was maintained in the system during growth. Commerical hydrogen was purified with a palladium diffuser (Model 8362, Matheson Gas Products, Newark, Calif.). The flowrates of all gases were set with metering valves and the flows were monitored with flowmeters. The total flow of hydrogen through the growth tube was 1.9 l/min. The ammonia flowrate was 350 ml/min and the HCl flowrate was 3 ml/min.

Electronic grade ammonia gas was obtained from Scientific Gas Products, Edison, N.J. Ultra high purity anhydrous hydrogen chloride (maximum impurity, 10 ppm nitrogen) was purchased from Precision Gas Products, Orange, Calif. Elemental gallium (99.9999% purity) was purchased from Alusuisse. These products were used as is, with no further purification.

Sapphire substrates with (0001) and $(1\bar{1}02)$ orientations, 250 microns thick and mechanically polished to a flat, mirror-smooth finish on both sides, were purchased from Insaco, Quakerstown, Pa. They were then cut into the required sizes by scribing them with a diamond scriber and cleaving them. The substrates were cleaned before use by first washing them in hydrofluoric and nitric acids and then boiling them successively in acetone, methanol, trichloroethylene, and isopropyl alcohol. The sapphires were then ready for mounting on the Trubore rod. A removable sample holder was used to properly position the substrate. This quartz holder, shown in Figure 3.2, was slipped over the end of the

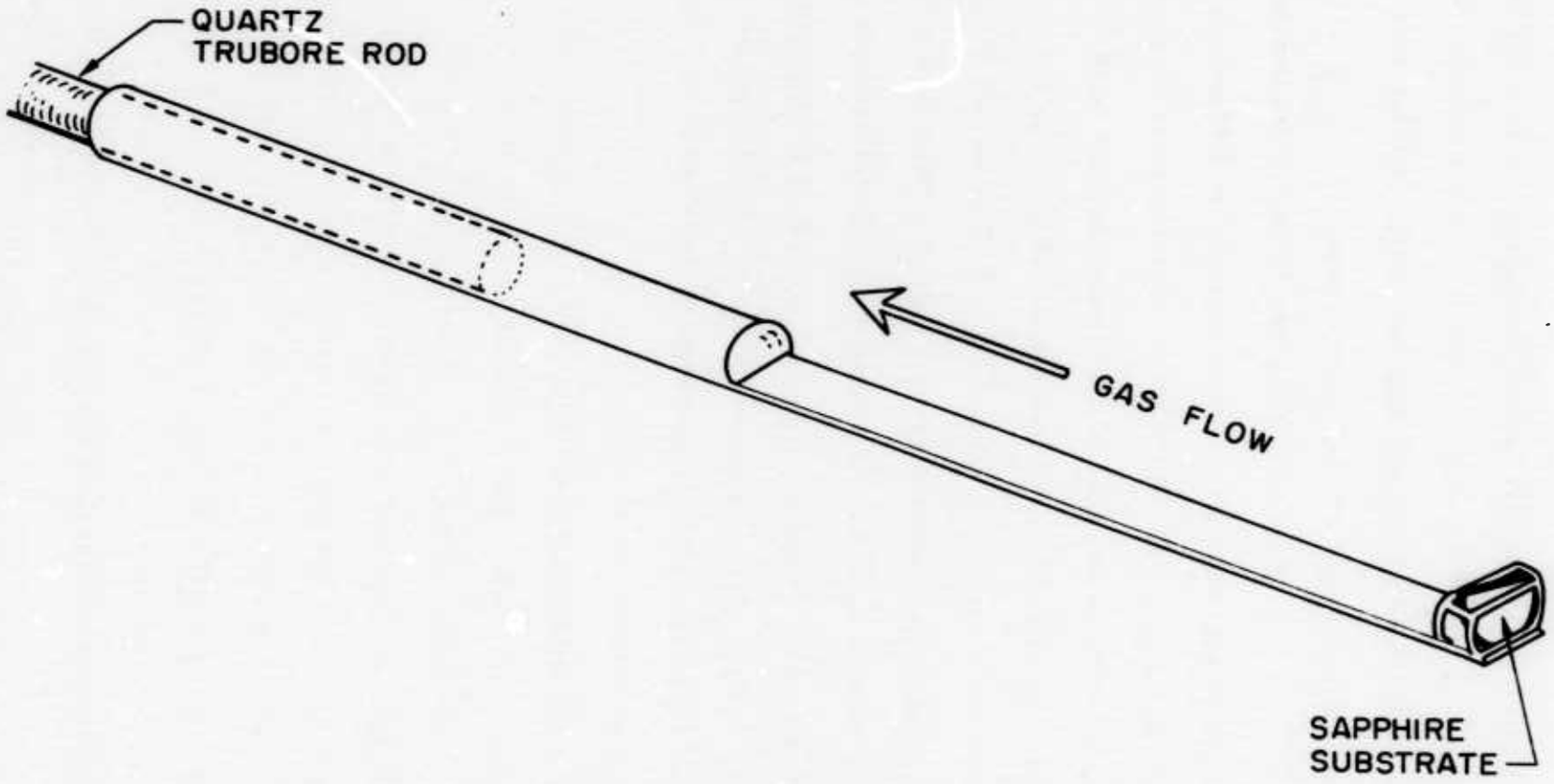

Figure 3.2 Quartz sample holder.

rod, rather than permanently attached to the rod, because of the great difficulty in dissolving GaN. The GaN grows upon the sample holder as well as the substrate, and eventually the holder is so grown over with GaN that there is no room to place a substrate on it. The only solvents for GaN (such as boiling NaOH and fused sodium pyrosulphate) also readily dissolve quartz. Thus the sample holder was simply replaced with a new one after a certain number of runs, but the costly Trubore rod remained serviceable throughout the investigation.

GaN would also deposit on the walls of the growth chamber if this tube weren't properly protected. Again it would not be possible to remove the GaN from the quartz. Therefore the growth zone was entirely lined with 0.005" thick graphite foil. This foil is quickly covered with a film of GaN, and therefore it plays no part in the chemical reactions occurring in the tube.

3.2 Doping Procedure

In order to grow doped GaN samples, a provision was made for incorporating dopants during the growth process. This was achieved by adding a sidearm tube to the main growth tube, positioned in the center temperature zone as shown in Figure 3.1. This sidearm had its own furnace and separate temperature controller. The dopant material was held in a small crucible at the end of a Trubore rod which again passed through a precision ground bearing. In the case of the sidearm, the Trubore rod was vertical and special provision had to be made to hold it in place and to move it since the entire growth apparatus was built inside a fume hood. The system used for positioning the crucible is

illustrated in Figure 3.3. The upper end of the Trubore rod was fastened to a chain which passed over a pulley system. The chain came down to the front of the system for easy access, where it was attached to a heavy brass block which could slide in a U-shaped brass trough. The brass block was positioned in the trough so as to place the dopant crucible at the desired position in the sidearm tube: outside of the sidearm furnace for undoped material, and at a carefully determined position inside the furnace for doped layers. The sidearm furnace had a fairly steep temperature gradient, from about room temperature to 1000°C in a space of 4". For dopants which have high vapor pressures and consequently are transported as their own vapors, it is clear that the temperature at which the dopant crucible is held is critical for determining the amount of dopant material in the gas phase. Many elements have low vapor pressures even at the highest temperatures attainable in the system (the furnaces are rated up to 1200°C, the temperature at which in addition quartz softens), and so there was provided a means for passing HCl over the sidearm crucible to produce volatile chlorides. If chlorides are used, the amount of dopant transported can be controlled by the HCl flowrate, rather than by the crucible temperature. However, no dopants requiring HCl transport were used in the present study. A profile of the temperature distribution inside the sidearm was taken by moving a thermocouple through its entire length. A plot of temperature vs. distance into the sidearm furnace was prepared, and these distances were marked off for the movable brass block. In this way it was possible to obtain the same vapor pressure for different dopant materials by positioning them in

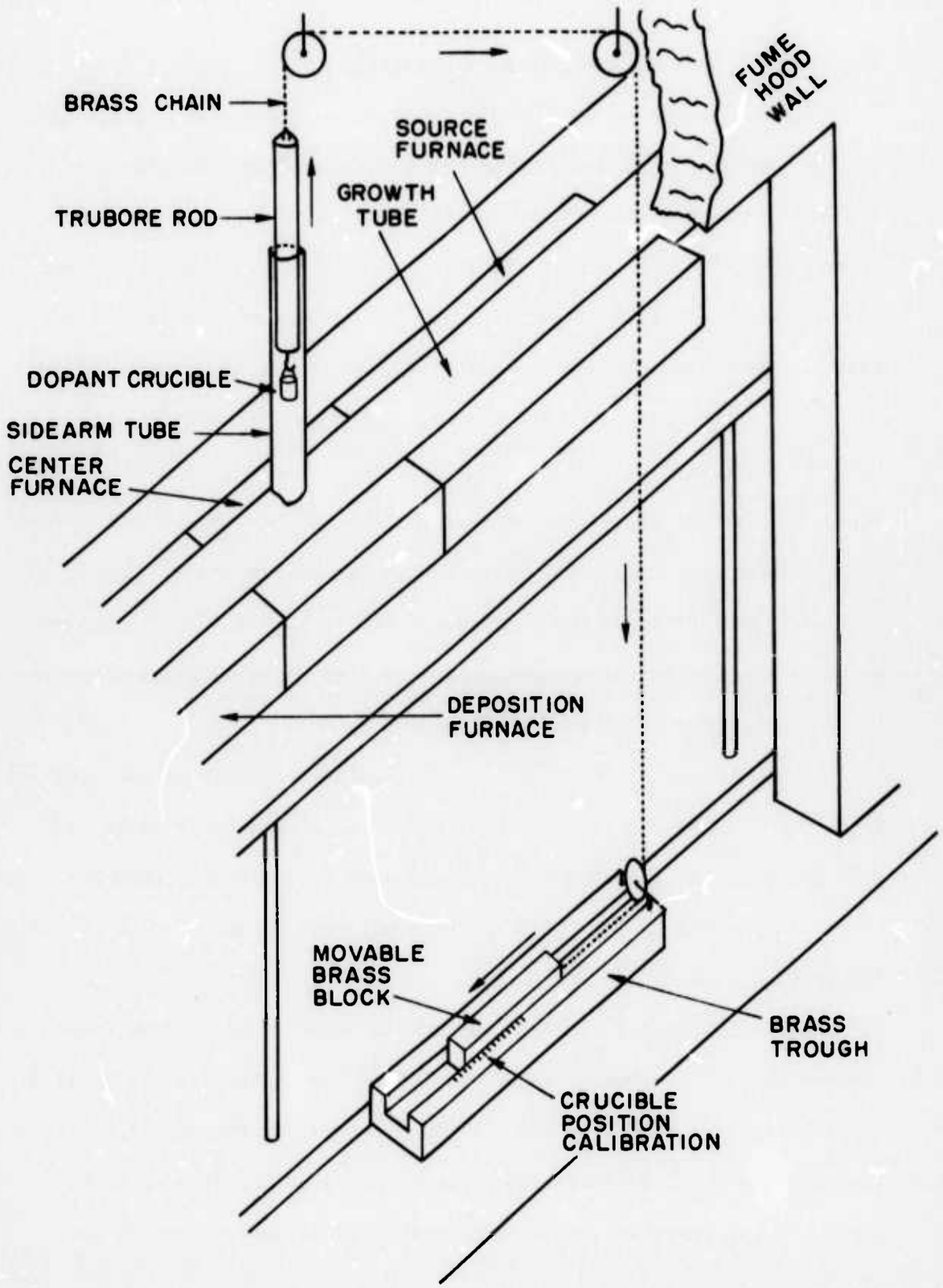

Figure 3.3 System for positioning dopant crucible in sidearm of vapor growth apparatus.

the crucible at the appropriate temperature.

It is interesting to consider the choice of dopants used for GaN. In the original work on the vapor phase growth of GaN [MARUSKA and TIETJEN, 1969] the first dopant studied was Zn. This is the most common p-type dopant used in the III-V compounds. Zinc served to make GaN insulating, but not conducting p-type. The next obvious choices were the other two elements of Group IIB, Cd and Hg, but these proved to have limited solubility and did not significantly alter the conductivity of samples. The next logical choice was to try elements of Group IIA, and of these, Mg was the most practical, since it has a high vapor pressure at reasonable temperatures and is not toxic. A couple of high-resistivity samples were grown with Mg doping, but the desired p-type conductivity was not obtained. Various other elements were then tried, but no other one gave insulating GaN.

As discussed earlier (Section 2.5), workers eventually obtained light-emitting diodes with Zn-doped GaN. Since Mg also produces insulating GaN, it appears that Mg should also be a possible dopant candidate for GaN LED's. As a consequence, both Zn and Mg were chosen for study as dopants in GaN.

The high-purity Zn used in the present study was obtained from Cominco American, Spokane, Wash. The Zn can be conviently placed in a quartz crucible, 3/4" long and 3/8" in diameter, at the end of the Trubore rod in the sidearm tube. The Zn comes in the form of shot, about 1/8" in diameter, and several pieces of it were placed in the crucible at a time.

Magnesium is more reactive than zinc and attacks quartz. Conse-

quently the high-purity Mg (Electronic Space Products, Los Angeles, Calif.) was held in a graphite crucible. The body of this crucible had the same dimensions as the quartz crucible. Originally a loop of platinum wire was used to hold the crucible to the quartz hook at the end of the Trubore rod. However, the Mg vapors attacked this wire (Mg and Pt form a low-temperature eutectic), and a new crucible with graphite "ears," shown in Figure 3.4, was machined. A platinum wire was still used at the top of the "ears," but this wire was now sufficiently far from the Mg vapors to remain intact. The Mg was obtained in the form of 1" cubic blocks, which were sawed into small pieces and cleaned in dilute HCl before use. When using Mg as a dopant, it was necessary to line the sidearm as well as the main tube with a graphite liner to reduce attack on the quartz. It has not proven possible to eliminate all attack because the two liners are perpendicular to each other and Mg vapors pass between them to the quartz tube at the place where they meet. It was necessary to repair the quartz tube after too much damage had occurred and the sidearm was in danger of breaking off.

The typical growth procedure for a GaN LED may be summarized as follows. First, the growth apparatus was cleaned and assembled. It was then flushed with high purity hydrogen. The sapphire substrate was inserted into the growth zone and the furnaces were turned on. When the proper temperatures were reached in the zones, the ammonia flow was started, to create an ammonia atmosphere. Next the HCl flow was started, and growth began. After a sufficiently thick undoped n-type layer was grown, the dopant crucible was lowered to its proper position, and the insulating layer was grown. The HCl flow was then stopped, the sample

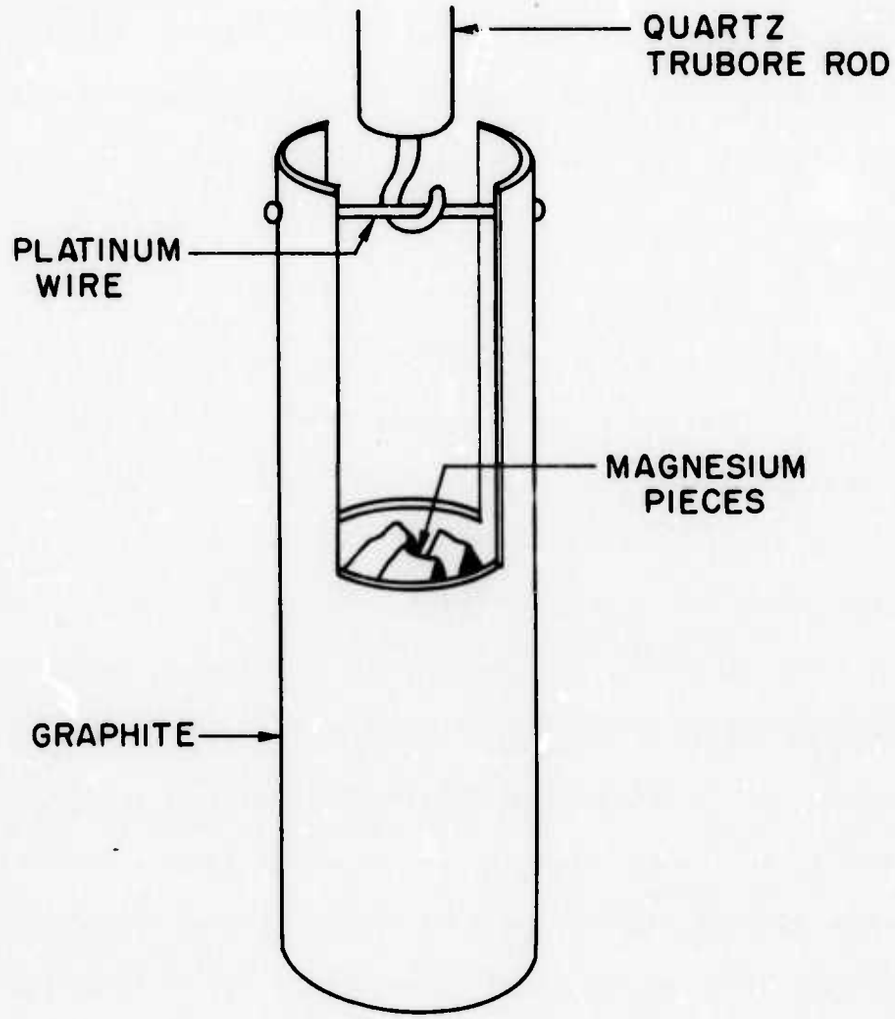

Figure 3.4 Graphite dopant crucible.

was withdrawn into the forechamber, and the large stopcock was closed, sealing off the furnace zones. Finally the sample was removed from the system and moved to the diode fabrication area.

3.3 Point-Contact LED's

The next step in the fabrication of a GaN light-emitting diode is to make electrical contact to the sample so that a potential difference may be applied to it and current will flow. The simplest contacts that can be made to a sample are point-contacts. Such contacts are made by touching two wires to the material. This is most easily done with micro-manipulators, which are spring-loaded and therefore apply some pressure to the wires touching the sample surface. This also allows precise positioning of the wires.

The surface layer of the GaN, grown as described at the end of Section 3.2, is electrically insulating. In order to make contact to the conducting n-type GaN below the i-layer, a large voltage (several hundred volts) had to be applied across both wires. In most cases an arc was passed between the two wires through the i-GaN, and the region directly under each wire point was burnt directly through to the conducting GaN. Then both contacts were "ohmic," i.e., the electric current I through the circuit was linearly proportional to the applied potential difference V: $I = (1/R)V$,* where R is the sample resistance. Notice that the insulating GaN had now been bypassed, but the i-layer is vital for electroluminescence. Electroluminescence does not occur

*More properly, Ohm's Law is expressed $(I/A) = \sigma F$, where I = current, A = area, σ = conductivity, and F = electric field. If $F = V/\ell$ and since $\sigma = (\ell/A)(1/R)$, where ℓ = length of sample, $I = (1/R)V$.

in a circuit where Ohm's Law is obeyed, because validity of this law implies very low electric fields, and it usually only obtains in systems lacking electrical junctions (in which high electric fields are found). Therefore, to obtain electroluminescence, one wire was arbitrarily moved to some other point on the sample surface. Light was then generated in the form of a small pin-point under this non-ohmic contact when a sufficient voltage was applied. Light was observed with either polarity of bias, but a brighter spot was observed when the non-ohmic wire was made positive.

3.4 Improved Large-Area Metal Contacts

A great improvement over the point-contact LED can be made by applying a large area metal contact to the surface of the GaN sample. In the first place, light emission will occur over a much larger area than possible with just a wire touching the surface, and secondly, with these large contacts a much lower voltage is required to turn on the LED. If the sample is cut into small pieces before LED fabrication is attempted, the process of making good electrical contact to the n-type region is also facilitated. An uncut wafer has an entirely insulating surface, but a chip of material, cut from a sample, obviously has easily contacted n-type material exposed around its entire periphery. It is not possible to contact the n-GaN through the substrate, a technique used for $GaAs_{1-x}P_x$ or GaP diodes, because of the high resistivity of sapphire ($\sim 10^{15}$ Ω-cm). Thus a useful technique for making a GaN LED is as follows. A chip is attached, with transparent glue or double-sided Scotch Tape, to a convenient support such as a

glass slide, sapphire side down. A metal contact is made to the center area of the GaN chip. Care is taken not to overlap any side of the chip, or an electrical short-circuit will result. Next, metal is attached to the edge of the wafer. It is permissible to touch sapphire, n-GaN, and i-GaN with this contact, because all the current flowing from it will pass into the n-layer. The other layers are highly resistive in comparison. Next, wires are touched to the two metal contacts, a bias is applied, current flows and electroluminescence is observed. A device of this type is sketched in Figure 3.5. The lead-in wires are held in place with dabs of epoxy. Notice that the emitted light must be viewed through the glass slide.

The following types of metal contacts and contacting procedures were used. A simple method employed indium metal which was cleaned and pressed into place. Unfortunately the pressure required was often enough to crack the sample. An alternative method was to evaporate a metal such as gold through a mask onto the sample. This provided good contacts but was a laborious procedure. In addition, such contacts were difficult to remove. A particularly useful technique makes use of a liquid metal such as indium-gallium. This liquid is simply painted on with a brush. It can easily be removed by dipping the slide in aqua regia. Many of the diodes made in this study had liquid indium-gallium contacts.

Diodes mounted on glass slides are not only a little unwieldy, they are also inconvenient for measurements at low temperatures. In addition, liquid metal contacts lack mechanical and thermal stability. To overcome these problems, a technique was developed for permanently

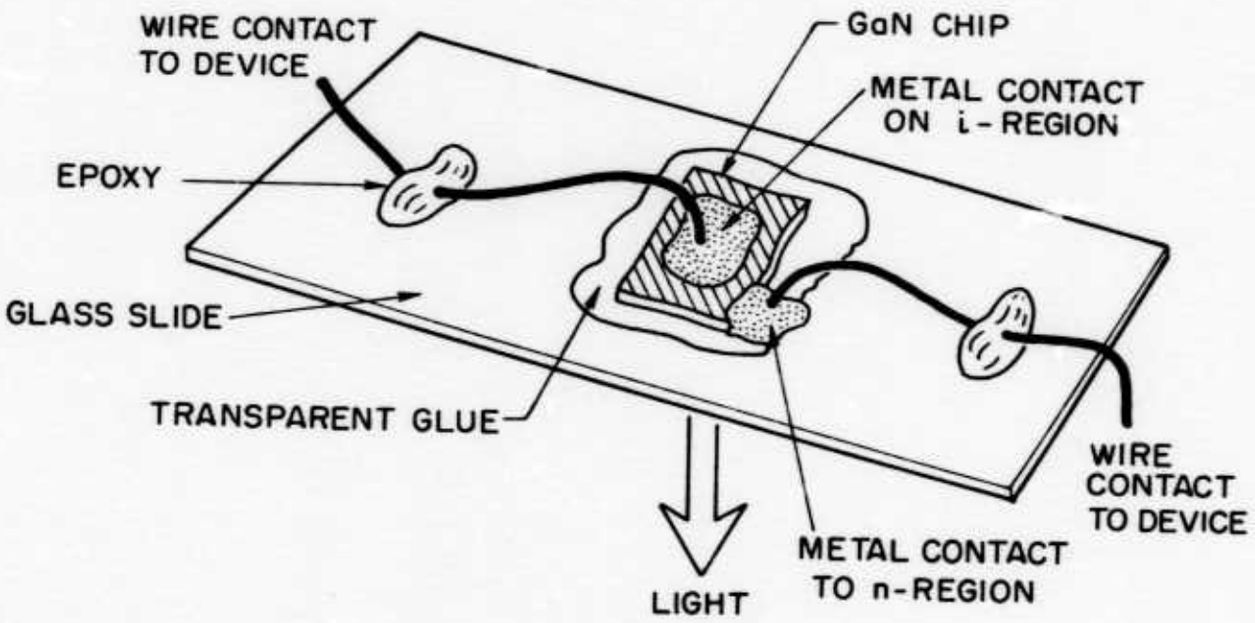

Figure 3.5 Gallium nitride light-emitting diode attached to a glass slide.

mounting diodes on standard TO-5 headers. A diode so mounted is sketched in Figure 3.6. Since the header is totally opaque, the chip must be mounted on it upside down, that is, sapphire side up. A good way to effect the attachment is to start with an indium amalgam, which is a liquid at room temperature. A globule of this liquid is painted on the surface of the i-GaN layer, and a small spot is painted on the side of the chip, in the usual way. The chip is then placed onto the metal header so that the large globule of liquid is between the header and the chip, while the small spot remains free. This device is then placed on a strip-heater in a hydrogen atmosphere and heated to 400°C for one minute. This heating serves to evaporate the mercury and solid indium contacts remain. The large contact now bonds the chip to the header. A tiny copper wire is used to contact the n-layer.

The technique just described is not very easy to carry out, because the chip can slide in the liquid amalgam before or during heating and short out. If liquid contacts can be tolerated, there is an easier method for attaching a chip to a header. First a hole is drilled through the center of the header, and then the chip is attached over the hole on the underside of the header with Duco Cement, so that the sapphire can be seen through the hole and the GaN i-layer is visible for painting from below. Wires can be attached in much the same way as they are attached to a glass slide diode.

3.5 Measurement of Wavelength and Intensity of Luminescence

The system used for studying the wavelength and intensity of electroluminescence in GaN diodes is shown in Figure 3.7a. The LED was

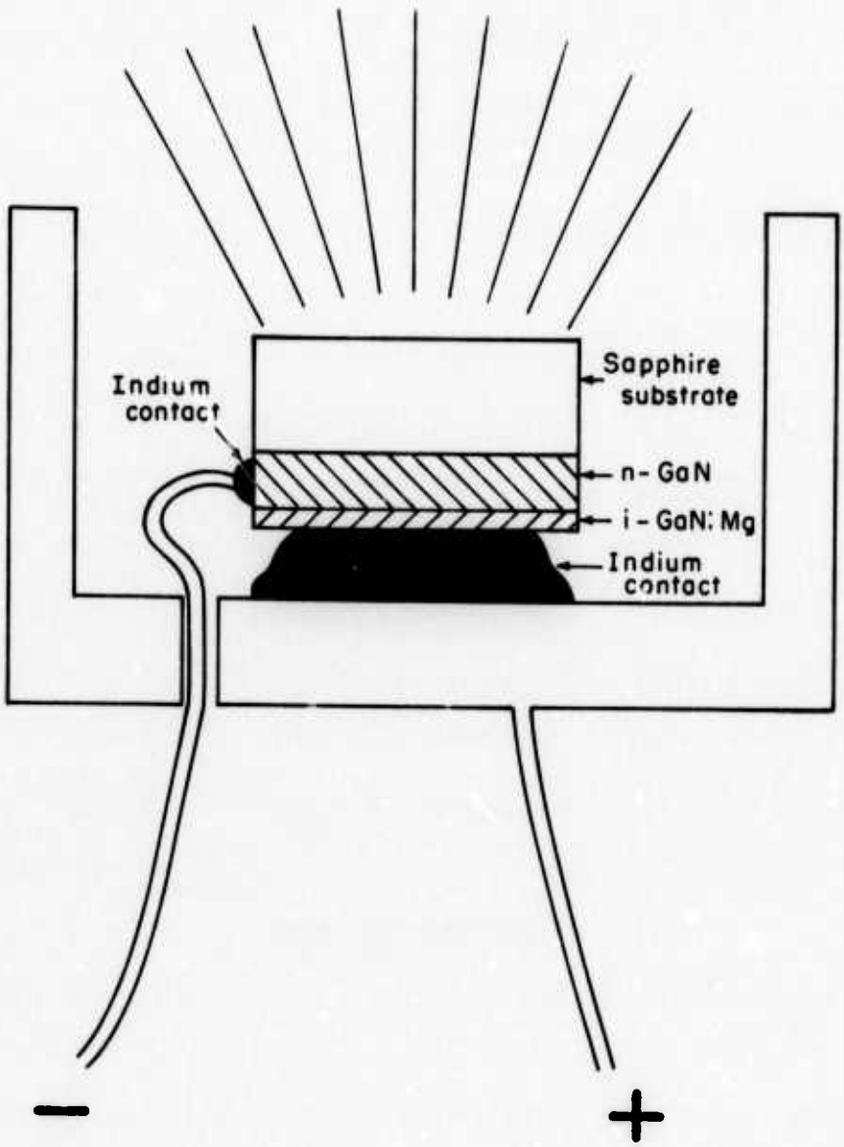

Figure 3.6 Schematic diagram of a gallium nitride light-emitting diode on a TO-5 transistor header.

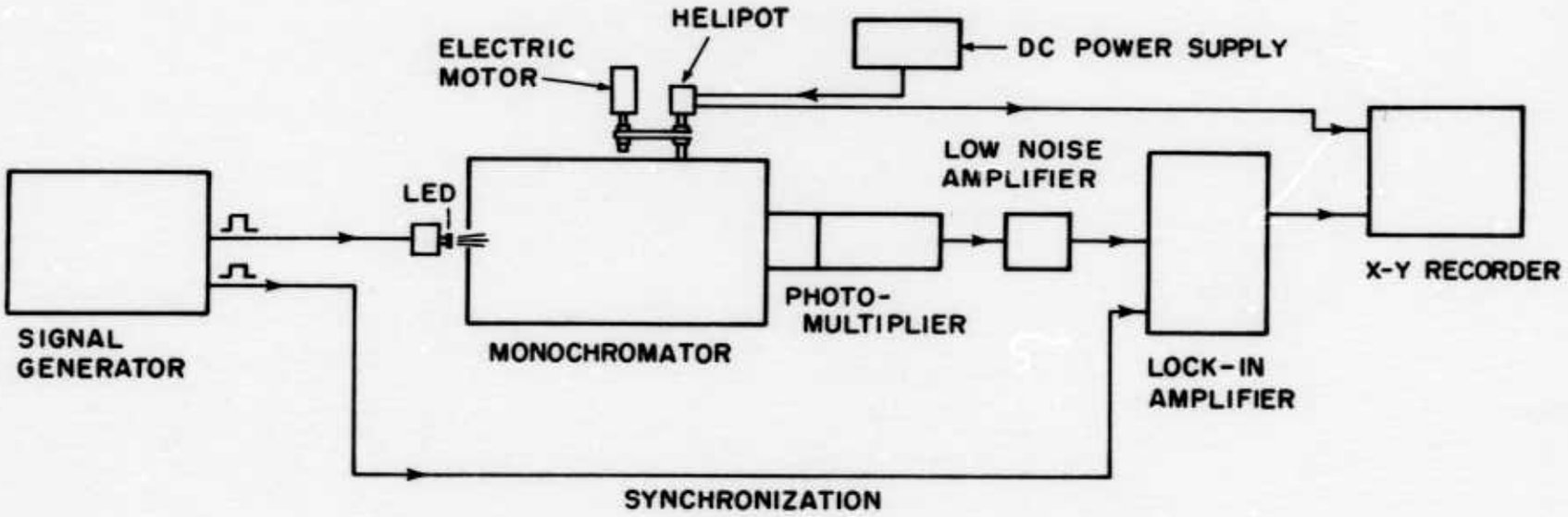

Figure 3.7a Experimental arrangement for measuring the wavelength and intensity of electroluminescence (schematic).

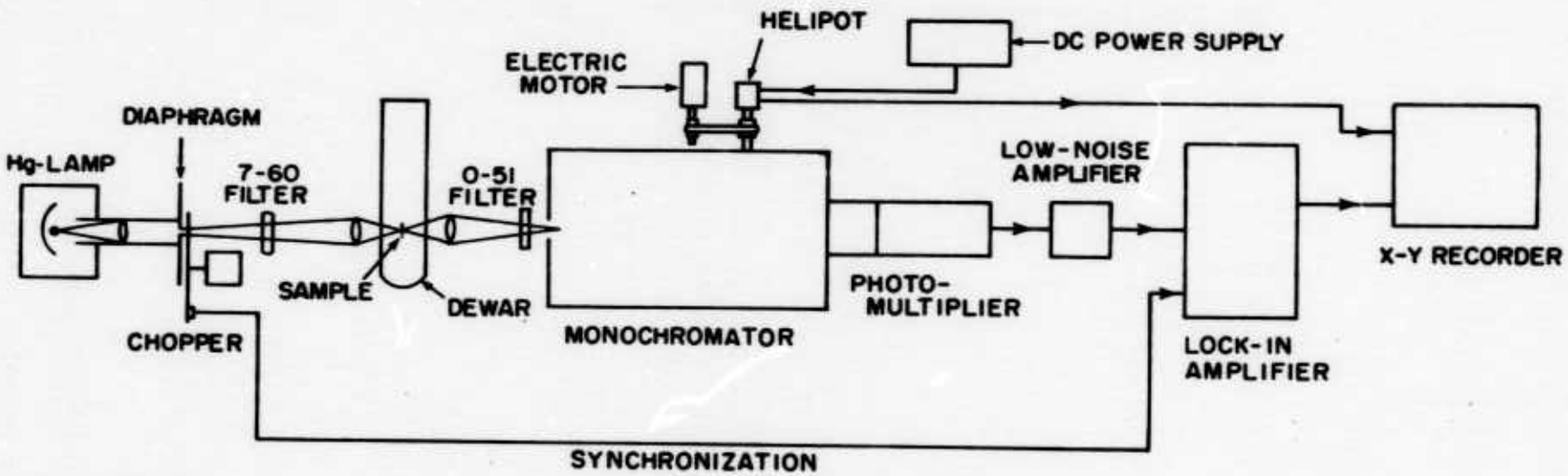

Figure 3.7b Experimental arrangement for measuring the wavelength and intensity of photoluminescence (schematic).

placed as close as possible (within about one inch) to the entry slit in the Bausch and Lomb Monochromator, so that as much light as possible was collected. The voltage for the diode was obtained from a Wavetek Model 111 Voltage Controlled Generator, which was set to produce square pulses of a convenient frequency (such as 300 Hz). Since the Model 111 can only supply up to 15 volts, a Tektronix Model 575 Diode Curve Tracer was used in experiments requiring higher voltages. This apparatus supplies up to 200 volts at 120 Hz, a frequency of operation which leads to some minor inconveniences since it is the second harmonic of the line frequency. When the curve tracer was used, all sources of light in the room, other than battery operated ones, had to be eliminated.

The light from the monochromator was directed into an RCA-7265 Photomultiplier, which has an S-20 photosensitive surface. The spectral response of the S-20 surface is shown in Figure 3.8. The response is approximately flat between 4000 and 4500 Å.

The output of the photomultiplier was fed to a Princeton Applied Research Model CR-4A Low-Noise Amplifier and then to a Princeton Applied Research Model JB-4 Lock-In Amplifier. Here it was synchronized with the signal generator, so as to exclude spurious light signals. The signal intensity was then plotted as a function of wavelength on a Moseley Model 135 X-Y Recorder. The wavelength of the monochromator (and also of the X-Y Recorder) was automatically driven by an electric motor and a Heli-pot, as shown in Figure 3.7a.

The modifications made to the system in order to study photoluminescence are shown in Figure 3.7b. The signal generator and the LED were removed, and the sample to be studied was positioned in a

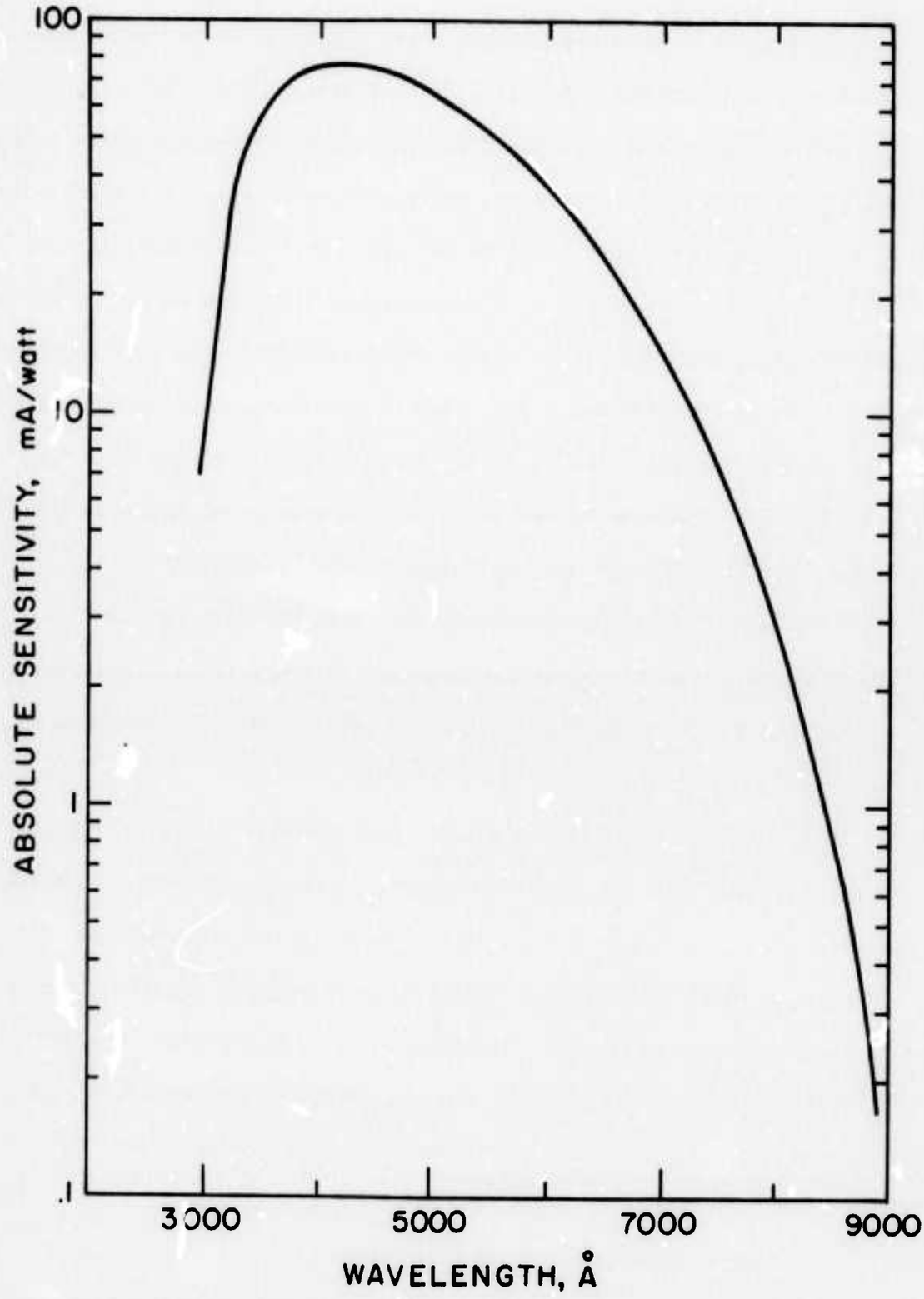

Figure 3.8 Spectral response of the S-20 photocathode.

dewar (which may be filled with liquid nitrogen) about 8" back from the monochromator. Photoluminescence was excited with a 500 watt high-pressure mercury light. This light was passed through a pin-hole, chopped, and focussed on the sample. The visible portion of the mercury arc spectra was removed with a Corning 7-60 filter, while the uv light from the source was prevented from entering the monochromator with a Corning 0-51 filter. Synchronization for the lock-in amplifier was obtained from the chopper.

3.6 Electrical Characteristics

The diode current-voltage (I-V) characteristics are conveniently measured with a Tektronix Model 575 Diode Curve Tracer. This apparatus displays the I-V curves on a cathode-ray tube and the trace can be recorded by photographing it with a polaroid camera. The curve tracer was instrumental in determining if pieces of material would make suitable diodes. It was also useful for finding the n-GaN layer from the side, and for determining if the contact to it was ohmic.

The Tektronix Curve Tracer has a lowest current scale of 0.01 mA/div, and in order to measure smaller currents (especially at low applied voltages), another system, shown in Figure 3.9 was used [FAHRENBRUCH, 1973]. Here the voltage was supplied by a battery connected across a variable resistor R1 and the current was determined by measuring the voltage across a fixed resistor R2 in series with the diode. This experimental arrangement was also used to measure photo-currents. For such measurements band gap light was supplied by passing light from a tungsten lamp through a monochromator and focussing the light on the

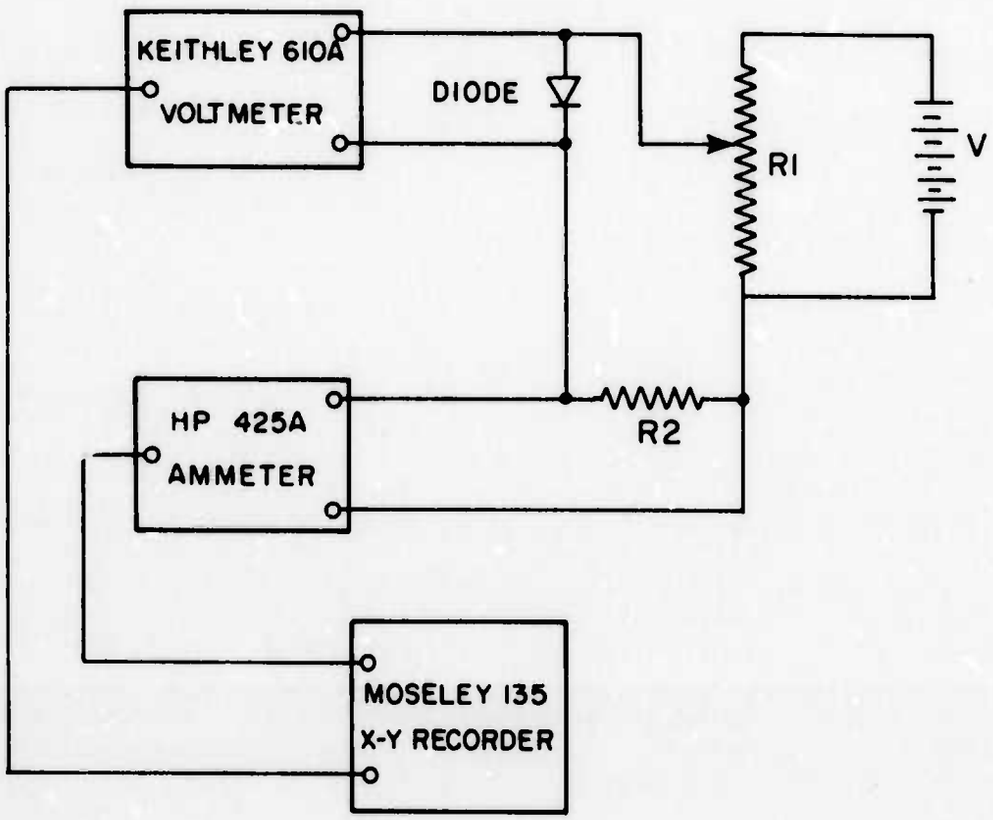

Figure 3.9 System for measuring I-V characteristics (schematic).

sample.

It was possible to measure the I-V characteristics at temperatures below room temperature by placing the devices in a dewar with liquid nitrogen in it. The liquid nitrogen level was kept below the position of the diode, and the diode was cooled by the gas streaming off from the liquid. The temperature was varied by simply adjusting the liquid level. A chromel-alumel thermocouple was used to monitor the temperature.

For elevated temperatures the diodes were placed in an oven equipped with a variable temperature setting.

Our test facilities did not include a calibrated detector for measuring diode efficiencies. Therefore a representative diode was sent to RCA Laboratories, Princeton, N.J., where such a test facility was available. Their apparatus was capable of simultaneously measuring the light power output as a function of power input and the I-V characteristics of a diode. The results of these two measurements are shown in Figures 4.8 and 4.11. A schematic diagram of the apparatus is shown in Figure 3.10. As the d-c bias across the diode is increased, the voltage across the diode and the current through it are sensed by logarithmic converters which feed their output to an x-y recorder, thus generating a log I vs. log V display.

Simultaneously with the I-V measurement, the dependence of the electroluminescent output power L_{out} on the input power P_{in} is recorded as a log-log plot on a second x-y recorder. The light emission of the diode is chopped and detected by the calibrated detector, and the output of the detector is synchronously amplified and converted into its logarithmic value. The logarithm of the input power, P_{in}, is obtained

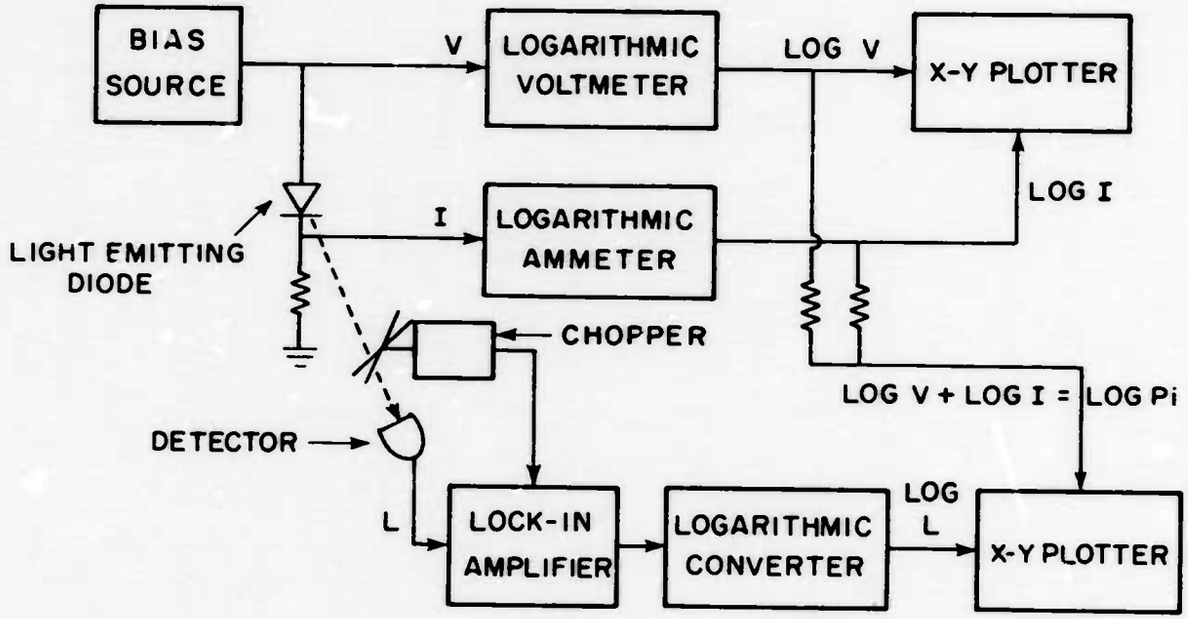

Figure 3.10 System for simultaneous measurement of power efficiency and I-V characteristics of a light-emitting diode (schematic).

by adding the outputs of the two logarithmic converters which are used to generate the I-V characteristics.

3.7 Scanning Electron Microscope

The scanning electron microscope (SEM) is an invaluable tool for studying the surface characteristics of samples. With this microscope it is possible to obtain high resolution topographic micrographs of metal and semiconductor surfaces with a range of magnification of up to about 10,000 times together with an extreme depth of field. It also permits the direct observation of electrical junctions.

The theory and operation of the scanning electron microscope has been described in detail in a textbook [THORNTON, 1968]. The principles of operation can be briefly summarized as follows. The microscope consists of an electron-optical column, a vacuum system (including the specimen chamber) and a signal detection and display system, as sketched in Figure 3.11. An Advanced Metals Research Model 900 scanning electron microscope was used in the present work. The electron beam is emitted from a cathode-ray gun with an energy of 1 to 30 KeV, and it is focussed and controlled with a system of magnetic lenses. The 100 Å diameter electron beam is swept across the sample in synchronization with a cathode-ray tube (CRT) on which the information is displayed.

The sample is placed in the specimen chamber on an adjustable stage so that the diode may be positioned under the beam and tilted to the angle required. The high energy electrons from the beam enter a short distance into the sample and lose their energy through collisions with electrons in the material. Some of the sample's electrons can

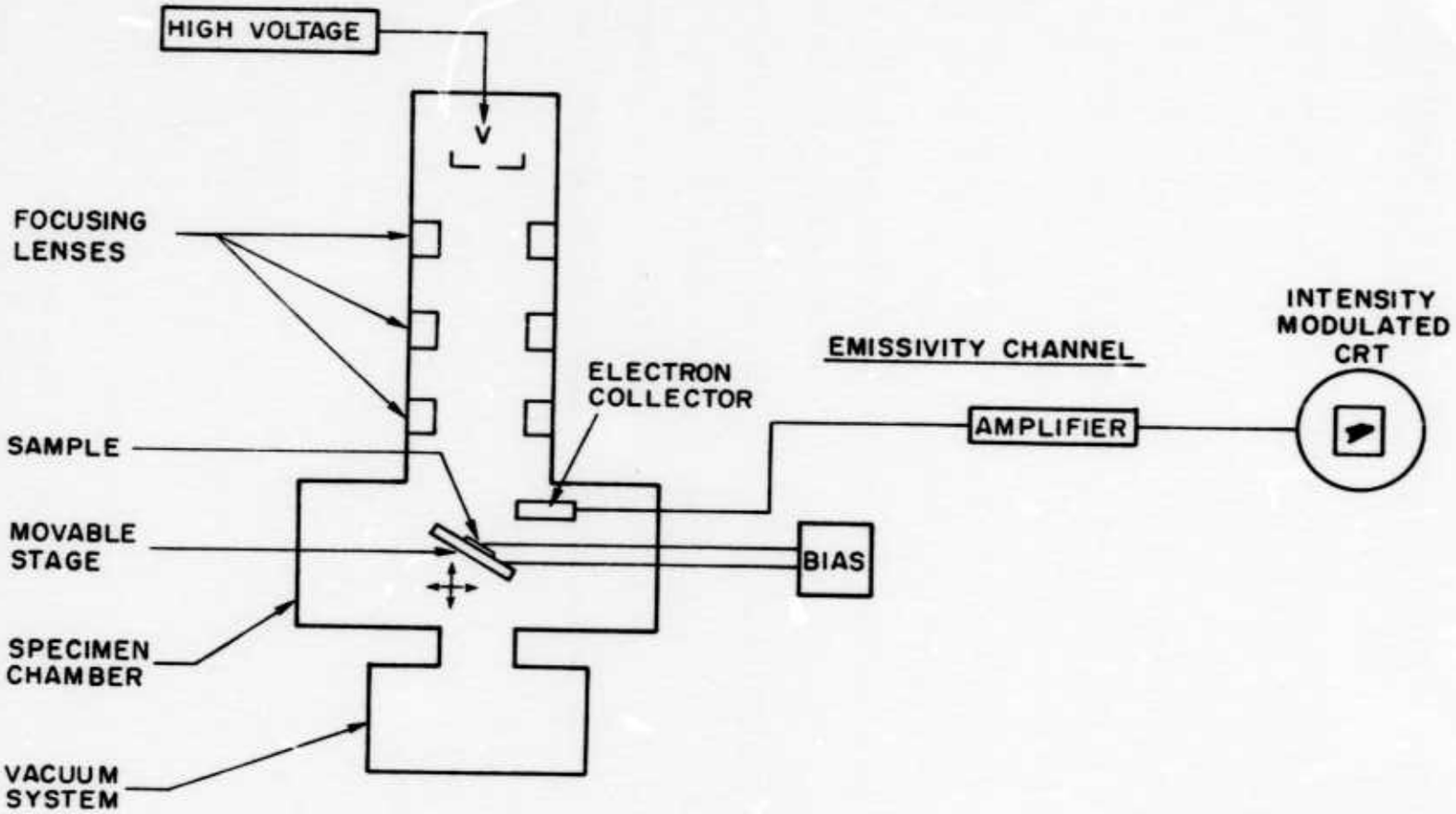

Figure 3.11 Schematic diagram of the scanning electron microscope.

therefore obtain sufficient energy to escape from it. Such electrons are termed "secondary electrons." The secondary electrons are collected and the resulting current is amplified and fed to the CRT. The pattern formed on the CRT corresponds to the surface geometry of the specimen as would be seen in an ordinary optical microscope, except that the depth of field in the scanning electron microscope is much greater. The contrast seen on the CRT picture is a direct result of the interaction of the electron beam with the sample surface topography. The number of secondary electrons produced varies with the angle with which the beam strikes a portion of the surface, and is smallest for a beam perpendicular to the surface (90°). The secondaries produced inside the material have randomly distributed momenta, and if the primary beam enters at a small acute angle, then more of the secondaries will be close enough to the surface to escape before they lose too much energy through phonon interactions. Few secondaries can escape from tiny holes and cracks in the specimen and these appear dark on the CRT. Steps show a very white front surface.

Another capability of interest is called "voltage contrast," which is primarily due to an electric field in the material. Such a field will either enhance or retard the emission of secondary electrons depending on its sign. Thus a p-n junction is easily detected, especially if a reverse bias is applied to it. The secondary emission is enhanced from the p-side (biased -) which appears bright, and retarded from the n-side (biased +) which appears dark. An electrical junction may even be visible with no applied bias presumably because of the smaller work function of the p region.

The variation in brightness across a sample can be displayed as a line across the CRT. The operator sets the primary beam to only sweep one line across the sample. The collected signal, which represents the number of secondaries produced at each point, is then displayed on the screen so that the x-axis is distance across the sample and the y-axis is signal intensity (number of secondaries). By taking two of these "line scans" at the same position across a sample, one with and the other without an applied bias, a good representation of the potential distribution across the diode can be obtained.

3.8 Transmission Electron Miscroscopy

Precipitates and dislocations have been observed in several III-V compounds and have been suggested as potential carrier recombination centers [RHINES, 1972]. Since the precipitates could be smaller than 500 Å in diameter, transmission electron microscopy (TEM) provides the only method for definitive examination. Dislocations are also readily observable in single crystalline materials by TEM because the lattice discontinuity they create leads to localized changes in diffraction conditions and consequent contrast in the transmitted image.

A 10 μm thick Mg-doped GaN layer on a 70 μm thick n-type layer, that had spalled off the sapphire substrate during post-growth cooling, was ultrasonically cut into 3 mm diameter discs for TEM examination. Low angle ion-milling was used to smooth the faceted surface of the i-layer, and then the n-layer and some of the i-layer were removed in a region near the center of the disc during a 65-hour bombardment on the n-layer side with 10 KV Ar ions in a Commonwealth Scientific Ion

Milling Machine. The sample provided an area larger than 500 μm^2 that was thin enough (<3,000 Å) for detailed TEM examination.

3.9 Proton Bombardment and Proton-Assisted Diffusion

It is sometimes possible to greatly increase the diffusion coefficients for dopant ions in semiconductors by bombarding the material in which the diffusion is desired with high-energy protons. These protons knock host atoms into interstitial positions, and the vacancies thus created can serve to allow the diffusion of the dopant species. If thermal processes alone are relied upon to create the necessary vacancies, high diffusion temperatures are required. The non-equilibrium concentration of vacancies created by proton bombardment can allow diffusion at significantly lower temperatures.

Several GaN samples were subjected to the proton bombardment process. Some were coated with a surface layer of Zn in an attempt at Zn diffusion while others were not. Beam currents of from 5 to 25 μA at 60 to 110 KeV were used on the samples held at 600-700°C as well as room temperatures. Bombardment times of up to five hours were used. The results are presented in Section 4.10.

Chapter 4

EXPERIMENTAL RESULTS

Undoped, Zn-doped, and Mg-doped GaN epitaxial layers have been grown and light-emitting diodes have been fabricated. Violet electroluminescence (peaking at 2.9 eV) has been obtained from GaN:Mg devices. In this chapter emission spectra and other diode properties are presented. These experimental results include diode electrical properties such as efficiencies, I-V characteristics, and luminous intensities; temperature dependences of diode properties; growth and surface morphology of the GaN material; the structural origin of the electroluminescence; capacitance measurements; and a structural study of the junction using the scanning electron microscope. In addition, LED's made from proton bombarded GaN are described.

The GaN diode electrical characteristics show rectification, and $I \alpha V^n$ with $2 \leq n \leq 3$ for forward bias (n-region negative). The violet electroluminescence is observed with this polarity of bias, while green light is emitted with reverse bias. The best external quantum efficiency obtained is 0.005% (forward bias). The light is shown to be generated from the cathode end of the insulating GaN region, in the form of discrete microscopic spots. These spots are correlated with the crystal structure.

The surface of the GaN layers is shown to be highly facetted. The insulating (doped) GaN layer is displayed in scanning electron micrographs, and the interface between the doped and undoped GaN regions is shown to follow the facetting of the surface. With an external bias

Preceding page blank

applied, potential gradients are shown to be developed only at the metal-insulator and the insulator-semiconductor interfaces.

4.1 Growth and Fabrication of GaN Light-Emitting Diodes

At the start of this investigation a number of undoped GaN samples were grown in order to establish the proper growth conditions for the particular vapor growth apparatus that was used. These conditions are further discussed in Section 4.5. Attention was then turned to Zn doping of the GaN. The doping was performed during the growth of the samples, because post-growth diffusions are not possible in GaN (Section 2.2). A number of samples were grown with the Zn doping crucible held at various temperatures. No changes in the GaN samples were noted for crucible temperatures up to 425°C, while between 425 and 500°C, an orange coloring of the normally colorless GaN set in. Above 500°C the resistance of the material began to increase noticeably, and samples grown with the Zn crucible held at 600°C, where the Zn vapor pressure is 10 Torr, were insulating with a resistivity > 10^6 Ω-cm.

Layers suitable for diode preparation were then grown. In these cases an undoped layer was deposited on the sapphire followed by a Zn-doped layer. The two layers were each usually grown for 1/2 hour, and the resulting epitaxial growth was in total about 100 microns thick. A deposition zone temperature of 900°C was used for all of the runs.

Point-contact light-emitting diodes were made from these samples. Point-contact devices have been described in Section 3.3. With about 70 volts applied to these contacts, green light peaking at 5150 Å (2.4 eV) was emitted under the non-ohmic wire. Such GaN:Zn diodes have

been reported in the literature [PANKOVE, MILLER, and BERKEYHEISER, 1971] and their growth was not pursued further. They were only prepared here to establish that the equipment was functioning properly.

After the initial work with Zn-doped GaN, major attention was concentrated on Mg doping. The Zn doping portion of the work had established that a Zn source temperature of 600°C, which gives a Zn vapor pressure of 10 Torr, was necessary to allow sufficient Zn to be transported to the growth zone to produce insulating GaN. Therefore when Mg doping was undertaken, the crucible with the Mg source was positioned in the sidearm at a temperature where the Mg vapor pressure was also 10 Torr. The required crucible temperature was 710°C. The GaN grown with the Mg crucible held at this temperature was light yellow in color and insulating. The next step was to grow the two layer (undoped + Mg-doped) structure of the type used for the Zn-doped diodes, and to discover if GaN:Mg light-emitting diodes could be made.

4.2 Emission Spectra of GaN:Mg Light-Emitting Diodes

The undoped + Mg-doped GaN layers are respectively n-type and insulating (i-type) and therefore form an n-i structure. A number of these n-i samples using Mg doping were grown, and point contacts were attached to them. Violet light emission was observed when about 150 volts bias was applied to the diodes. This was the first time that electroluminescence had been observed in Mg-doped GaN. The emission spectrum of a point-contact GaN:Mg LED is shown in Figure 4.1. This emission spectrum peaks at 4250 Å (2.92 eV), in the violet region of the visible spectrum. The light emitted from these point contact diodes was a pin-

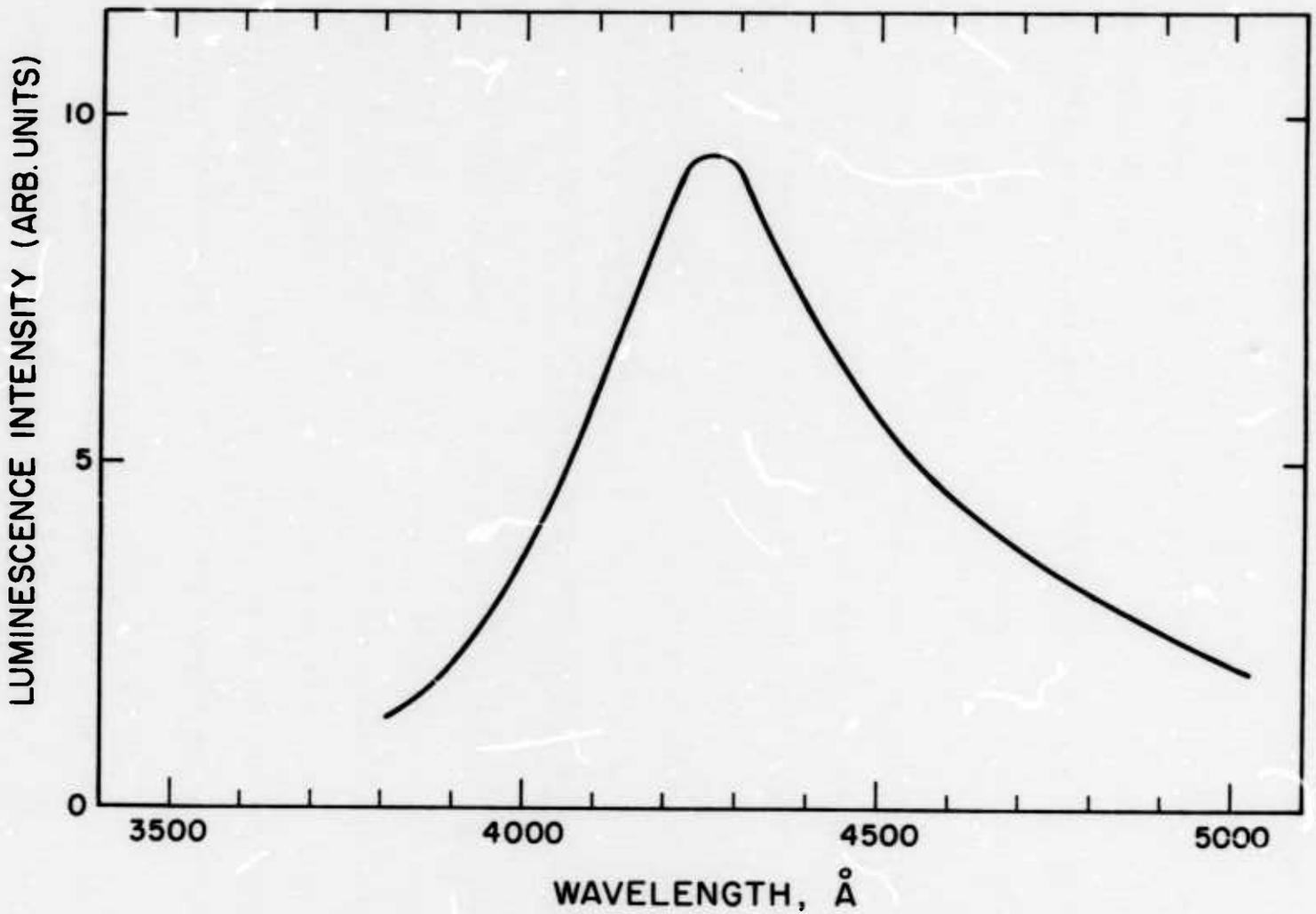

Figure 4.1 Electroluminescence spectrum of point-contact GaN:Mg light-emitting diode (sample #6·8·72).

point source, intense enough to be seen in a well-lit room.

Following the successful growth and fabrication of the first GaN:Mg violet light-emitting diodes, attention was directed towards producing diodes with large-area contacts. The various schemes for fabricating such diodes have been described in Section 3.4. All of these cases require that a metal contact be deposited on top of the doped layer, so that the structure then consists of a metal (m), an insulating (i) region, and a conducting (n) region. Such a structure forms an m-i-n diode. The metal contact was typically 2 mm x 2 mm in area, with the GaN chip just slightly larger in size than this contact. It was much easier to make electrical and optical measurements on the m-i-n than on the point-contact diodes, and no further work was done on point-contacts.

Figure 4.2 displays the spectrum of the electroluminescence from diode #6·28·72, which had its peak at the shortest wavelength found, 4150 Å (2.98 eV). Although it is interesting to note that such short-wavelength electroluminescence is possible from GaN:Mg, this result occurred only in one sample and was not reproducible. The type of light emission spectrum that was seen on a regular basis in diodes made from material from various growth runs is shown in Figure 4.3. The peak occurs at 4325 Å (2.86 eV), in the violet region of the spectrum. This emission peak is 575 Å (400 meV) wide at half-maximum. There is considerabl blue light emitted as well as violet, and since the eye is more sensitive to blue than to violet, the diodes appear deep blue-violet in color to the human observer.

The position of the peak of the emission shifts to shorter wave-

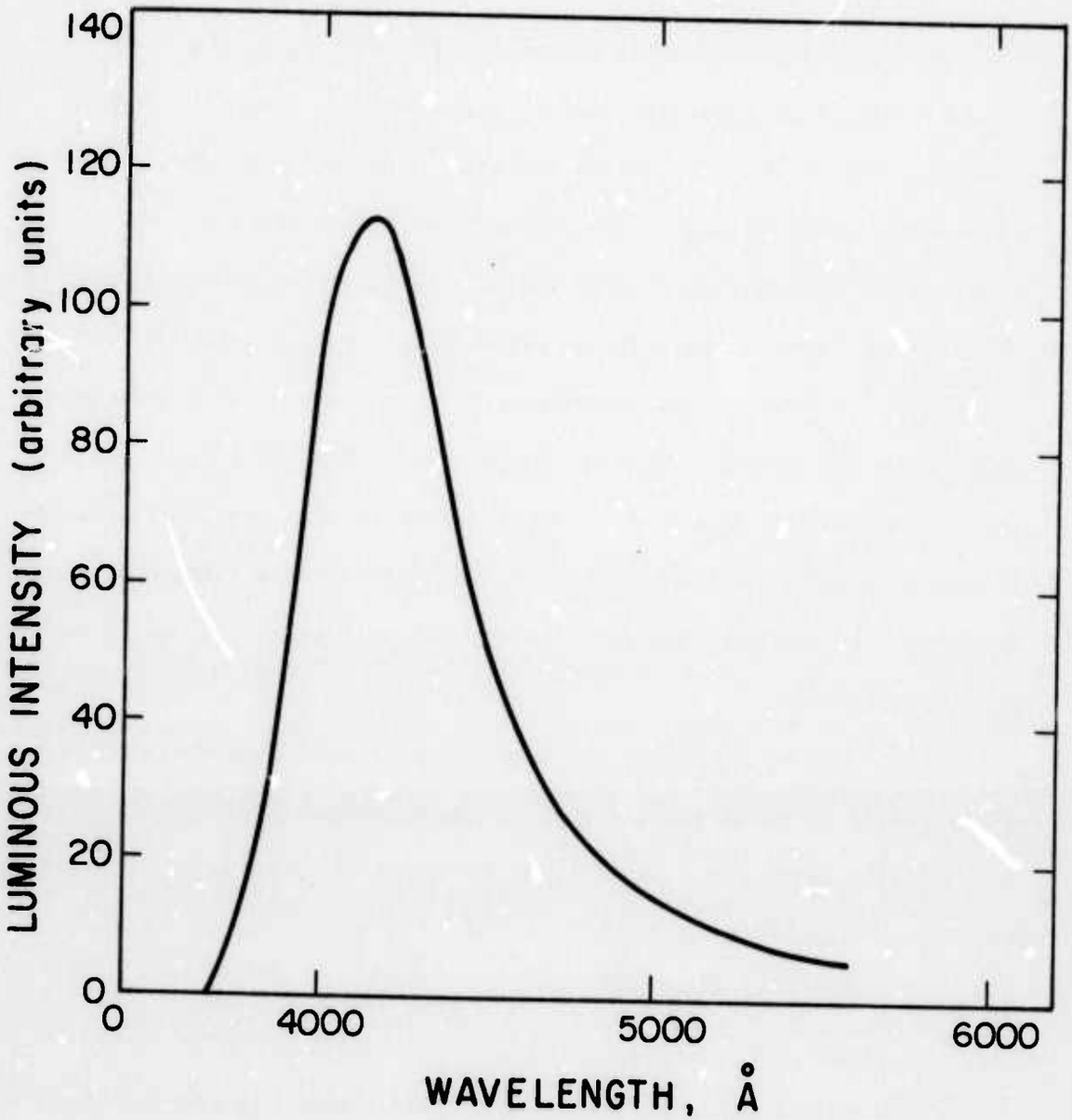

Figure 4.2 Electroluminescence spectrum of GaN:Mg m-i-n diode, sample #6·28·72 (forward bias).

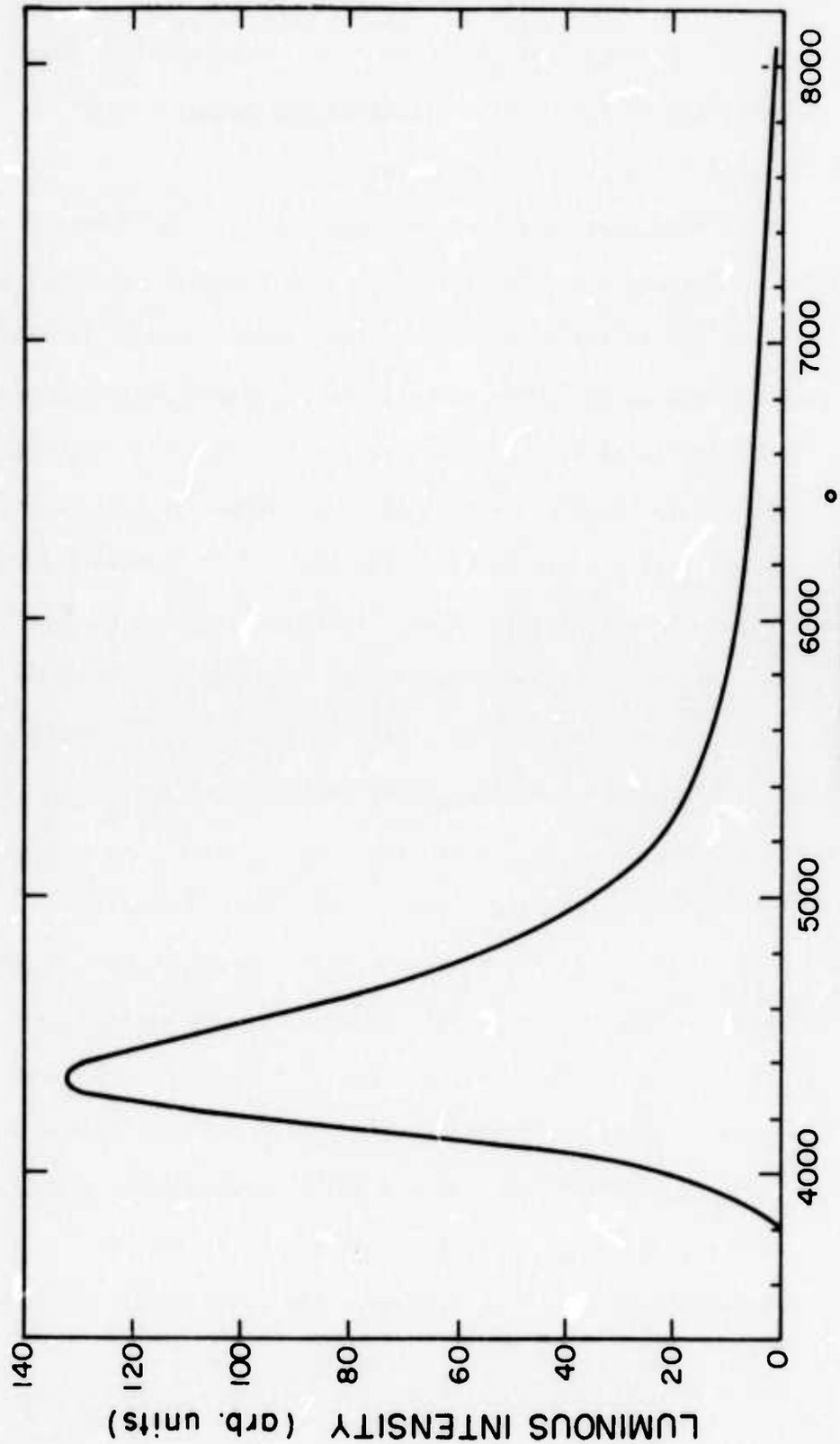

Figure 4.3 Electroluminescence spectrum of typical GaN:Mg m-i-n diode (forward bias).

lengths as the bias voltage applied to the diode is increased. This shift is shown in Figure 4.4. The position of the emission peak reached a constant value at higher voltages.

All of the diodes just described were operated with a "forward bias" applied. "Forward bias" is defined to mean that the metal contact to the insulating region (or else the non-ohmic point-contact) is biased positive with respect to the n-GaN contact (or the ohmic point-contact). However, light emission is often but not always observed with "reverse bias." The diodes show rectification, and it is necessary to apply much larger voltages to obtain appreciable current flow (and light-emission) with reverse bias than with forward bias. In many cases the diodes "punch-through" and burn out (become short-circuits) as the voltage is increased in an attempt to observe reverse-bias electroluminescence. However, some diodes have successfully been operated in reverse bias, and a spectrum is shown in Figure 4.5. The peak wavelength is at 4820 Å (2.57 eV), which is light-blue in color. Another less intense peak occurs at 6000 Å (2.07 eV) in the yellow-orange. These are not the same emission peaks as the one seen with forward bias. There is also considerable green and yellow light emitted, and the diodes appear green in reverse bias due to the eye's sensitivity. With the use of a proper power supply arrangement it is possible to switch such a diode alternately from violet to green by changing polarity. This may have practical applications in signaling systems. The reverse-bias electroluminescence also exhibits a shift of the emission peak to shorter wavelengths as the magnitude of the applied voltage is increased. This is shown in Figure 4.6.

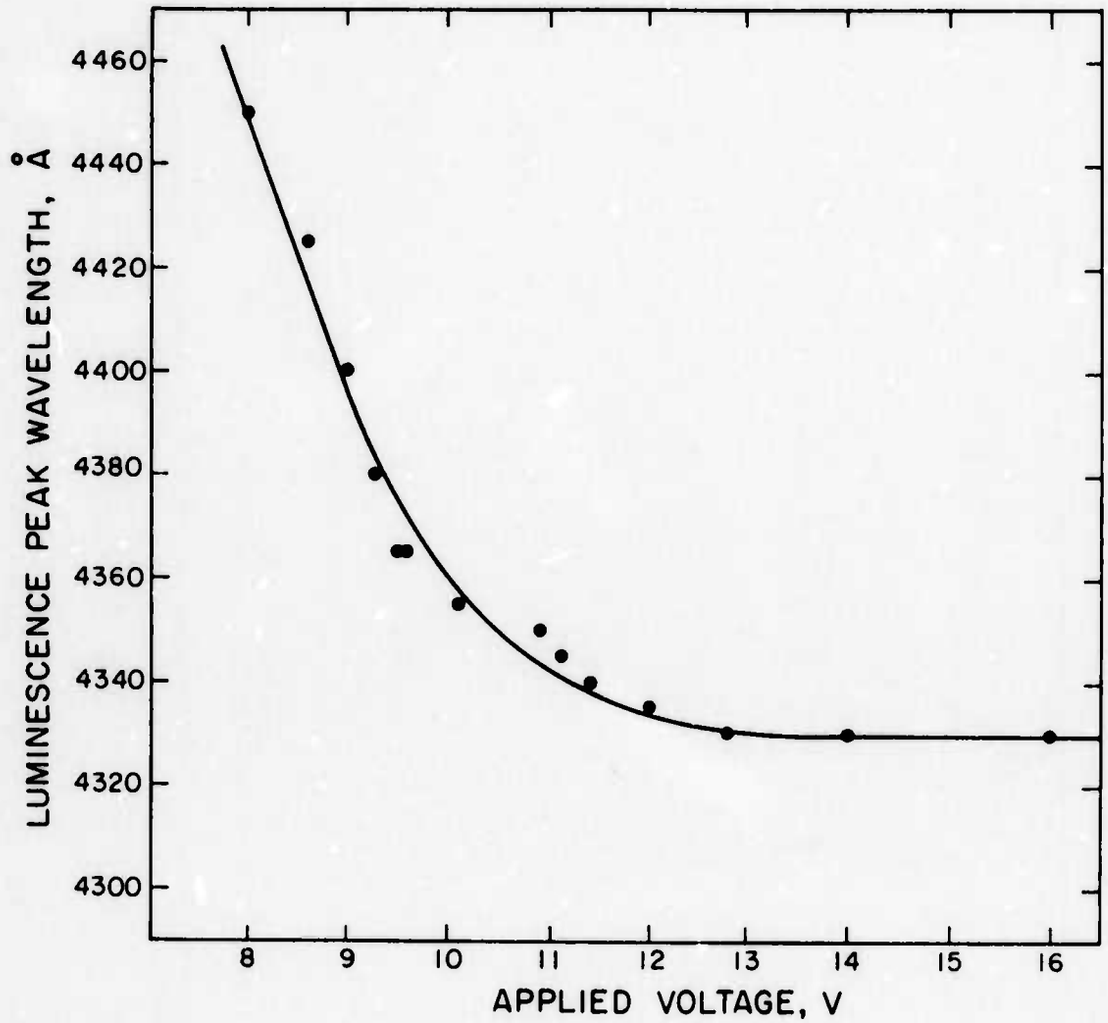

Figure 4.4 Dependence of the peak wavelength of the emission on applied voltage (forward bias).

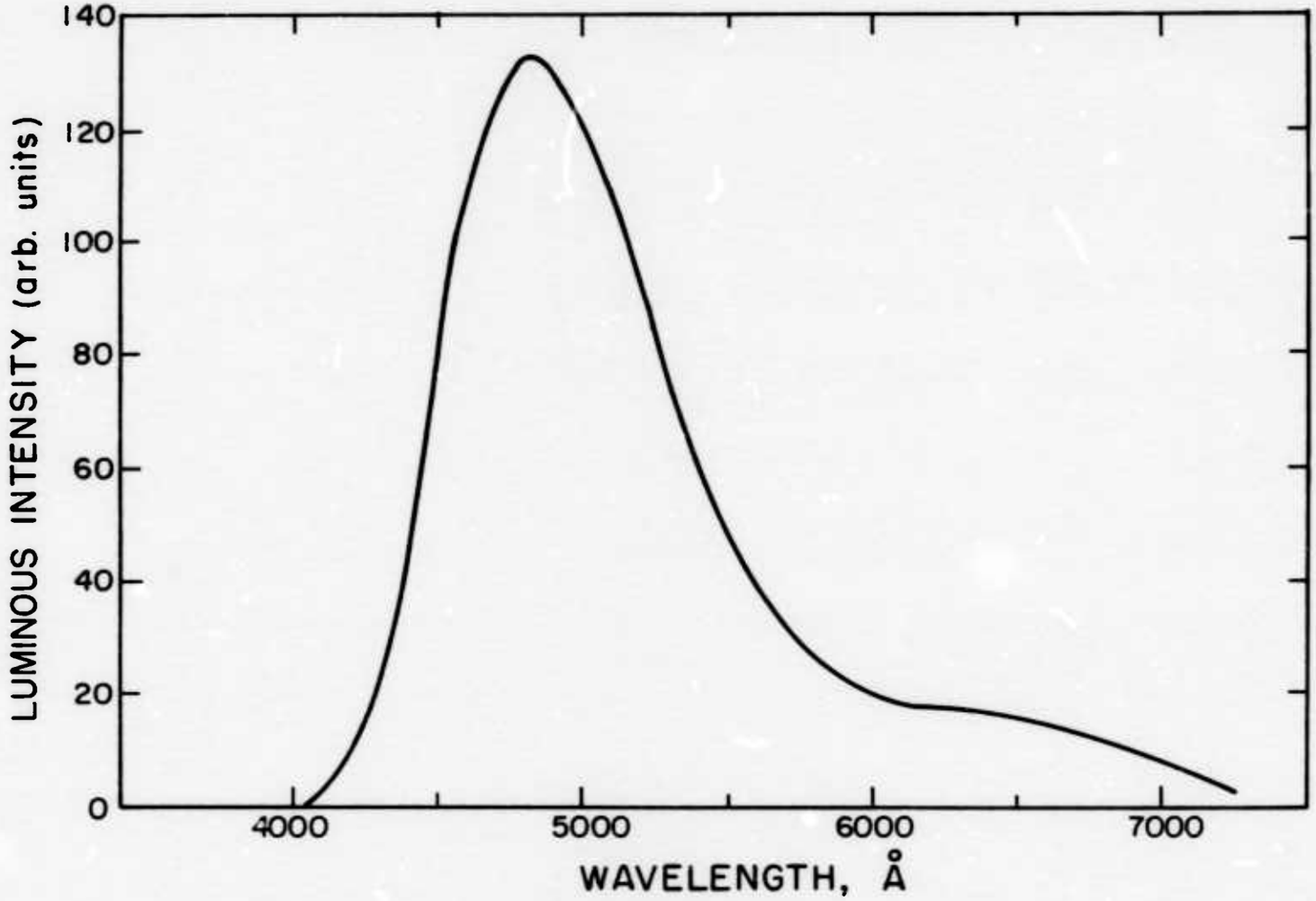

Figure 4.5 Typical reverse-bias electroluminescence spectrum for GaN:Mg m-i-n diodes.

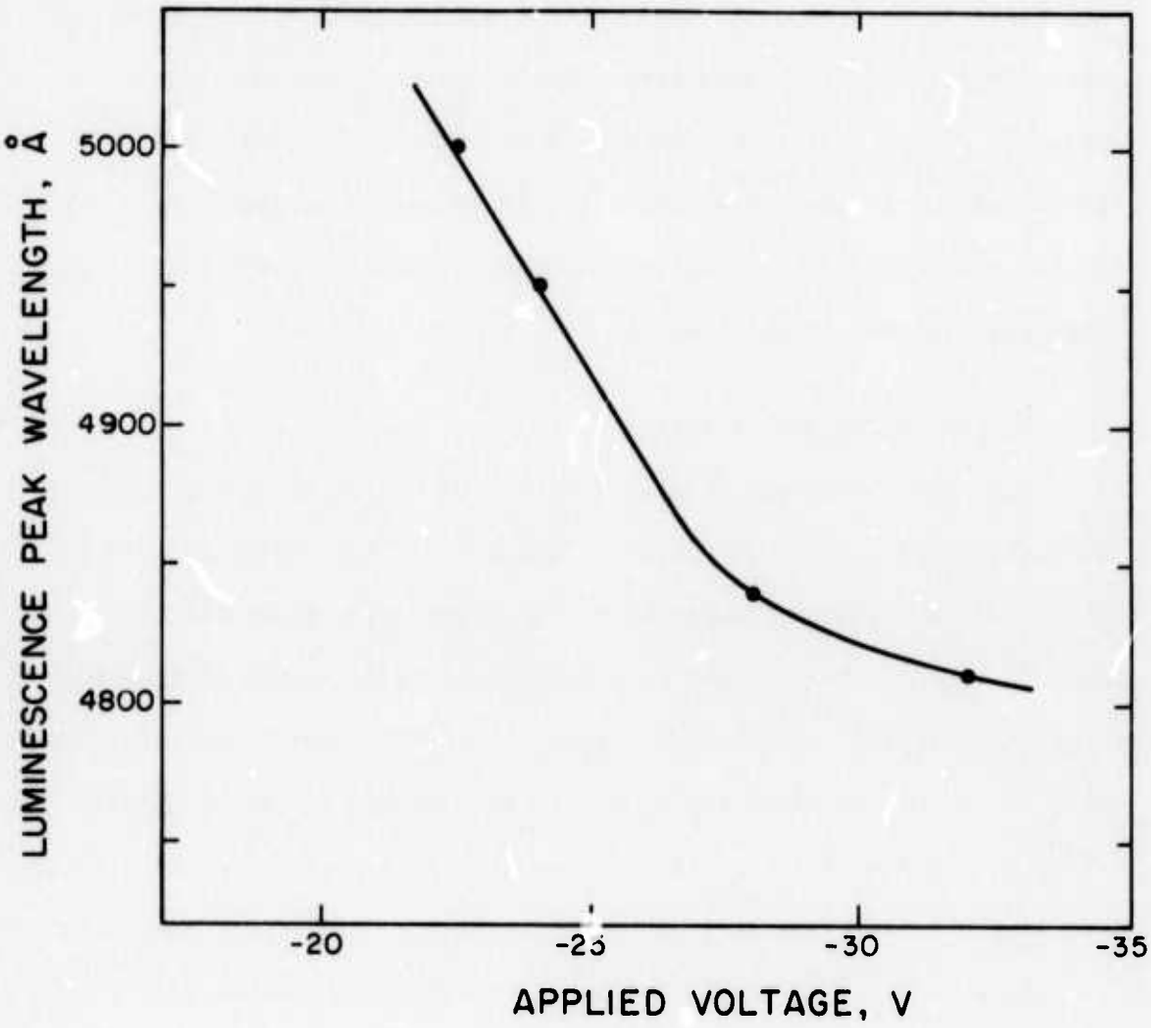

Figure 4.6 Dependence of the peak wavelength of the emission on applied voltage (reverse bias).

In order to better understand these light-emitting diodes, the photoluminescence of Mg-doped GaN was studied. The set-up used has been described in Section 3.5. The photoluminescence was excited with a high-pressure mercury vapor lamp. The emission spectrum obtained is shown in Figure 4.7. The peak occurs at 4250 Å (2.92 eV) which indicates that Mg forms a level about 0.5 eV above the valence band in GaN. Notice that the photoluminescence spectrum closely resembles the forward-bias electroluminescence spectra.

4.3 Electrical Characteristics

The light power output as a function of electrical power input for a representative diode is shown in Figure 4.8. The measurement technique was described in Section 3.6. A forward-bias power efficiency of about 0.001% can be obtained at a typical operating power (0.1 watt). Since the external quantum efficiency is related to the power efficiency by a factor of $qV/h\nu$ (Section 1.3), it is a simple matter to obtain external quantum efficiencies from Figure 4.8, and the external quantum efficiency as a function of applied voltage is plotted in Figure 4.9. A maximum external quantum efficiency of 0.005% has been found for forward-bias electroluminescence. Reverse-bias electroluminescence is about an order of magnitude less efficient.

The typical shape of diode I-V characteristics, as measured on the Tektronix 575 Curve Tracer, is shown in Figure 4.10. It is apparent that rectification does occur with these diodes. The current drawn by a particular sample is dependent on the contact area, but since the emitted light shows a very nonuniform pattern, as will be described in

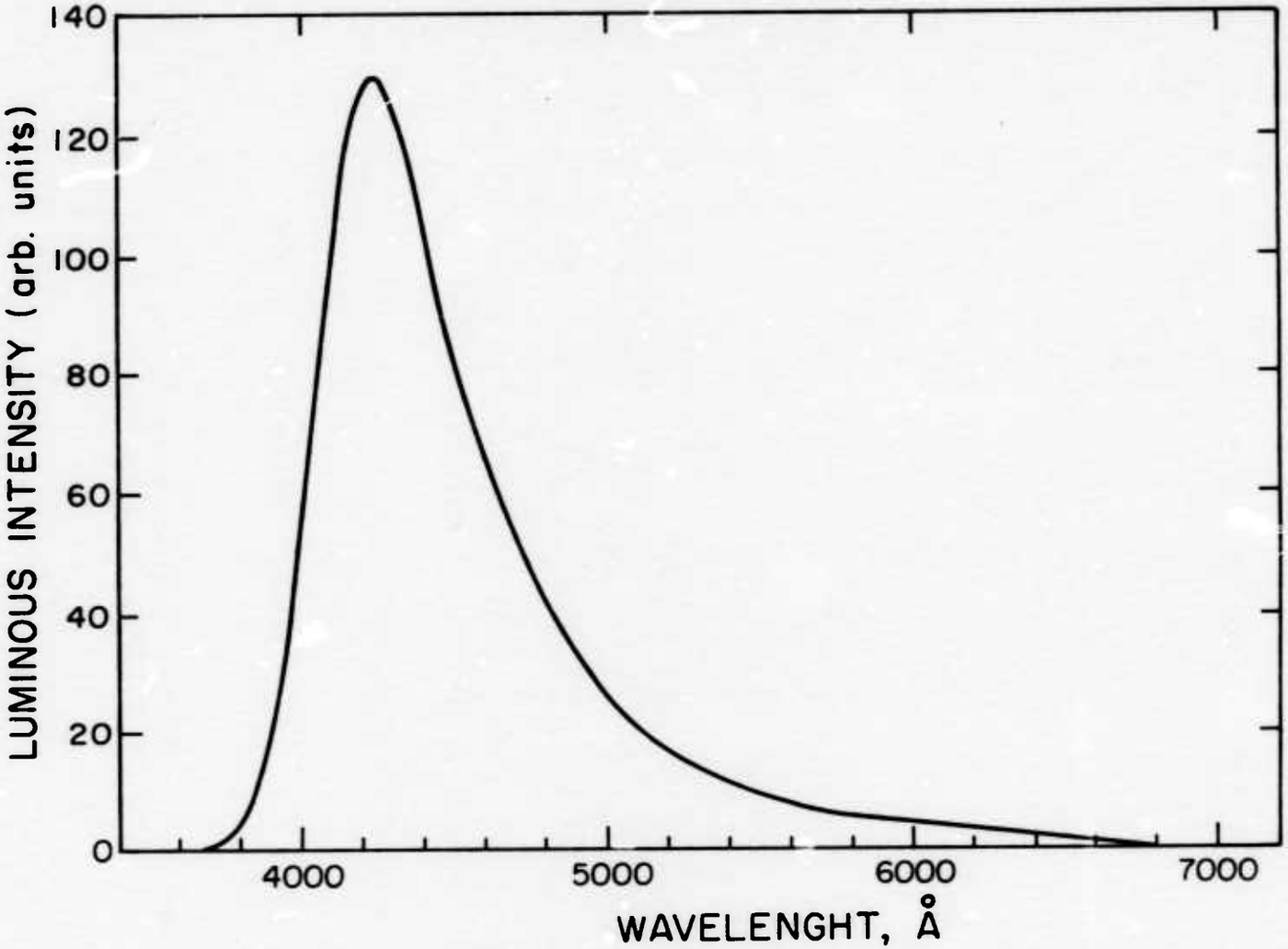

Figure 4.7 Photoluminescence spectrum of Mg-doped GaN.

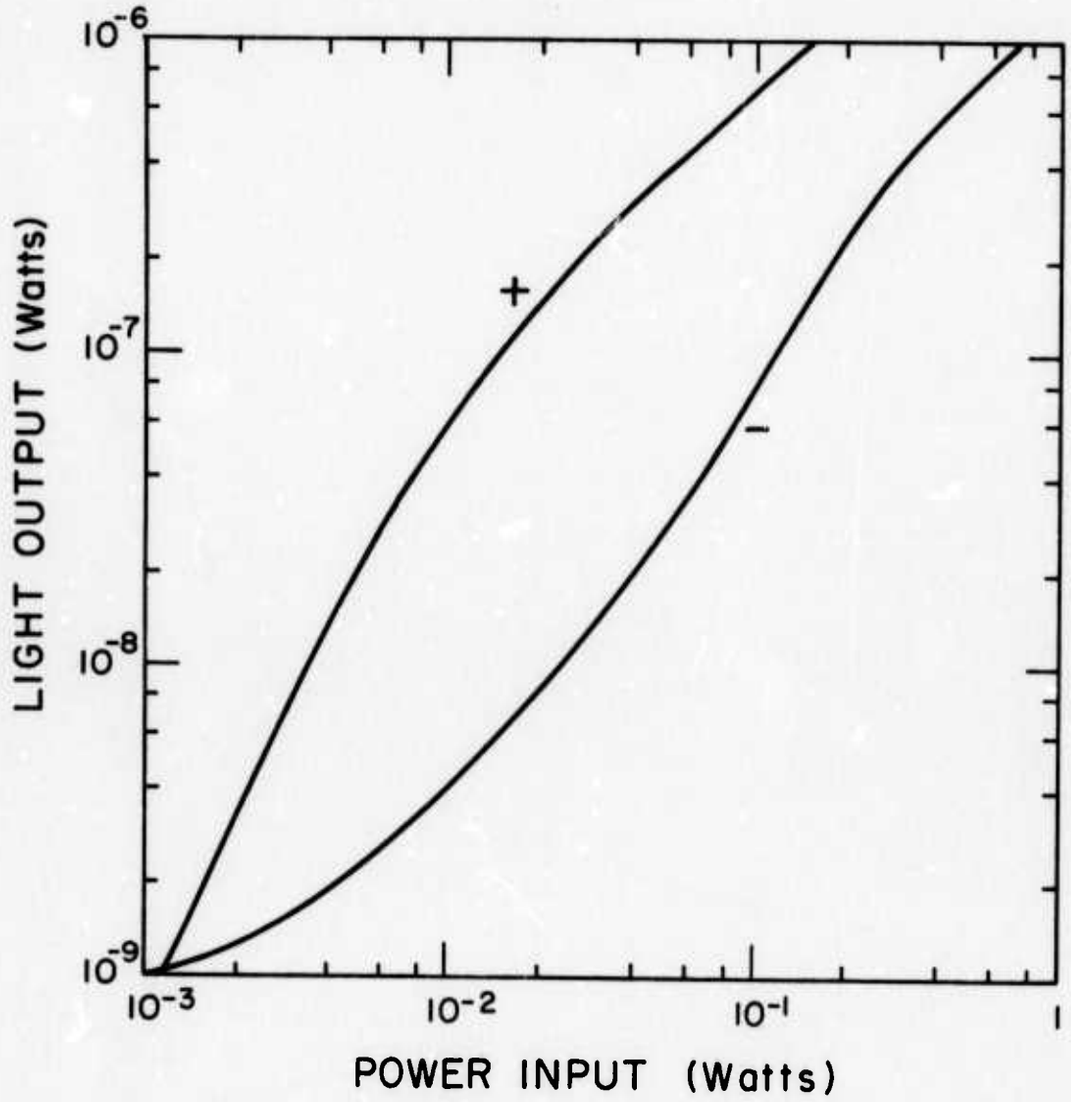

Figure 4.8 Dependence of light power output on electrical power input for GaN:Mg light-emitting diodes.

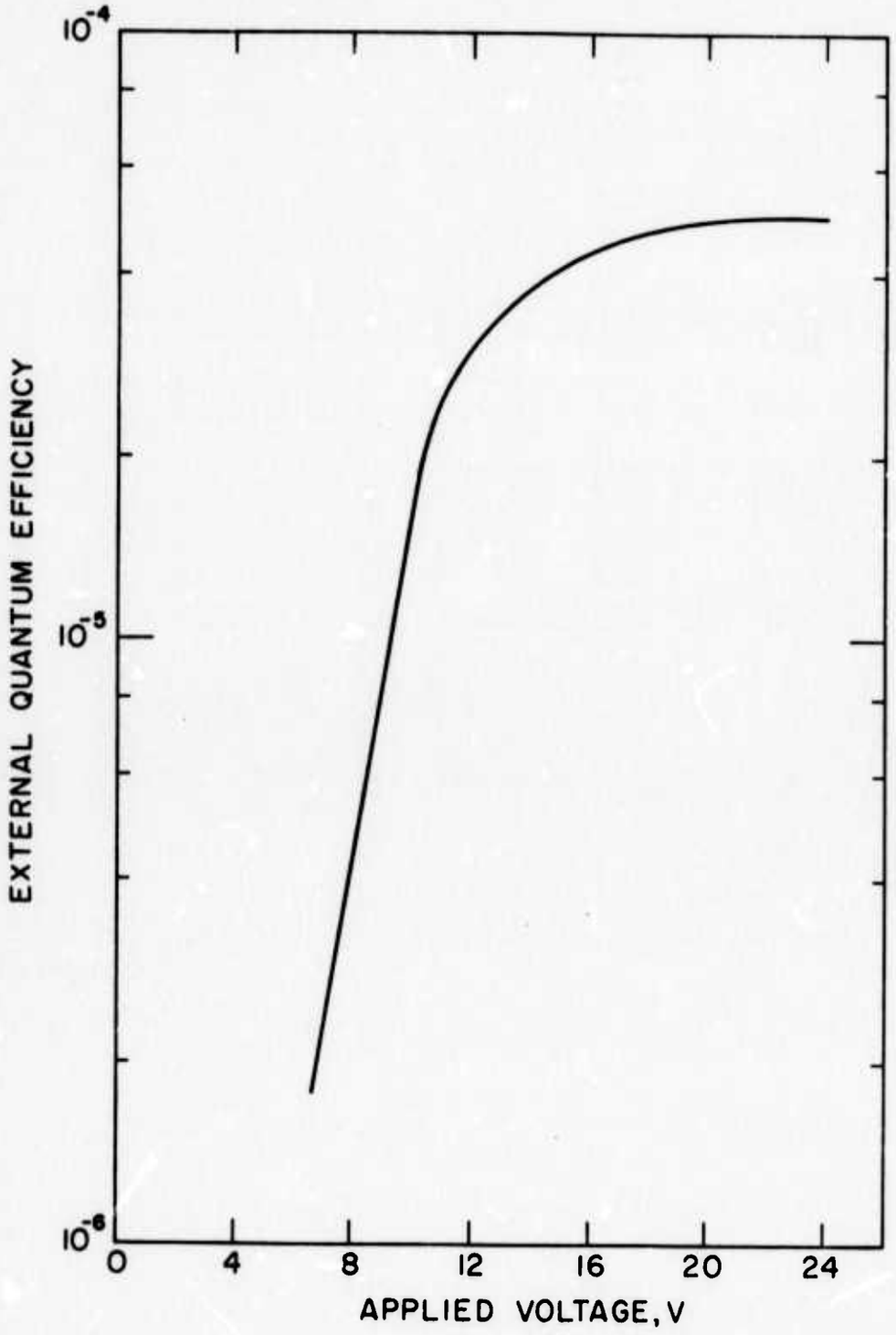

Figure 4.9 External quantum efficiency of GaN:Mg light-emitting diode.

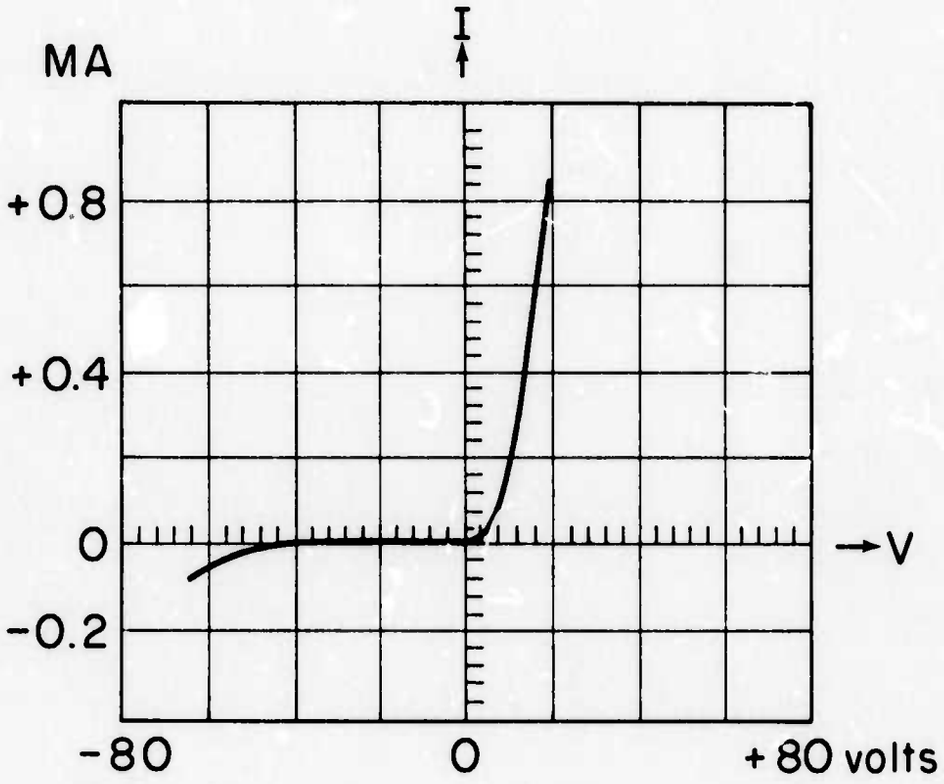

Figure 4.10 Typical diode I-V characteristic.

Section 4.6, it is not possible to ascertain the current density. A log-log plot of current-voltage characteristics is presented in Figure 4.11. With forward bias (+), $I \alpha V^3$ when about 20 volts is applied. This is the voltage necessary for light emission from a diode to be easily visible in a well-lit room. At lower biases the exponent n in the power law $I \alpha V^n$ becomes larger than 3. Numerous experiments have shown that this exponent is not always 3 in the range of 10 to 30 volts for various Mg-doped diodes, and it in fact varies between 2.0 and 3.0 for different samples. In Zn-doped diodes, a value of n = 2 has been reported [PANKOVE, MILLER, and BERKEYHEISER, 1971].

The luminous intensity L (at the peak wavelength) is plotted as a function of applied voltage in Figure 4.12. L is seen to increase superlinearly with V.

4.4 Temperature Dependence of Luminescence and Electrical Characteristics

The electrical properties of the diodes were measured as a function of temperature. Only diodes bonded with a solid metal contact to a header proved useful for these measurements. The major problem encountered in all cases was mechanical separation of the contacts from the device due to differences in thermal expansion coefficients. If the diodes were rapidly immersed in liquid nitrogen, they fractured for the same reason. Thus in all cases the LED's were slowly cooled as described in Section 3.6, and measurements were taken at various temperatures down to the vicinity of, but not including, liquid nitrogen temperature. An example of the current and luminous intensity which were measured at a constant applied voltage and various temper-

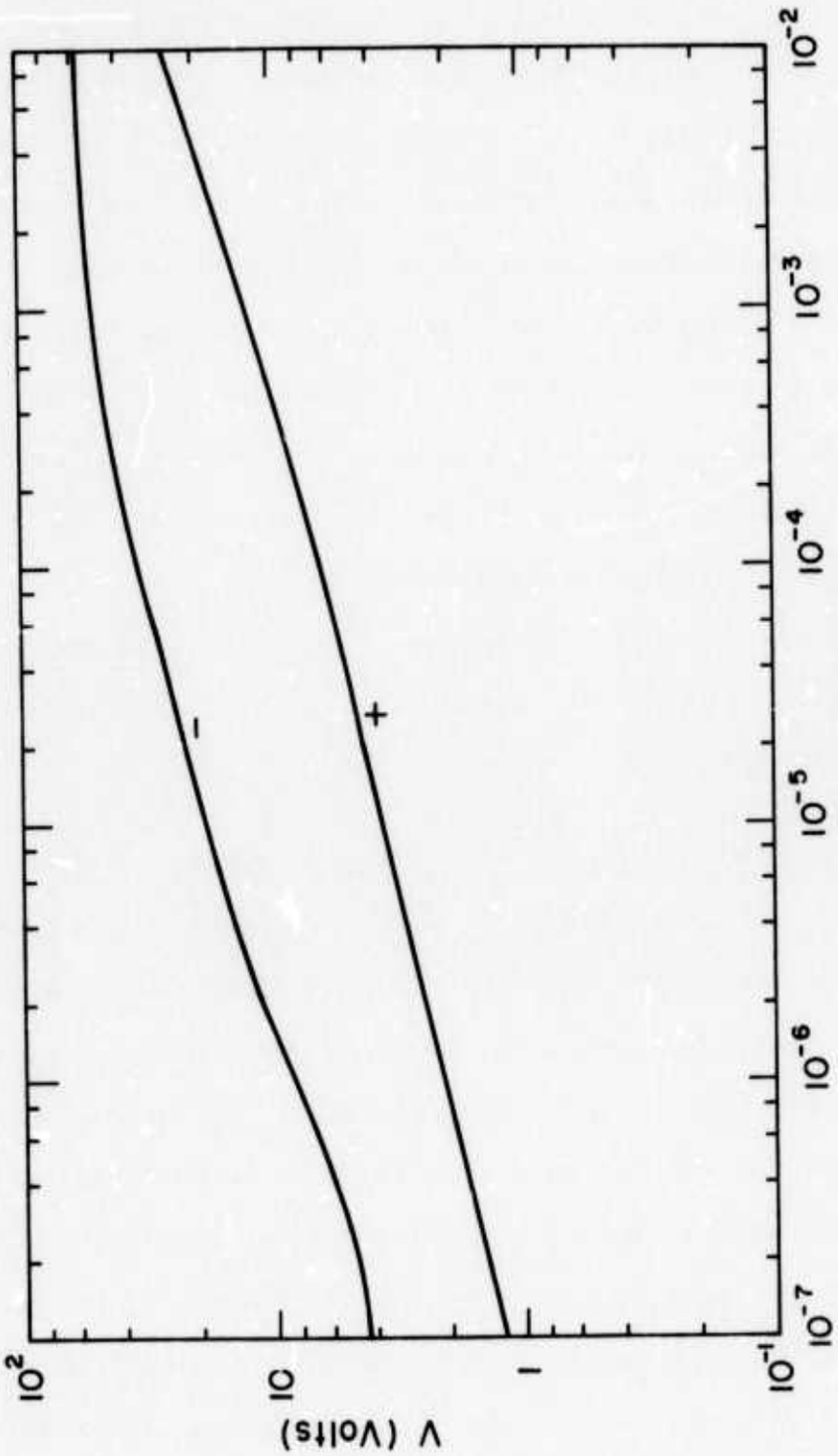

Figure 4.11 Log-log plot of diode I-V characteristic (sample #7·7·72).

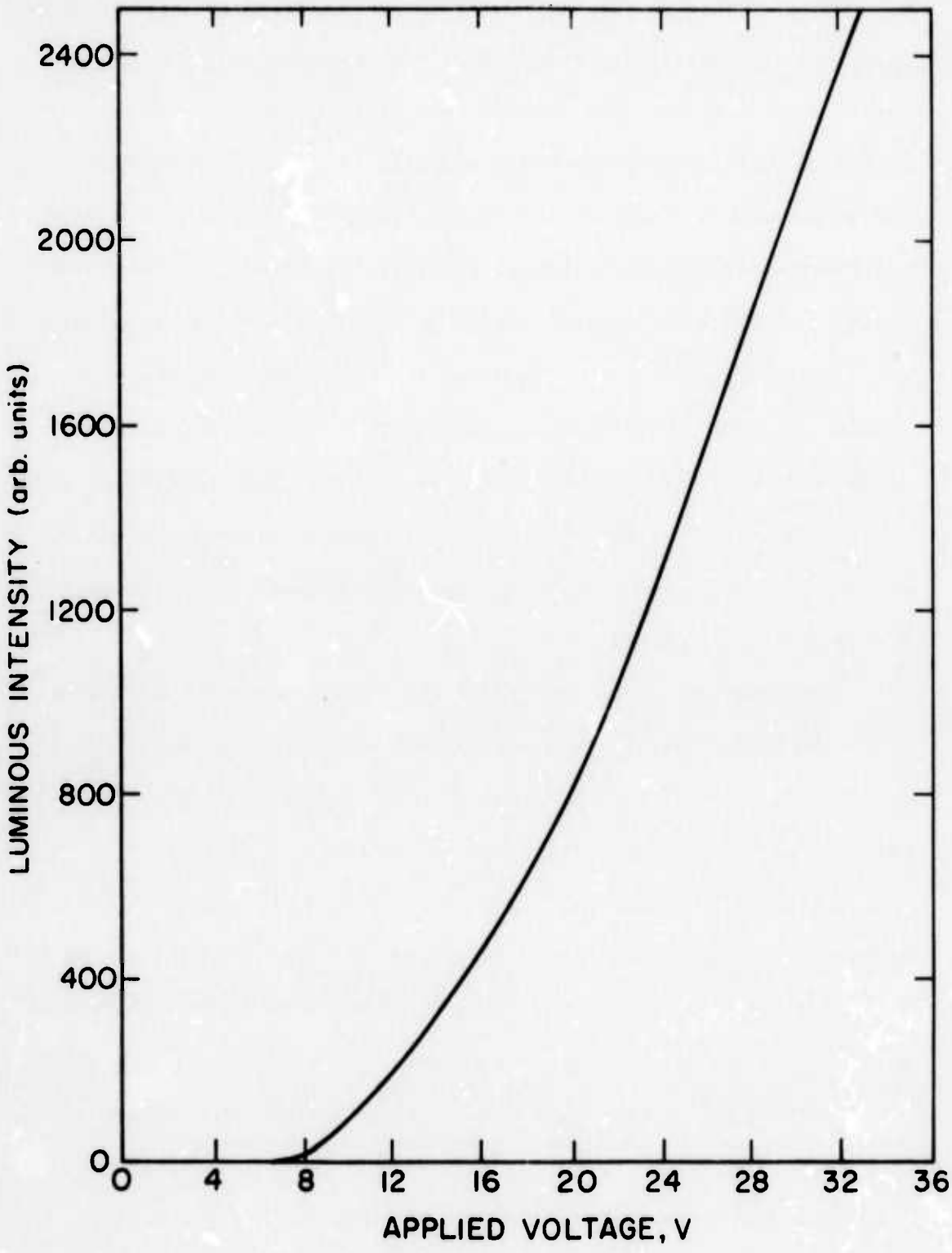

Figure 4.12 Luminous intensity as a function of applied voltage.

temperatures for a particular LED is shown in Figure 4.13. The current decreases with decreasing temperature corresponding to an activation energy of 0.13 eV for this sample. The luminous intensity first increases with lower temperatures and then decreases with an activation energy of 0.06 eV. Thus the diode efficiency increases by more than two orders of magnitude in going from room temperature to about 125°K, yielding an external quantum efficiency of about 1% at low temperatures.

All other diodes measured showed similar characteristics. No changes in these characteristics were found in samples measured at elevated temperatures, up to 450°K. In all cases the activiation energy for the temperature dependence of the current was between 0.1 and 0.2 eV, and the activation energy for the luminous intensity decrease was always smaller, typically 0.05 eV.

The temperature dependence of I and L for another diode is shown in Figure 4.14. Here the characteristics were taken for a number of constant applied voltages between 10 and 40 volts. The activation energies are independent of the applied voltage.

There is little change in the shape or peak wavelength of the electroluminescence in going to lower temperatures. A shift of the peak to higher energy by 0.05 eV has been observed between room temperature and 110°K.

No shift with temperature was found for the GaN:Mg photoluminescence spectrum. However, the intensity of the photoluminescence increased with decreasing temperature and then reached a saturation value at low temperatures, as shown in Figure 4.15. The temperature-dependent region of photoluminescent intensity had an activation energy

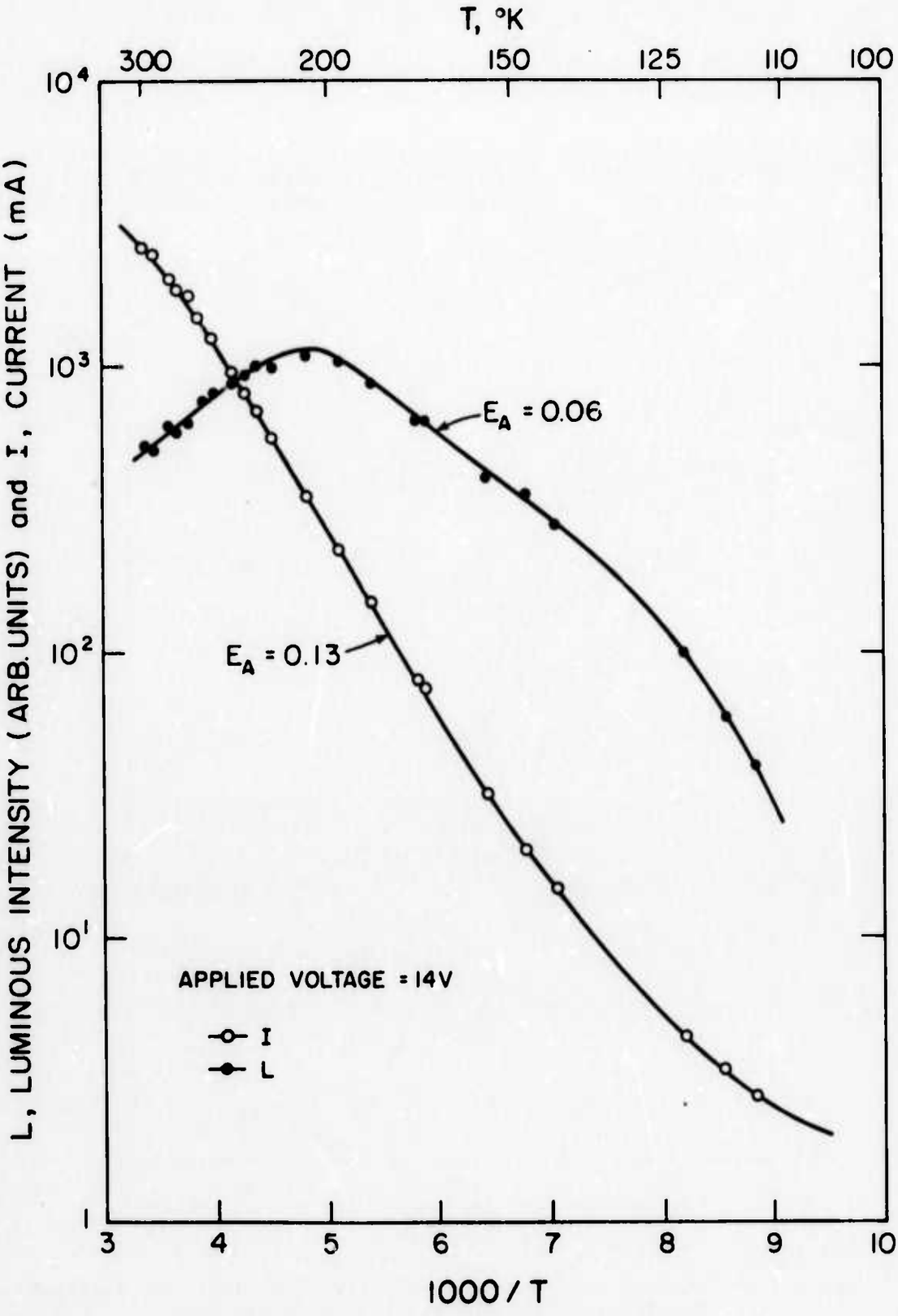

Figure 4.13 Temperature dependencies of diode current and luminous intensity at constant voltage.

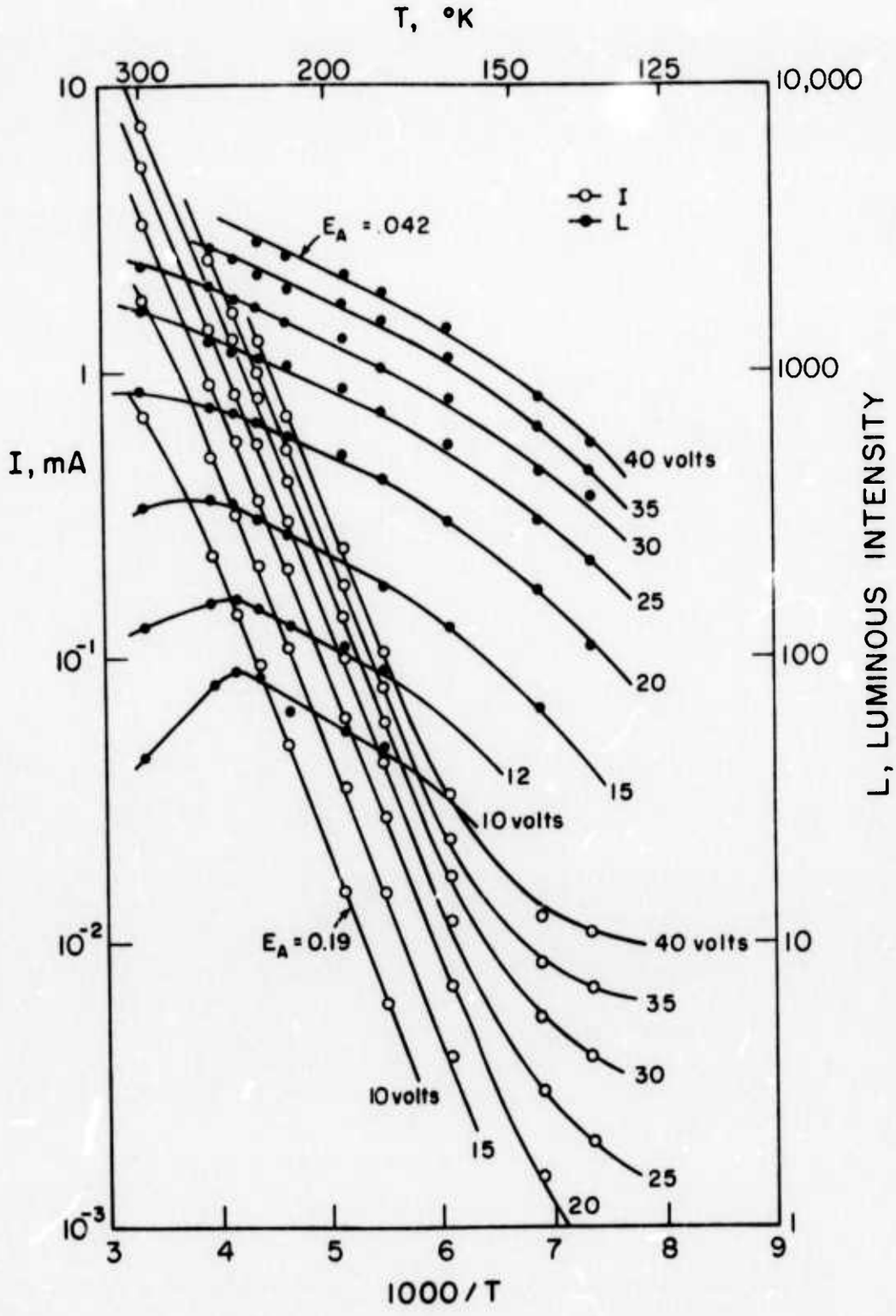

Figure 4.14 Temperature dependencies of diode current and luminous intensity at various constant voltages.

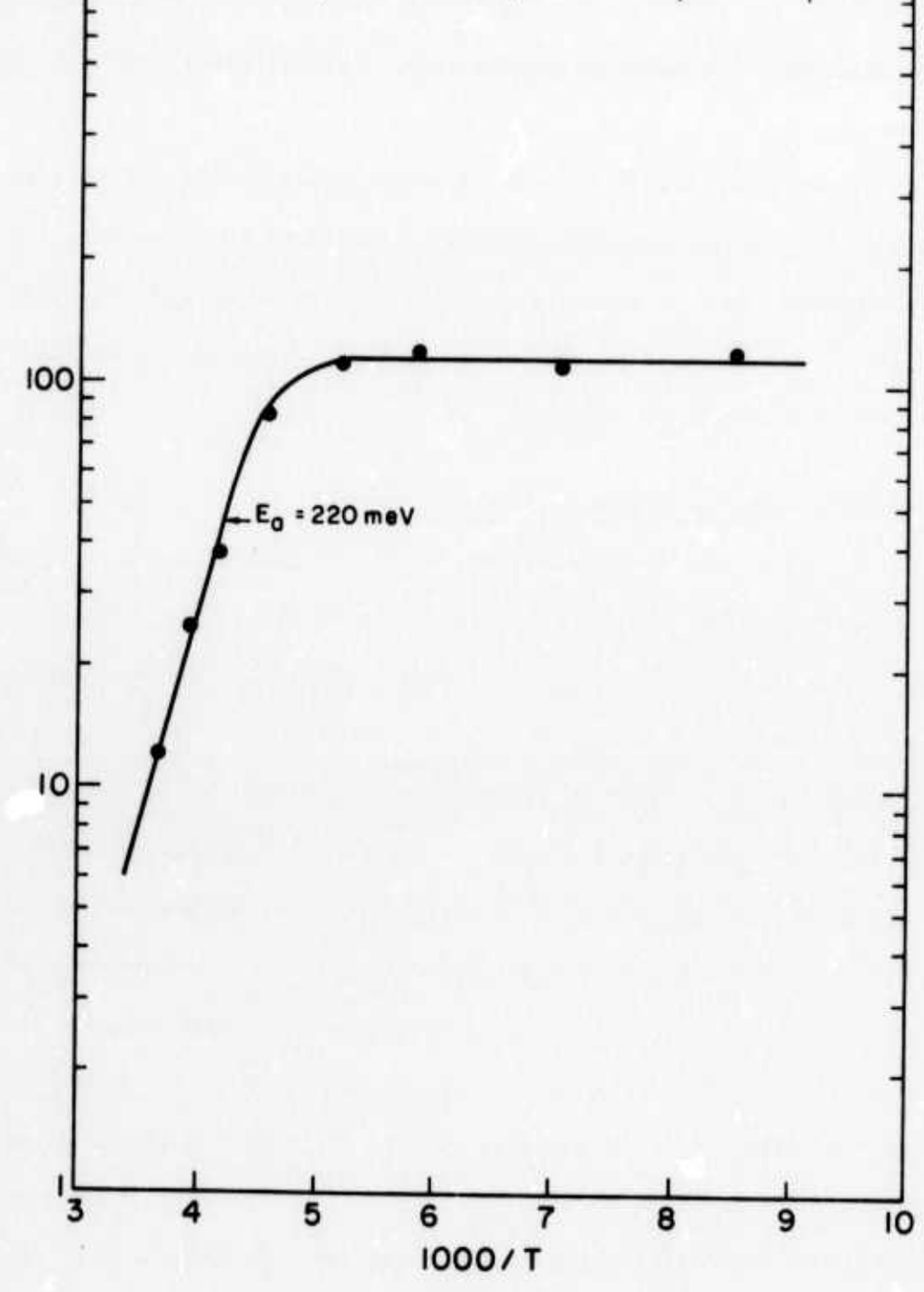

Figure 4.15 Temperature dependence of photoluminescence intensity.

of 220 meV. This behavior is typical of most materials [LEVERENZ, 1949]. The knee in the curve corresponds to the temperature for the onset of nonradiative recombinations. This temperature is about 200°K for Mg-doped GaN.

Measurements of the reverse-bias electrical characteristics as a function of temperature gave results very similar to those obtained with forward bias. Activation energies for the dependence of diode current on temperature (at constant voltage) were found to be about 0.2 eV, independent of voltage.

4.5 Growth and Surface Morphology of GaN

The growth and surface morphology of the GaN epitaxial films were studied in order to obtain a better understanding of the processes which control the operation of the LED devices. Gallium nitride crystallizes with the hexagonal wurtzite structure. It was found that a large number of GaN nuclei are formed on the sapphire substrate during the chemical vapor deposition (open-flow vapor phase growth) process. This is reasonable since the deposition temperature used was several hundred degrees below the expected equilibrium temperature for the chemical reaction. These nuclei grow to form separate hexagonal islands of GaN, and an example of these islands is shown in Figure 4.16. This photograph was taken at 5000X magnification in the scanning electron microscope. The deposition occurred on an (0001)-oriented sapphire substrate, and the GaN islands have the same orientation. Notice that the individual islands have the form of hexagonal columns, with the respective sides of each column parallel to those of all the other columns. Given

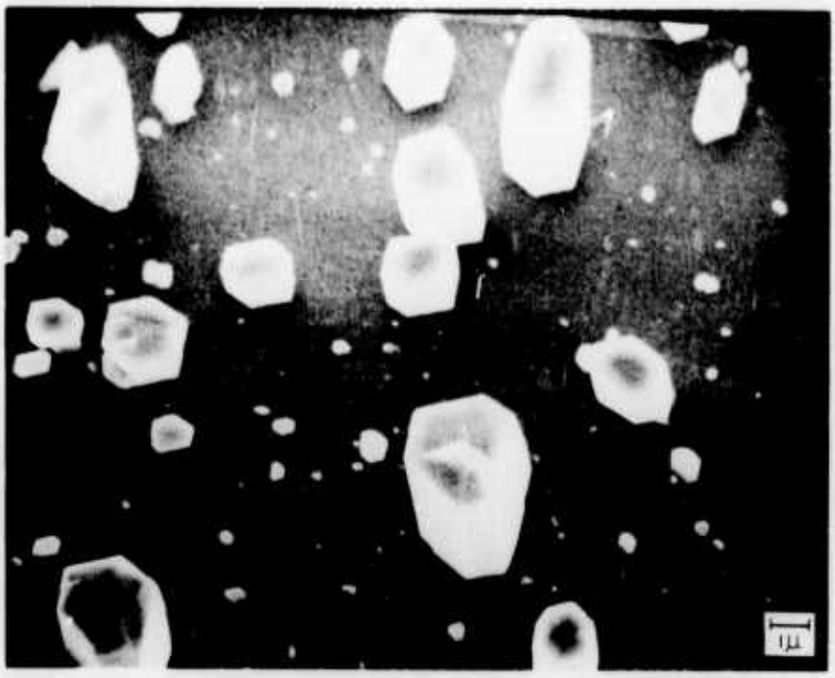

Figure 4.16 Hexagonal islands of GaN nucleated on (0001)-sapphire.

sufficient time, all of these islands coalesce. This is clearly shown in Figure 4.17, where separate GaN islands on the (0001)-oriented sapphire substrate are still visible on the right side of the photograph (2000X magnification) while a continuous film has formed on the left side. However, the original island pattern is still visible in the coalesced area, which exhibits a facetted surface. This suggests that the various islands may not be exactly aligned.

Two examples of the types of GaN surface which occur for films grown on $(1\bar{1}02)$-oriented sapphire substrates are shown in Figures 4.18 and 4.19. The type of facetting shown in the scanning electron micrograph of Figure 4.19 is more commonly found. In either case the c-axis of the GaN is not perpendicular to the substrate as it was for the (0001)-oriented material. The GaN was found to have a $(10\bar{1}3)$ orientation when grown on $(1\bar{1}02)$-oriented sapphire, and the angle between the $(10\bar{1}3)$ and (0001) planes in GaN ($c/a = 1.62$) is 32°, so the minimum angle between the c-axis and the surface plane of the sapphire substrate is 58°.

The size of the facets is directly related to the position of the substrate in the growth tube. The size decreases with distance downstream from the ammonia inlet tube, as shown in Figure 4.19A. Therefore the number of islands nucleated must increase with distance downstream. It may simply be that the reactants are depleted as the gases flow downstream and the growth rate of the nucleated islands decreases, allowing time for additional islands to nucleate before the substrate surface is covered over, or else there may be a small temperature gradient in the deposition zone. The thickness of the deposit shows a

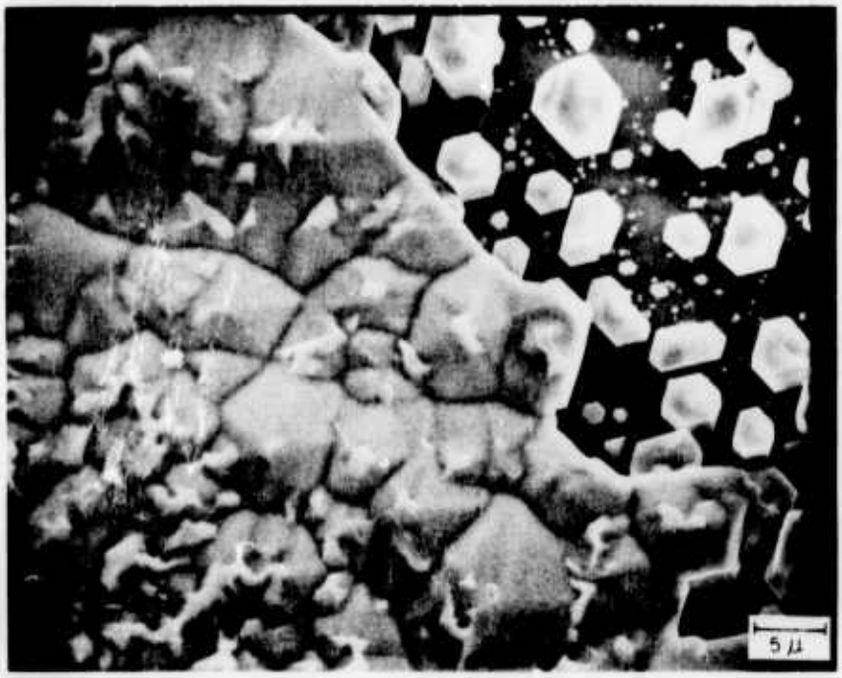

Figure 4.17 Hexagonal islands of GaN, which have coalesced to form a continuous film on the left side of the picture. (0001)-orientation.

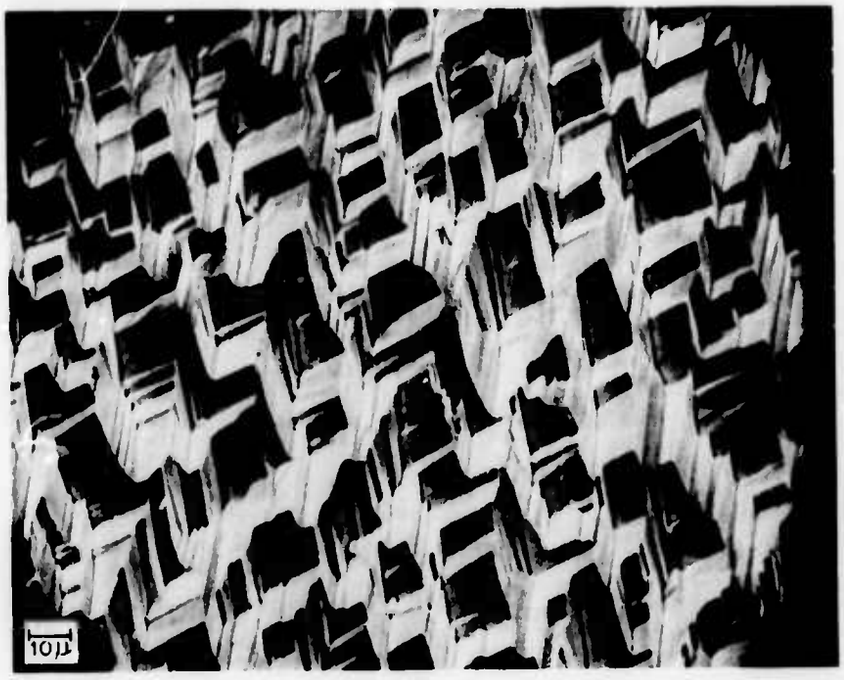

Figure 4.18 Surface of gallium nitride sample #5·19·62, grown on $(1\bar{1}02)$-sapphire.

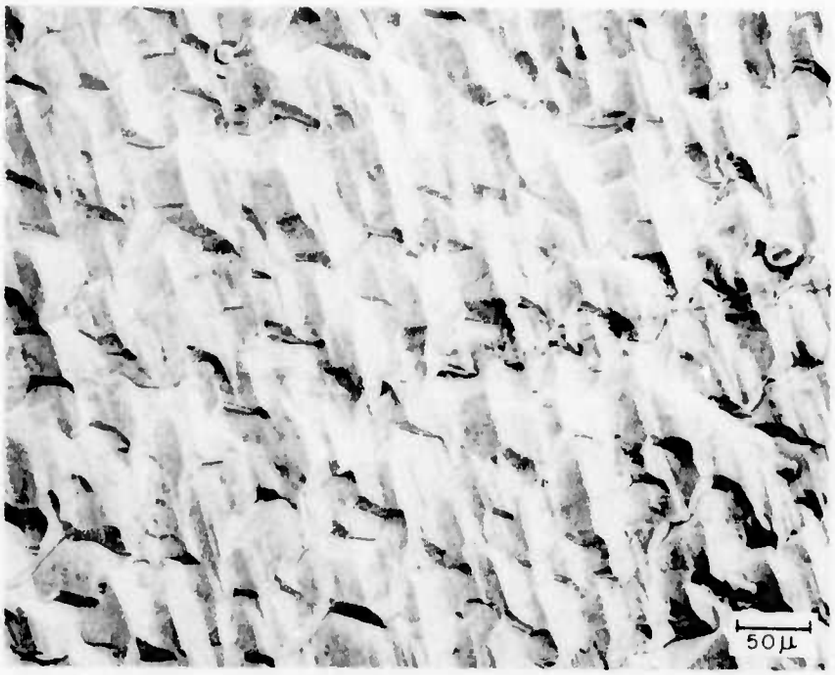

Figure 4.19 Typical facetted surface developed in GaN grown on $(1\bar{1}02)$-sapphire.

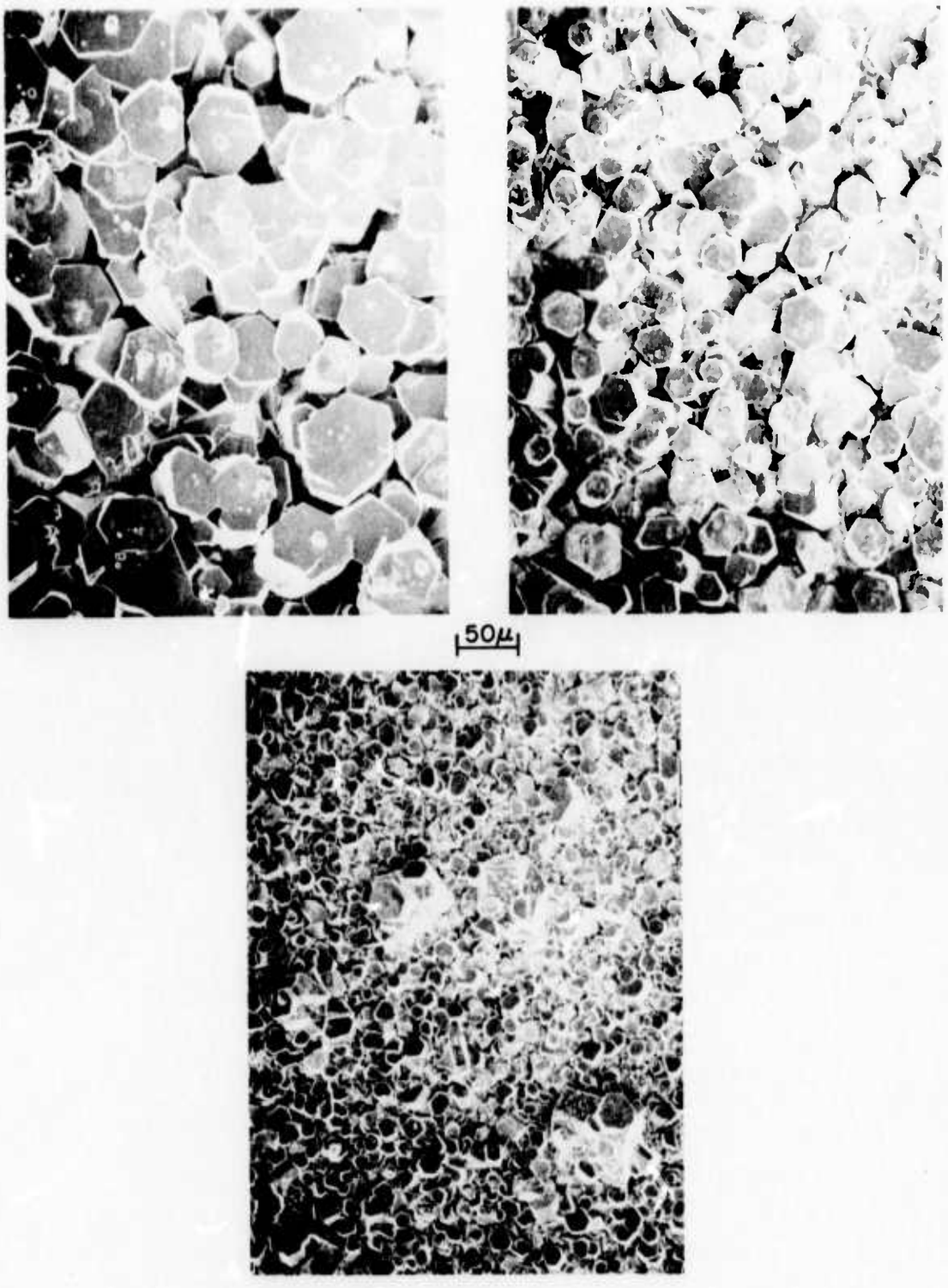

Figure 4.19A Gallium nitride films on quartz substrates, showing crystallite size at various distances downstream from the ammonia inlet: (a) 2"; (b) 3"; (c) 4". Magnification 200X.

marked decrease with distance downstream. Diodes were grown at various positions in the deposition zone at the beginning of this study, and it was found that the best (brightest) ones were grown at a position about 7.5" inside the deposition furnace. Many problems with reproducibility of highly luminescent material were encountered and remain unresolved.

A Laue pattern for one of the typical facetted GaN films grown on $(1\bar{1}02)$ sapphire is shown in Figure 4.20. The pattern shows only spots, which are indicative of a single crystal. There are no rings which would indicate a polycrystalline sample. Therefore, even though many nuclei are involved in the formation of a GaN film, the result is a single crystal. It must be observed that the Laue pattern spots are not pin-points but instead show a slight smearing, characteristic of slight crystalline misalignment. There are probably subgrain boundaries between the grown-together islands.

4.6 Pattern of Light Emission

It has now been shown that GaN films on sapphire substrates consist of microscopic islands which have grown together to form a continuous, single-crystalline epitaxial layer with a facetted surface. The microscopic study was extended to actual operating LED's, in order to discover how the light emission is correlated with the structure of the crystals.

A device is shown externally illuminated and magnified 28X in the optical microscope in Figure 4.21. This chip of GaN had spalled off the sapphire substrate. A small number of GaN layers spalled off the

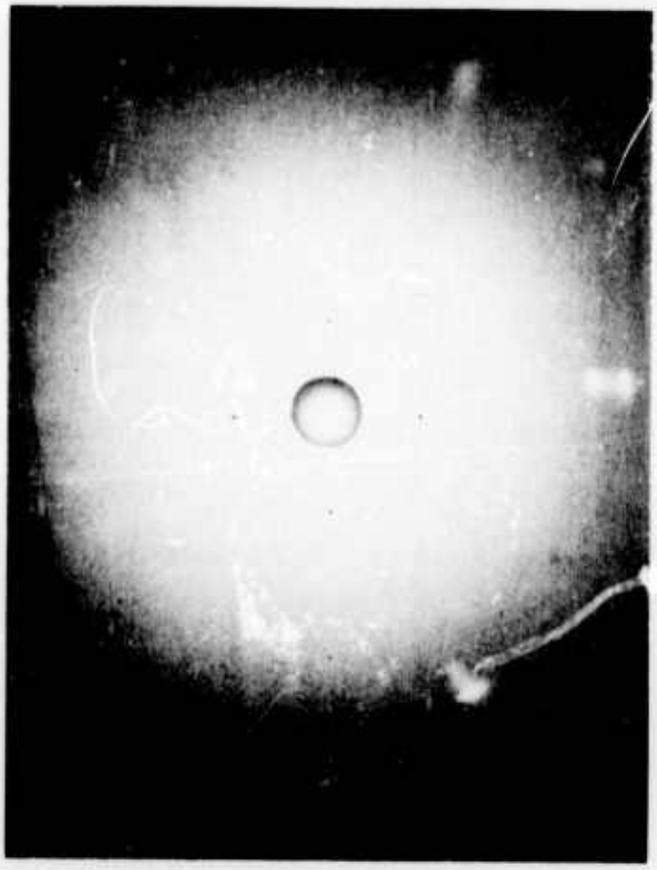

Figure 4.20 Laue pattern of $(10\bar{1}3)$-GaN (grown in $(1\bar{1}02)$-sapphire substrate).

Figure 4.21 Gallium nitride light-emitting diode with external illumination. The (1102)-sapphire substrate is removed, exposing the n-GaN layer. Magnification 28X.

sapphire substrates while cooling down to room temperature due to the large thermal expansion mismatch. Such chips were especially suited for emission pattern observations, because with the sapphire substrate out of the way, it was then possible to focus the optical microscope onto the light pattern at magnifications as high as 200X. If a sapphire substrate intervened between the microscope lens and the actual GaN LED, then a diffuse light pattern was observed.

The light emission does not occur uniformly throughout the material; rather, it takes the form of small, discrete spots. The pattern of light spots which occurred when the device shown in Figure 4.21 was forward biased is shown in Figure 4.22. Another diode was observed at a higher magnification, 200X, in the optical microscope, and the light spot pattern is shown in Figure 4.23. This photograph was exposed for six minutes, and the spots appear larger on the film than they actually are, due to the long exposure. Visual observations of the spots in the microscope indicate that they are less than 10 microns in diameter.

The same region of the LED of Figure 4.23 is shown with external illumination in Figure 4.24. The spot pattern has been superimposed onto this photograph. It can be seen that the light spots are of the same order of size as the crystal facets, and no more than one spot occurs in any facet although some facets are without spots. For comparison, the facets can be seen more clearly in the scanning electron micrograph shown in Figure 4.19.

A spotty light emission pattern is also observed with reverse bias. Most of the spot positions are different from the ones seen when a diode is forward biased, but a few appear to be the same. In addition, the

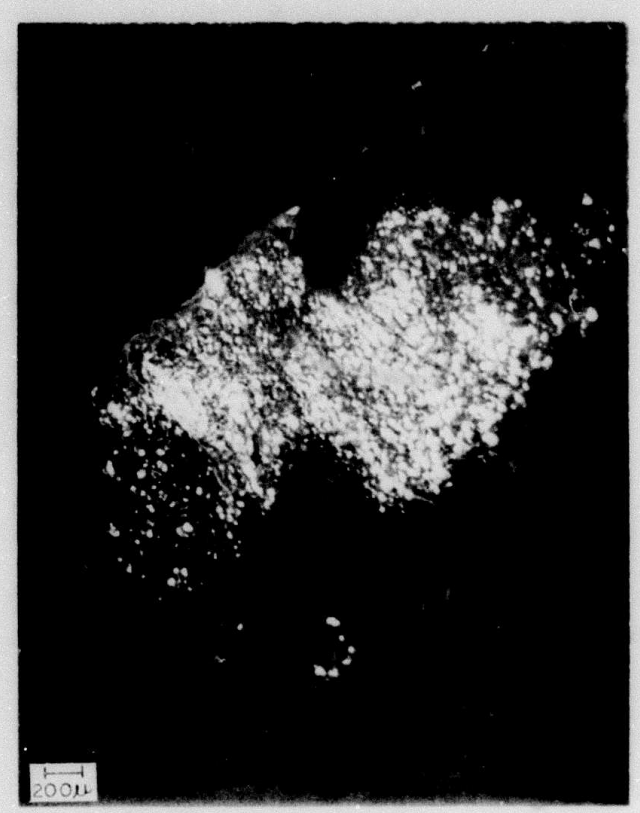

Figure 4.22 Light spot pattern observed during forward biasing of the diode shown in Figure 4.21. Magnification 28X.

Figure 4.23 Light spot pattern of forward-biased diode at 200X magnification.

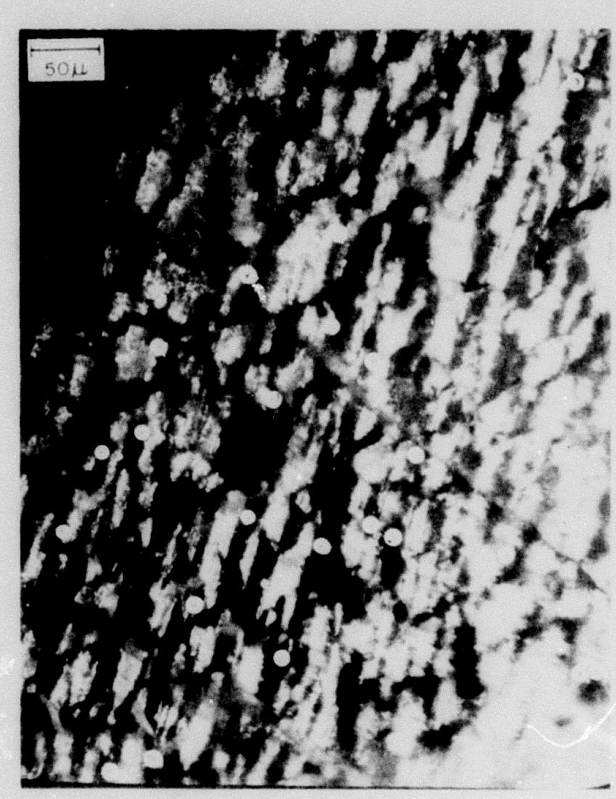

Figure 4.24 Same diodes as in Figure 4.23 with external illumination and light spot pattern superimposed (200X). $(10\bar{1}3)$-orientation.

two peaks shown in Figure 4.5 are generated from different spots: the more intense spots are blue while the others are yellow-orange. The series of photographs displayed in Figures 4.25, 4.26, and 4.27 shows a device with external illumination, forward bias, and reverse bias respectively. The marked change in the light spot pattern which occurs when the bias polarity is changed is clearly demonstrated.

It has been observed that the light spots turn on in a definite, reproducible order as the applied voltage is increased, and once all the spots are lit, they just become brighter as the voltage is further increased. As the voltage is turned back down, the spots go out in reverse order. Highly luminescent devices have large numbers of closely spaced light spots, all of which turn on over a short range of voltage increase (about 2 to 3 volts), while the poorest diodes have only a single light spot, which increases in brightness but which burns up before another spot can turn on. The voltage increase necessary to turn on one other spot in such diodes can be more than 10 volts. Single-spot diodes are not useful for visual displays.

Any GaN LED will burn up and become a short circuit if the applied voltage is continuously increased. In all cases the position of the brightest light spot overheats and burns, and a tiny black dot is left in the GaN at this point. The device can be salvaged by simply altering the metal contact so that it does not touch this black dot.

It should be noted that the spottiness of the light emission from GaN LED's is not discernible to the unaided eye, and therefore the devices appear to be quite uniformly illuminated. The presence of a sapphire substrate helps to diffuse the light and to increase the

Figure 4.25 Gallium nitride light-emitting diode #12.7.72 with external illumination. (10$\bar{1}$3)-orientation.

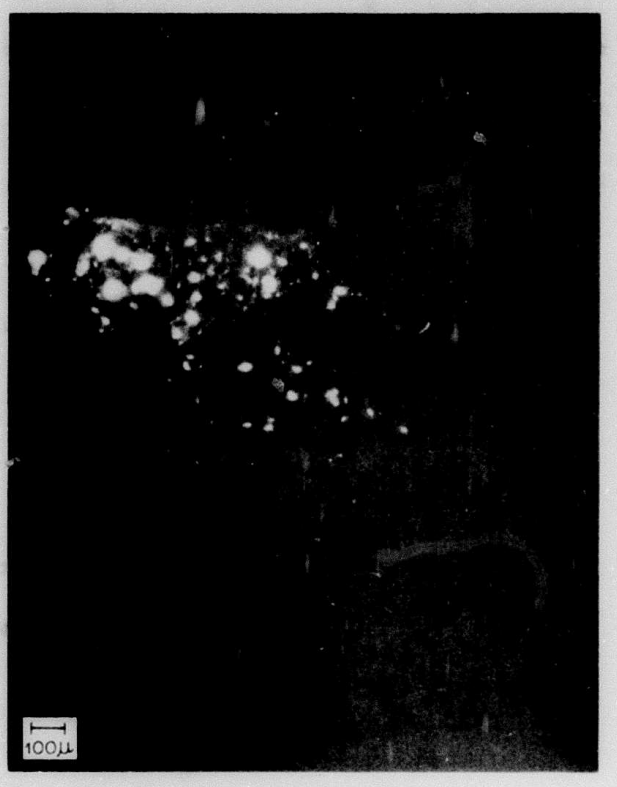

Figure 4.26 Gallium nitride light-emitting diode #12·7·72 (cf. Figure 4.25) with forward bias, illustrating light spot pattern.

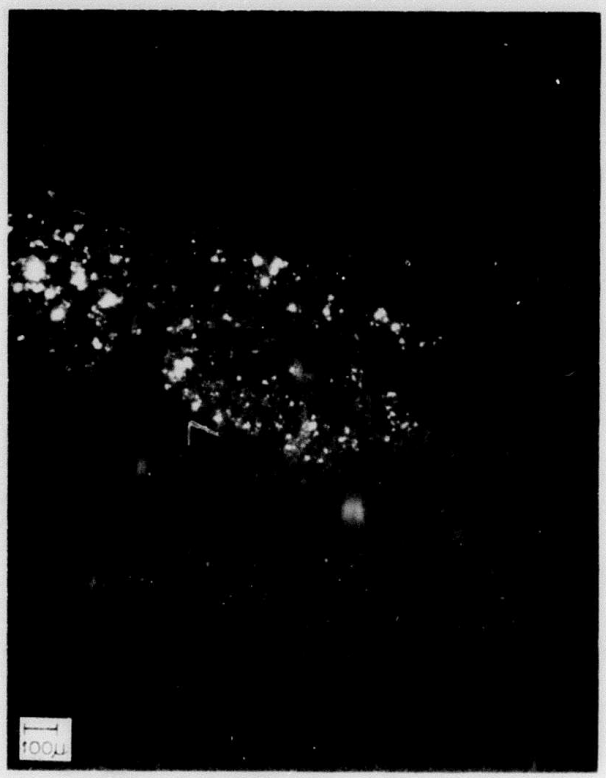

Figure 4.27 Diode #12.7.72 (cf. Figure 4.25) with reverse bias, illustrating different set of light spots appearing with reverse bias than forward bias.

uniform appearance of the LED's. The generation of light in the form of spots does not detract from the appearance of the LED's to a viewer, but of course it does result in a loss of efficiency since only a small portion of each device actually contributes to the light output.

Now that it has been established that the light emission pattern consists of a number of discrete spots, it is of interest to determine where the light is actually created inside the device. That is, is the light formed at the metal-GaN:Mg (m-i) junction, the GaN-GaN:Mg (i-n) junction, throughout the bulk of the GaN:Mg layer, or within the undoped GaN layer? In order to answer this question a sample was mounted perpendicular to a glass slide, so that the various regions (m, i, and n) were visible on the top surface. Figure 4.28 is an optical micrograph of the sample and shows, on the right, the sapphire substrate (with an arrow on it, pointing to a triangular mark used as a reference), in the center the GaN n- and i-layers which are indistinguishable in this picture, and on the left the metal contact to the i-layer. This sample is then shown with forward bias applied (and without external illumination) in Figure 4.29, magnified 500X. One of a number of the light spots which were particularly close to the top edge of the chip is clearly seen at the center of the photograph. It occurs about one-eighth of the way from the metal contact on the i-layer to the sapphire substrate. Another spot, similarly positioned, can be seen at the bottom of the picture. In the next section it will be shown that the exact position of the i-n junction is one-eighth of the way across the GaN.

Once again, reverse bias light proved more difficult to study.

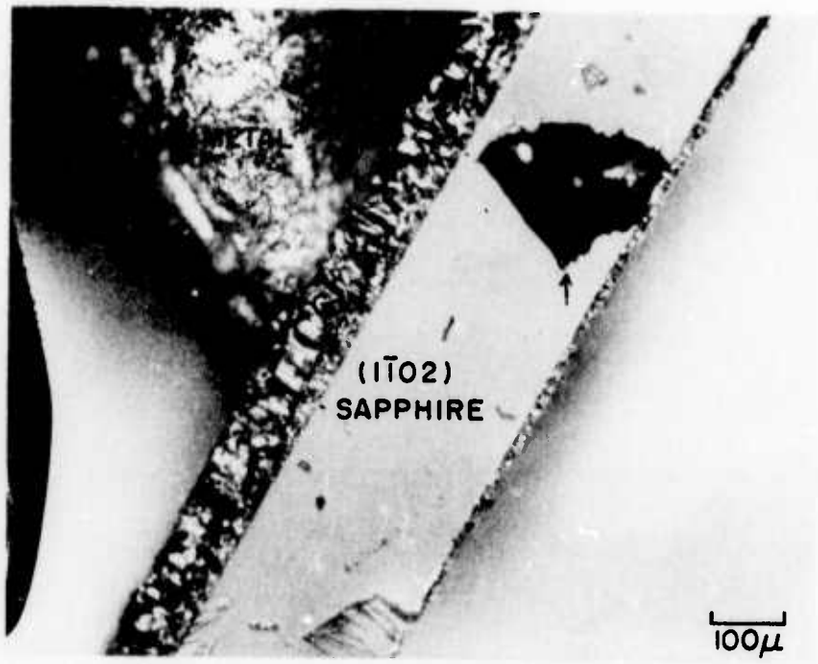

Figure 4.28 Diode mounted perpendicular to a glass slide showing sapphire substrate, GaN, and metal contact.

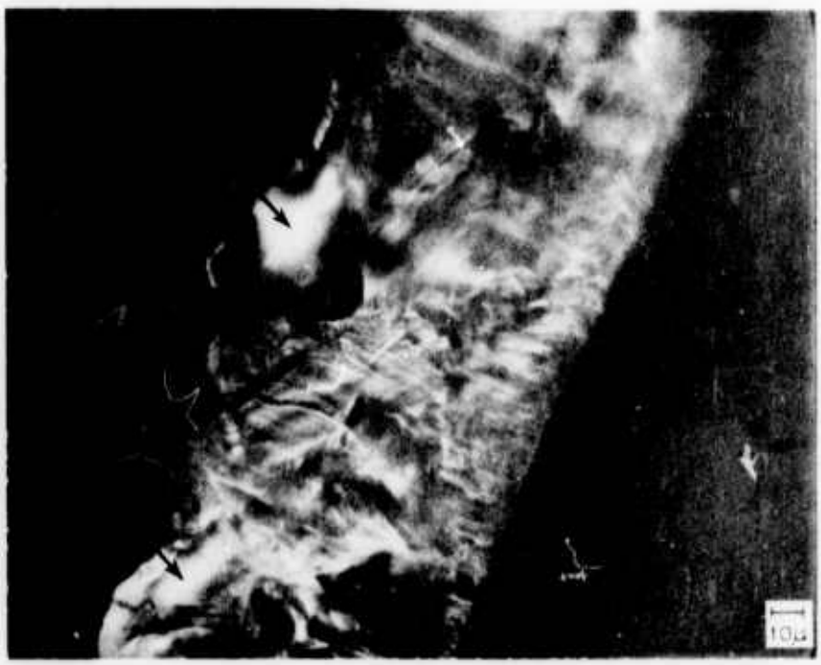

Figure 4.29 Light spots observed when diode shown in Figure 4.28 was forward biased. The light spots occur within the GaN region. Magnification 500X.

The size of the reverse bias light spots, when viewed through the n-layer was the same as the forward bias spots. However, none could be clearly seen and photographed from the junction side of the sample. The reverse-bias light appeared to come from the m-i junction. There definitely were no signs of light spots anywhere within the i- or the n-regions, and the metal-GaN:Mg interface appeared to glow. The problem involved in actually photographing the light seemed to be that the metal contant came within about 10 microns of the surface on which the microscope was focussed. It was very difficult to paint the contact any closer to the edge, because of the problem of getting it over the side and onto the n-region, which would cause a short-circuit. For this reason no light generated at the m-i junction would be visible along the very edge of the chip. Therefore the origin of the reverse-bias light remains in doubt, although it is likely that it is generated at the m-i junction.

4.7 Characteristics of the Insulating (Mg-Doped) Region

It was now appropriate to make a more detailed study of the insulating Mg-doped GaN layer in the diodes. The Mg concentration in the doped material was determined by electron microprobe analysis, and concentrations of 2-6 x 10^{20} atoms/cm^3 were found. In addition, one Zn-doped sample was analyzed with the microprobe and proved to contain 6 x 10^{19} atoms/cm^3, which is similar to the Mg concentrations. It is not known what percentage of the dopant is electrically active.

The addition of a large quantity of dopant affects the lattice parameters of GaN. In Table 4.1 are shown the lattice parameter measure-

	a, Å	c, Å	Data Source
GaN	3.189	5.185	MARUSKA and TIETJEN, 1969
GaN	3.190	5.17	FAULKNER et al., 1970
GaN	3.189	5.185	ILEGEMS and MONTGOMERY, 1973
GaN	3.190	5.184	PRESENT STUDY
GaN:Mg	3.194	5.192	PRESENT STUDY

Table 4.1 Lattice Parameters of Undoped and Mg-Doped GaN

ments of a number of investigations (including the present one) on undoped GaN and the a and c values for Mg-doped GaN (from the present study). The a and c values for the doped material were found to increase by an average of 0.14 and 0.21%, respectively, over the values for undoped material. Since the tetrahedral covalent radii of Mg and Ga are respectively 1.40 and 1.26 Å, if 4×10^{20} Mg atoms are substituted for Ga among the 4.4×10^{22} lattice sites of GaN, then the unit cell should expand by 0.10%, in good agreement with the experimental results.

Further studies of the insulating region in the diodes were made with the SEM. Diodes were attached to glass slides with the side (and hence the two junctions) up, as described in the previous section. A clear picture of such a diode arrangement is shown in Figure 4.30, which has a magnification of 25X. In the next three SEM photographs, Figures 4.31 through 4.33, this device is shown at 100X magnification and with zero, positive, and negative bias, respectively. In this set of photographs, the facetted nature of the GaN surface is again apparent. The surface is actually quite jagged. Here, too, the actual extent of the insulating region is beginning to be distinguishable. It is especially noticeable with negative bias, where it shows up as a white band.

The width and shape of the i-layer is clearly distinguishable in Figure 3.34, which was taken with negative bias at 500X magnification. The difference in contrast between the n- and i-layers is a result of voltage contrast in the SEM. The very white region is the front surface of the i-layer which is visible because the metal contact does not come all the way up to the edge, and should be disregarded. The i-layer is light gray and the n-layer is dark gray. The i-layer is from 10 to 25

Figure 4.30 Perpendicular view of diode #12·13·72, as seen in the scanning electron microscope. The entire device (including the (1102)-sapphire substrate) and the two metal contacts (to the n- and i-layers) are visible. Magnification 25X.

Figure 4.31 Scanning electron micrograph of diode #12·13·72 at 100X magnification--no bias. $(1\bar{1}02)$-oriented sapphire substrate.

Figure 4.32 Scanning electron micrograph of diode #12-13-72 at 100X magnification with forward bias (+22 volts).

Figure 4.33 Scanning electron micrograph of diode #12·13·72 at 100X magnification with reverse bias (-22 volts).

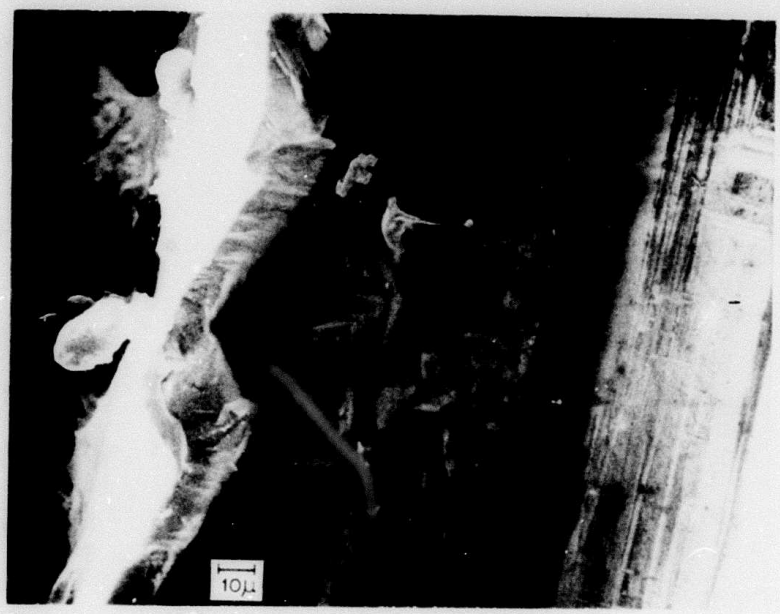

Figure 4.34 Scanning electron micrograph of diode #12·13·72 at 500X magnification with reverse bias. The insulating (Mg-doped) GaN layer can be clearly distinguished. $(1\bar{1}02)$-oriented sapphire substrate.

microns wide, but over most of its extent it is just the 10 micron width. This thickness variation is caused by the different rates of growth of different facet planes. Notice that the m-i junction and the i-n junction are parallel, and that both have a jagged appearance (conforming to the facets). Notice also that the i-n junction is about one-eighth of the way from the front face to sapphire substrate. Thus the light spots seen in Figure 4.29 were in fact generated at the i-n junction.

The n-GaN was grown for one-half hour and the i-GaN for one-quarter hour in the diode shown in Figures 4.29 and 4.34. However, the n-layer is eight times as thick as the i-layer. Therefore the presence of Mg in the vapor during the growth of GaN reduces the growth rate to only one-fourth of that of undoped material.

The last three SEM photographs of this series, Figures 4.35 through 4.37, were taken with a magnification of 1000X. Figure 4.35 was taken without any bias applied to the diode, while Figure 4.36 shows positive bias and Figure 4.37 shows negative bias. During the slow scanning of these last two photographs, the bias was switched off for a short time, as indicated on the figure, in order that one may compare in the same picture the biased and unbiased conditions. Notice that biasing the metal contact positive renders it black and that the same black condition occurs for the n-GaN region when it is biased positive, as expected. In these high-magnification photographs one can see that the i-n junction can have a rather complicated shape.

Figure 4.38 is typical of the structure of Mg-doped GaN seen in the transmission electron microscope. The lighter regions are

Figure 4.35 Scanning electron micrograph of diode #12·13·72 at 1000X magnification with no bias.

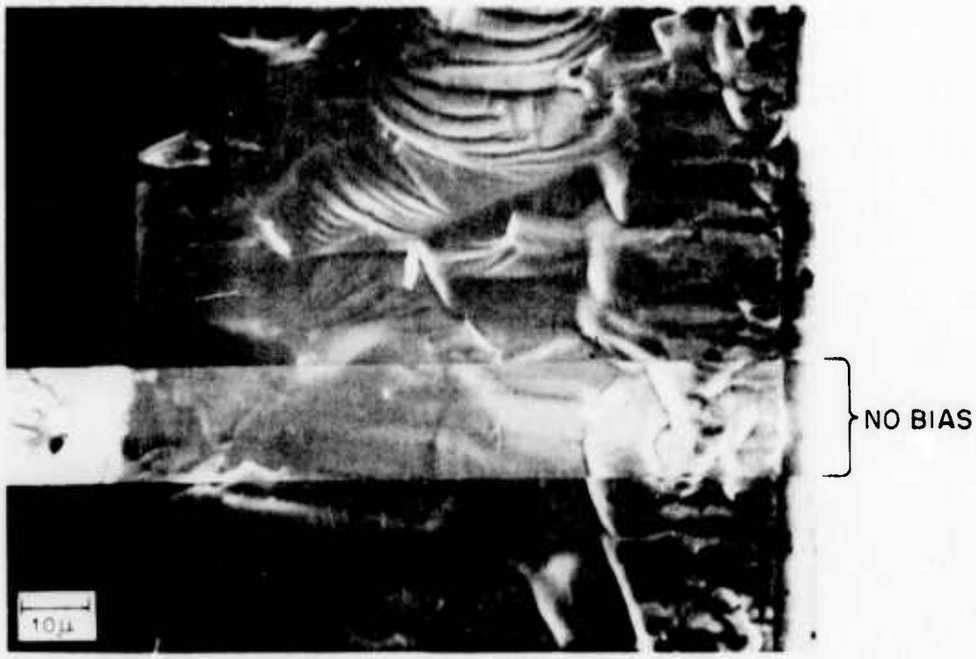

Figure 4.36 Scanning electron micrograph of diode #12·13·72 at 1000X magnification with forward bias. The bias was removed during part of the scan, as indicated.

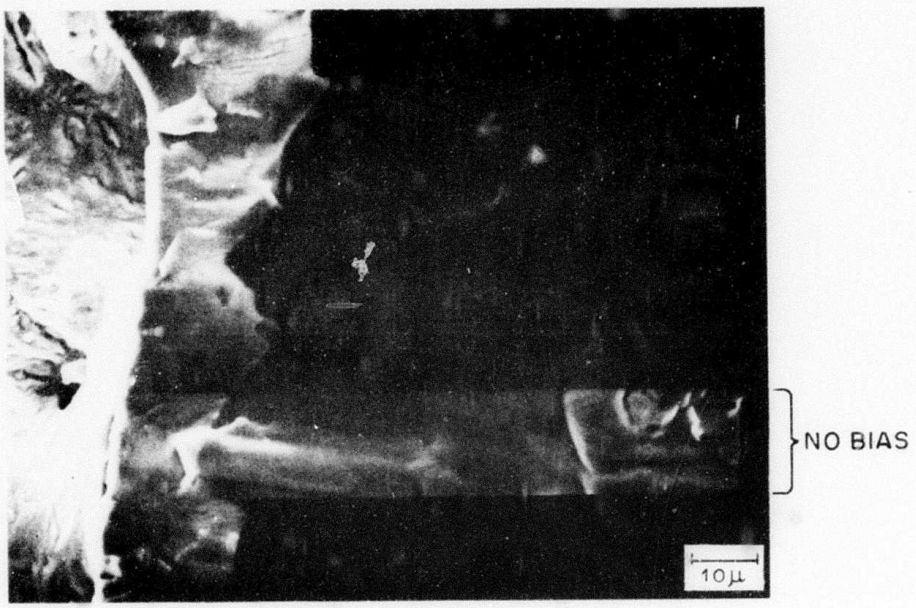

Figure 4.37 Scanning electron micrograph of diode #12-13-72 at 1000X magnification with reverse bias. The bias was removed during part of the scan, as indicated.

Figure 4.38 Transmission electron micrograph of insulating (Mg-doped) region of a GaN LED. Notice no evidence of precipitates or dislocations. Magnification 240,000X.

apparently caused by non-uniformities in sample thickness that were created during thinning. Detailed examination revealed no evidence of precipitates or dislocations. Grain boundaries were not observed, as was expected, because of the small size of the thinned area as compared to the known grain size. Selected area diffraction yielded a distinct, single crystalline GaN pattern. It can be concluded that the i-layer is precipitate-free and that the dislocation density is less than 10^5 cm^{-2}.

4.8 Electrical Potential Distribution

A good approximation of the electrical potential distribution within a diode can be obtained by taking line scans in the SEM with and without an applied bias. In the ordinary display mode of operation, the SEM scans successive lines in order across a sample. However it can be set to continuously sweep across just one line, and to display the number of secondaries collected across the sample on this line as a trace on the CRT. Two such traces are displayed in Figure 4.39, taken at 1000X magnification for the same line across the sample, with and without forward bias. These traces are superimposed on a standard secondary electron image of the region of which the line is a part, and thus the photograph consists of a total of three exposures. The same line was traced with and without forward bias at 2500X magnification in Figure 4.40. The traces with 0, -6, -12, and -18 V (reverse bias) at 2500X magnification are shown in Figure 4.41. Since for a topographically and compositionally uniform sample the number of secondary electrons emitted from any point on the sample is dependent on the voltage at

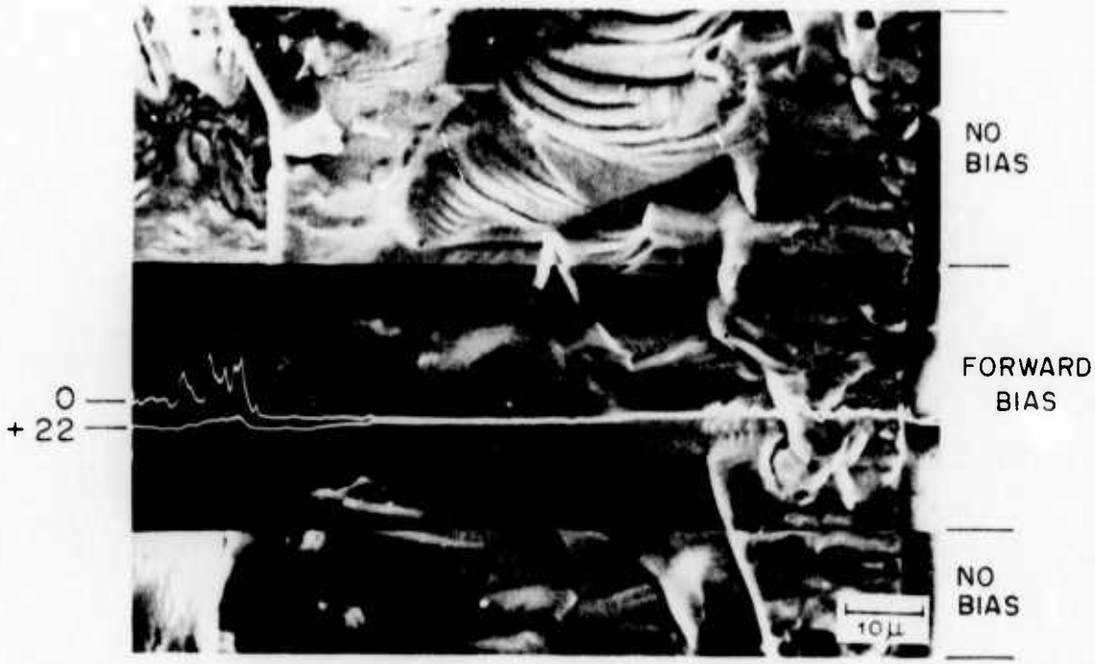

Figure 4.39 Superimposed zero bias and forward bias line scan traces and SEM photograph of a gallium nitride light-emitting diode. Magnification 1000X.

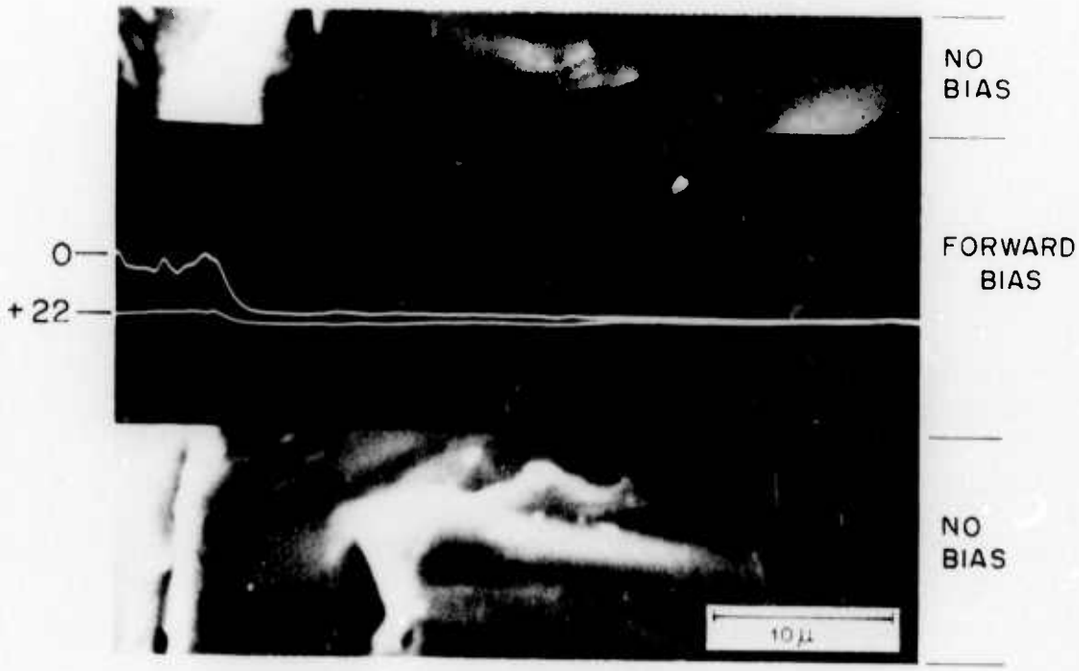

Figure 4.40 Superimposed zero bias and forward bias line scan traces and SEM photograph of a gallium nitride light-emitting diode. Magnification 2500X.

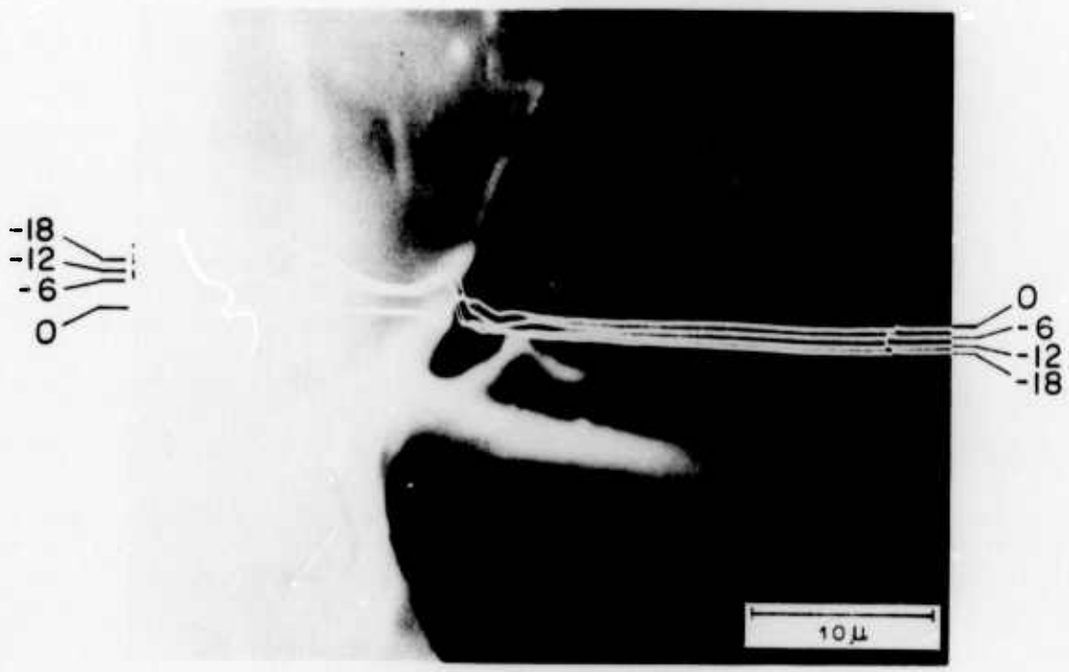

Figure 4.41 Superimposed zero bias and reverse bias (-6, -12, and -18 volts) line scan traces and SEM photograph of a gallium nitride light-emitting diode. Magnification 2500X.

that point [MacDONALD and EVERHART, 1965], and since the height of the line scan trace is directly proportional to the number of secondary electrons collected, it is possible to display the voltage profile across the diode for an applied bias. This has been done for both forward and reverse bias in Figures 4.42 and 4.43 respectively. Gradients in potential occur in either case at both the m-i and the i-n junctions, and nowhere else.

The potential distribution of GaN LED's has recently been obtained with a fine wire probe and electrometer by other workers [J. I. PANKOVE, private communication]. The forward-bias distribution is exactly the same as the one obtained in the present study in the SEM. However, the reverse-bias potential distribution obtained with the wire probe shows the entire potential gradient at the m-i junction. The reason for the different distributions in reverse-bias is not known.

It should be noted that in Figures 4.39 through 4.41 the front edge of the i-layer is once again visible on the left side of the photographs. This edge contributes some spurious peaks to the line scan, and it has been discounted in Figures 4.42 and 4.43, which are only supposed to have one linear dimension. The width of the i-layer is not the same in Figure 4.42 and Figure 4.43 because these measurements were not taken on the same sample, although the photographs presented here were the best ones obtained in this study for each of the two bias situations.

4.9 Diode Capacitance

Diode capacitance and conductance measurements were made with a

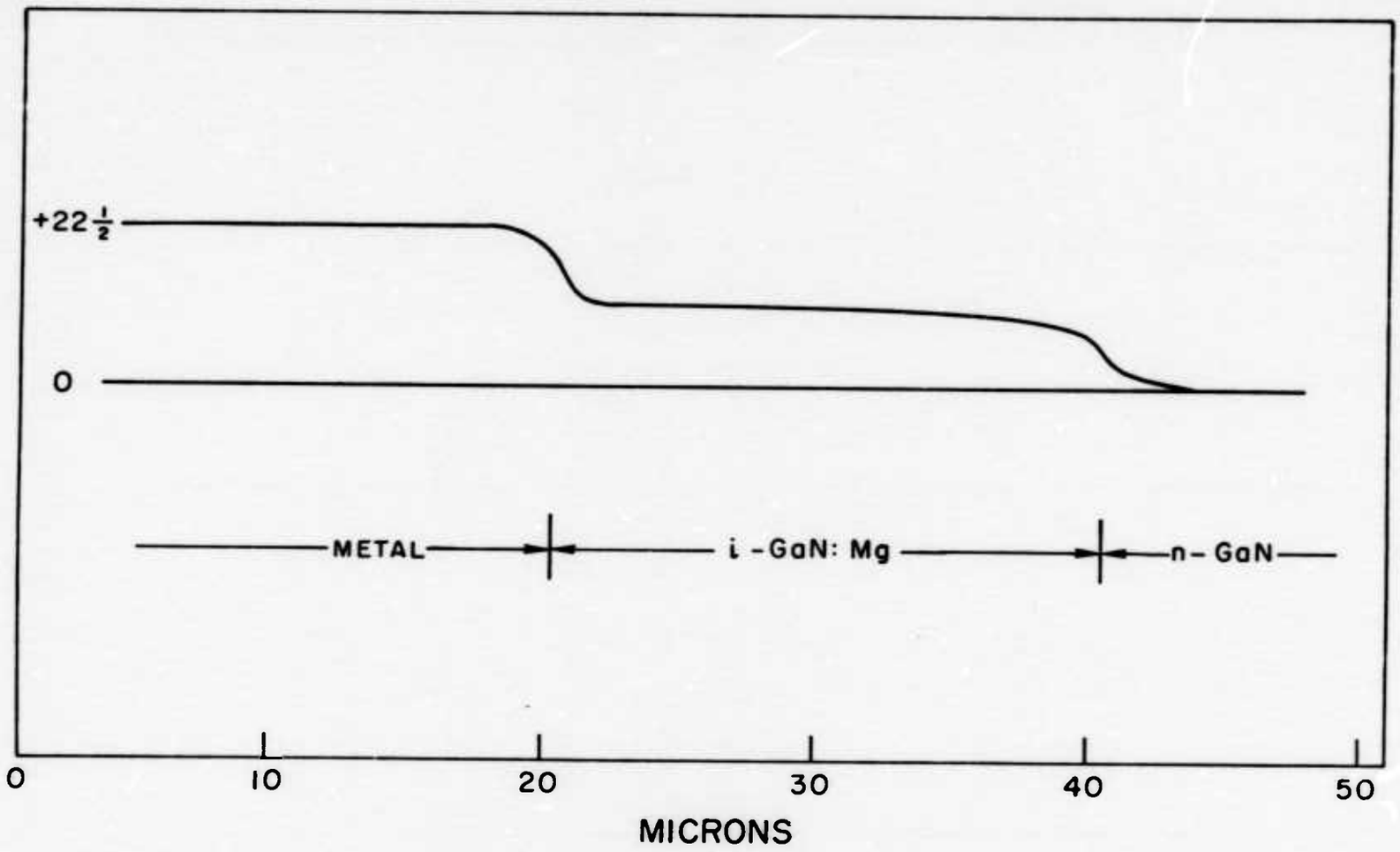

Figure 4.42 Electric potential distribution across a gallium nitride light-emitting diode when forward bias is applied.

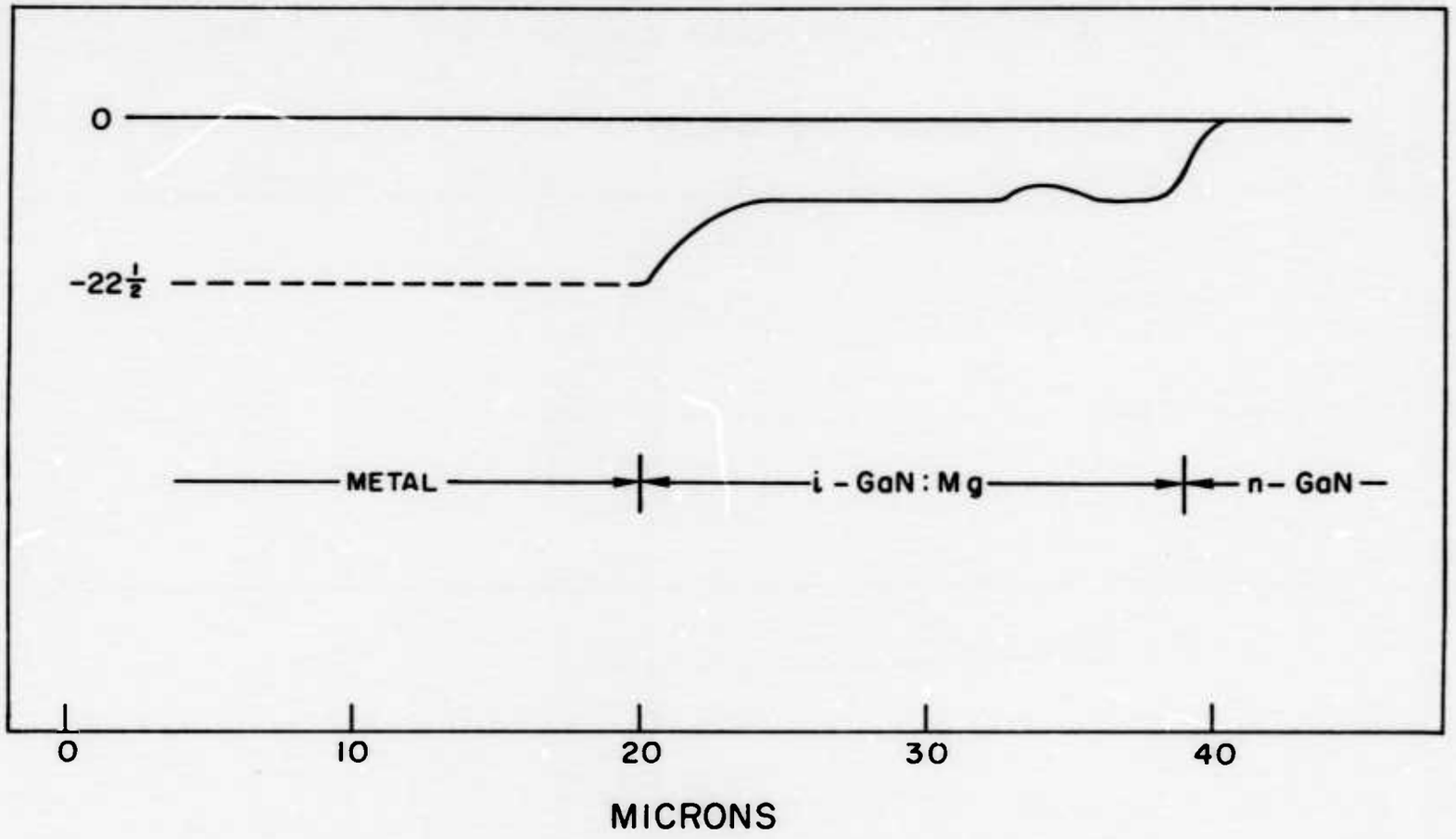

Figure 4.43 Electric potential distribution across a gallium nitride light-emitting diode when reverse bias is applied.

Boonton Electronics Model 75D Direct Capacitance Bridge. This instrument uses a 1 MHz test frequency and is capable of supplying up to 150 V d-c bias. The voltage dependences of the capacitance and conductance were of the same form for all GaN diodes tested, and the results for a representative diode are shown in Figure 4.44. In this figure, $1/C^2$ is also plotted as a function of applied voltage. The form of this plot suggests two diodes connected back to back, so that one is always "reverse biased." An ordinary p-n junction diode will only show a linear $1/C^2$ vs. V plot for "reverse bias" (i.e., n biased positive with respect to p) voltages. This linear portion can be extrapolated to the value of the junction barrier potential, which will be about +1 V. This extrapolation is not possible for the GaN m-i-n diodes because of the capacitance of the i-layer, which exists in addition to the junction (actually two junctions are involved) capacitance. In Figure 4.43 the capacitance of the diode is 1[illegible]0 pF with zero bias applied. For purposes of comparison it is appropriate to calculate this capacitance from other data. It is known that the i-layer is 10^{-3} cm wide from measurement in the SEM. Using

$$C = \frac{\varepsilon A}{d}, \qquad (4.9.1)$$

with $\varepsilon = 5.5\ \varepsilon_o$,

and $A = 4 \times 10^{-2}\ cm^2$,

then $C = 19.5$ pF,

which is smaller than the measured value by a factor of 7. The measured

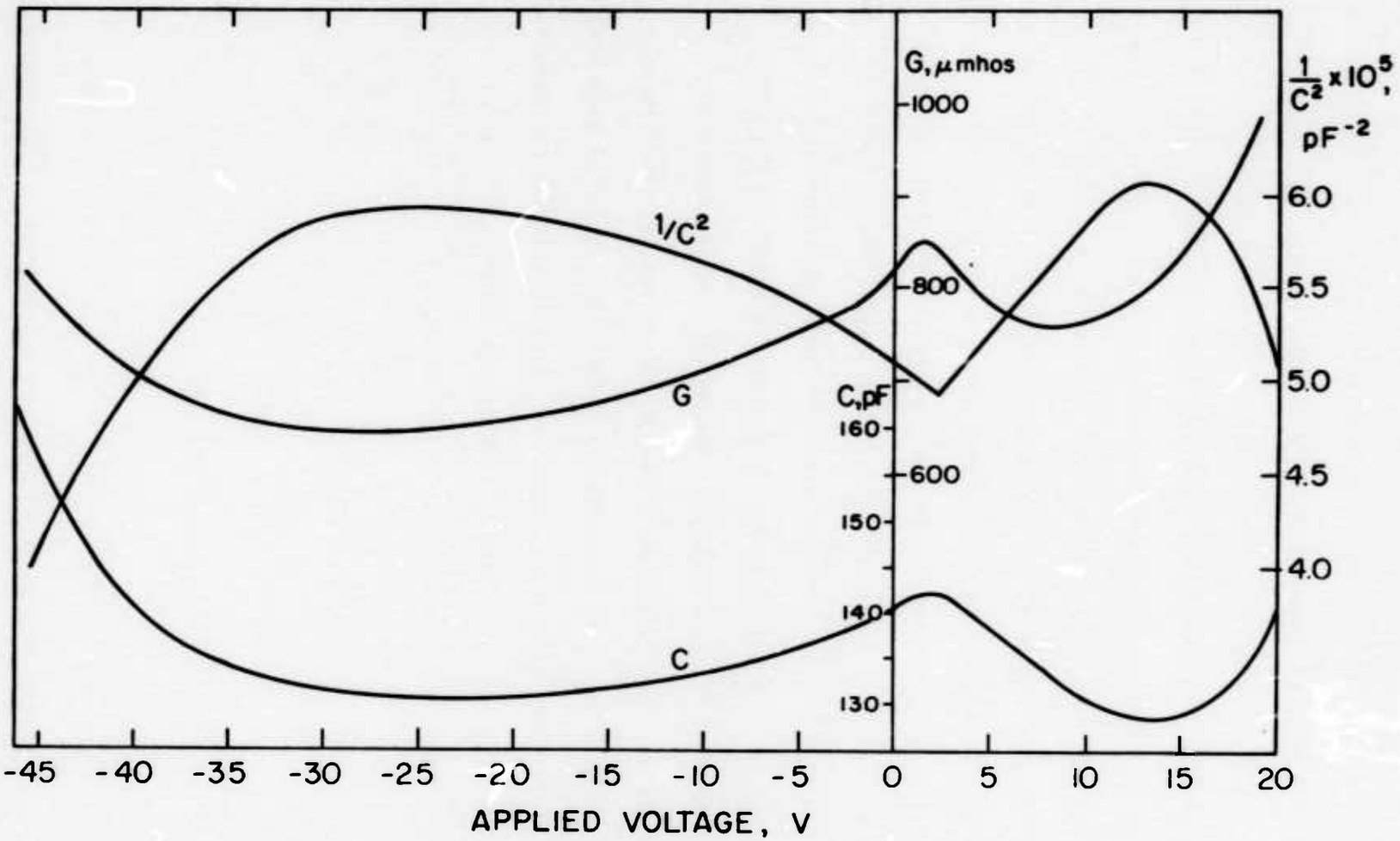

Figure 4.44 The capacitance and conductance as functions of applied voltage for a typical GaN diode. Also included is the quantity, $1/C^2$, as a function of voltage.

capacitance is directly proportional to the area of the metal contact on the i-layer, so the discrepancy is not due to current spreading across the surface of the i-layer. This suggests that the effective width of the i-layer may be smaller than the observed width, perhaps because of conducting precipitates along the subgrain boundaries.

Use may be made of the depletion approximation (total depletion of free carriers in a junction region of width w) to calculate the carrier concentration. With this approximation,

$$\frac{1}{C^2} = \frac{2V}{q\varepsilon N} , \tag{4.9.2}$$

where

$$N = \frac{N_A - N_D}{N_A N_D} . \tag{4.9.3}$$

The value of N may be obtained from the slope of the $1/C^2$ vs. V plot,

$$N = \frac{2}{q\varepsilon[d(1/C^2)/dV]} . \tag{4.9.4}$$

With either bias polarity, a value of $N \approx 10^{16}$ cm^{-3} is found. From Hall Effect measurements on undoped n-type GaN samples an average value of $N_D = 7 \times 10^{18}$ cm^{-3} has been found. Thus the value of $N = 10^{16}$ cm^{-3} calculated above could be N_A by Equation 4.9.2. This number is far less than the total Mg concentration (10^{20} cm^{-3}). Therefore it may be that all of the Mg is not electrically active, or else that Mg doping tends to increase the concentration of native donors (nitrogen vacancies) to produce self-compensation.

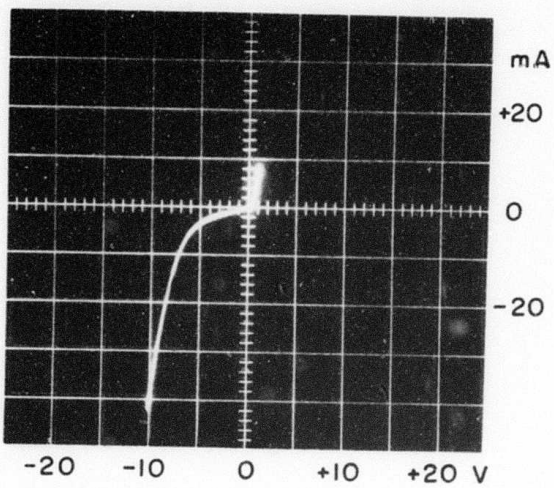

Figure 4.45 Current-voltage characteristic of a GaN m-i-n diode prepared by proton bombardment.

4.10 Proton Bombardment and Proton-Assisted Diffusion

The GaN samples subjected to the proton bombardment treatment in all cases acquired insulating surface layers. These i-layers were very thin, and it was not possible to distinguish them from the remaining untouched GaN with the SEM. No evidence for Zn diffusion was found in samples which had been coated with Zn before the bombardment treatment. Electron microprobe analysis was used to detect the presence of Zn in the layers. The instrument has a Zn detection limit of 300 ppm. The electron beam in the probe had a penetration depth of 1.5 microns, but the diffusion depth was unlikely to have been more than 0.5 micron. Since GaN contains 4.4×10^{22} gallium atoms per cm^3, and considering the detection limit of the probe and the diffusion depth, about 5×10^{19} zinc atoms per cm^3 would have had to have been included in the samples for detection. Thus if any was included, it had to have a lower concentration. Significantly, photoluminescence studies failed to show the peak found in GaN samples doped with Zn during growth.

Even though Zn apparently did not diffuse into the bombarded GaN samples, they did exhibit electroluminescence. Since the surface layers of these samples were insulating, diodes were fabricated by the techniques used for the Mg- and Zn-doped samples, as described in Section 3.4. The diodes made from proton bombarded material emitted yellow-green light, but only with reverse bias. With forward bias applied, these diodes were ohmic. The type of I-V characteristic found for these diodes is shown in Figure 4.45.

Chapter 5

DISCUSSION

The experimental results presented in Chapter 4 are discussed with the aim of developing a model for the operation of the GaN light-emitting diodes. This discussion is primarily concerned with the basic conduction mechanisms in diodes and with the mechanisms for electroluminescence. The seven conduction processes considered are: (1) minority carrier injection in a p-n junction; (2) Schottky emission; (3) Frenkel-Poole emission; (4) tunnel or field emission; (5) space-charge-limited current; (6) Ohmic electron hopping; and (7) ionic conduction. It will be shown that quantum mechanical tunneling through a triangular potential barrier at the cathode is the only mechanism consistent with the data. The three mechanisms for electroluminescence, minority carrier injection, internal field emission, and impact ionization, are discussed, and although it is always very difficult to absolutely distinguish the internal field emission process from the impact ionization process, evidence in support of impact ionization in the GaN LED's will be given. Finally, the growth, fabrication and operation of a GaN LED is described from a microscopic point of view.

5.1 Basic Mechanisms for Diode Operation

We wish to develop models to explain the diode electrical characteristics and the electroluminescence. A good understanding of the mechanisms responsible for the device operation is essential if the diode performance is to be improved. Therefore let us summarize the important properties and features of the LED's which were described in detail

Preceding page blank

in the chapter on Experimental Results, and which have direct bearing on an elucidation of the mechanisms involved.

a) It is possible to obtain violet light-emitting diodes using GaN:Mg m-i-n structures.

b) The electroluminescence with forward bias consists of a broad spectrum (400 meV half-width) which peaks at 2.9 eV.

c) Photoluminescence in GaN:Mg shows a similar spectrum which also peaks at 2.9 eV.

d) The reverse bias electroluminescence spectrum is different than the forward bias electroluminescence and photoluminescence spectra; peaks occur at 2.6 and 2.0 eV.

e) The light emission occurs as a pattern of small, discrete spots, which are of the same order of size as the GaN crystal facets.

f) The light is emitted at the cathode (i-n junction) with forward bias, and apparently also at the cathode (m-i junction) with reverse bias.

g) Laue patterns indicate that the GaN is single crystalline, but the surface shows a strongly facetted structure. For this reason, the m-i and i-n junctions are not planar, but follow the facetted nature of the growth.

h) The diode I-V characteristics show rectification. With forward bias applied, $I \alpha V^n$ where $2 \leq n \leq 3$ in the region of light emission (15-25 volts), while $n > 3$ at lower voltages.

i) The diode current at constant voltage exhibits a small activation energy with temperature of 0.1-0.2 eV. This activation energy is independent of the applied voltage.

j) When a bias is applied, potential gradients appear at both the m-i and the i-n junctions in the diodes, but not over the bulk of the insulating (i) region.

First of all, it is apparent that a single, simple, standard p-n junction is not involved. The GaN diode I-V characteristics do not fit Schockley's p-n junction equation,

$$I = I_o[\exp(qV/kT)-1], \qquad (5.1.1)$$

over any current and voltage range. GaN has not been doped conducting p-type. Rather than a p-n junction, an insulating region is the essential component of the GaN light-emitting diodes. Therefore it is proper to consider the basic conduction processes in insulators as summarized in Table 5.1 [SZE, 1969]. Six possible processes which can control the current flowing through an insulator are listed in this table. Some of these processes may be occurring simultaneously in series or in parallel in a particular type of device, but the overall rate of carrier flow is usually controlled by the slowest process for processes in series, and by the fastest process for processes occurring in parallel. The first three processes listed in the table give control of the current at the electrodes, while the last three operate throughout the bulk of the insulator.

The basic conduction processes in insulators may be summarized as follows. In the Schottky emission process, thermionic emission of carriers across the metal-insulator interface or the insulator-semiconductor interface is responsible for current flow. Frenkel-Poole emission is due to field-enhanced thermal excitation of trapped electrons

Table 5.1

Basic Conduction Processes in Insulators

Process	Expression†	Voltage and Temperature Dependence
Schottky Emission	$J = A^*T^2 \exp\left[\frac{-q(\Phi_B - \sqrt{qF/4\pi\epsilon_i})}{kT}\right]$	$\sim T^2 \exp\left(\frac{-B + aV^{1/2}}{kT}\right)$
Frenkel-Poole Emission	$J \sim F \exp\left[\frac{-q(\Phi_B - \sqrt{qF/\pi\epsilon_i})}{kT}\right]$	$\sim V \exp\left(\frac{-B + 2\,aV^{1/2}}{kT}\right)$
Tunnel (or Field) Emission	$J \sim F^2 \exp\left[-\frac{8\pi\sqrt{2m^*}(q\Phi_B)^{3/2}}{3qhF}\right]$	$\sim V^2 \exp(-b/V)$ or, $\sim V \exp(-b/V^{1/2})$
Space-Charge-Limited	$J = \frac{8\epsilon_i \mu V^2}{9d^3}$	$\sim V^2$
Ohmic	$J \sim F \exp(-\Delta E_{ae}/kT)$	$\sim V \exp(-c/T)$
Ionic Conduction	$J \sim \frac{F}{T} \exp(-\Delta E_{ai}/kT)$	$\sim \frac{V}{T} \exp(-d'/T)$

†A^* = effective Richardson constant, Φ_B = barrier height, F = electric field, ϵ_i = insulator dynamic permittivity, m^* = effective mass, d = insulator thickness, ΔE_{ae} = activation energy of electrons, ΔE_{ai} = activation energy of ions, $B = q\Phi_B$, $a = (q^3/4\pi\epsilon_i dk^2)^{1/2}$

Positive constants independent of V or T are b, c, and d'.

into the conduction band. For trap states with coulomb potentials, the expression involved is virtually identical to that for Schottky emission. Tunnel emission is either due to field ionization of trapped electrons into the conduction band or to electrons penetrating a potential barrier at a junction. Space-charge-limited current results from carrier injection into a region in which no compensating charge is present. In some respects it is analogous to the process which governs the operation of a vacuum tube. The ohmic mechanism applies to thermally excited electrons hopping between isolated states. Ionic conduction describes the diffusion of ions under the influence of an electric field.

The voltage and temperature dependencies of the current for the six basic conduction processes in insulators are presented in Table 5.1. In order to establish the actual mechanism responsible for the diode electrical characteristics, these voltage and temperature dependencies are compared with the experimental results found for the GaN LED's.

Ionic conduction can be eliminated since GaN is not expected to be an ionic conductor. The electrodes would soon become polarized and current flow would cease, or else electrolysis would occur. Instead, GaN LED's have been operated continuously for weeks with no sign of degradation in their electrical or luminescent properties.

There is no evidence for an ohmic hopping mechanism of conduction. The expression for this process,

$$J \sim F \exp(-\Delta E_{ae}/kT), \qquad (5.1.2)$$

does not fit the diode electrical properties.

The Schottky and Frenkel-Poole emission processes also involve

expressions which are not consistent with the experimental results. The Schottky process involves the thermal excitation of carriers over a potential barrier of height Φ_B. This potential barrier is lowered by the applied electric field. The voltage and temperature dependence of the current may be expressed as

$$J \sim T^2 \exp \frac{-B + aV^{1/2}}{kT} , \qquad (5.1.3)$$

where B is equal to $q\Phi_B$ and a is a constant independent of V and T, defined in Table 5.1. Therefore the barrier height can be calculated from the thermal activation energy measured at a constant voltage. Consider a forward-biased GaN LED. The barrier to be surmounted is at the i-n junction. The height of this barrier may be estimated as follows. The band gap of GaN is 3.4 eV. The Fermi level in the i-region may be assumed to lie near the middle of the gap, while it lies at the conduction band edge in the n-region. Therefore Φ_B is equal to about 1.7 eV. The maximum photovoltage (which equals the barrier height) has been measured to be 1.6 volts for GaN:Zn LED's [PANKOVE, MILLER, and BERKEYHEISER, 1971]. In the present study a barrier height of at least 0.63 volts was measured using a mercury lamp excitation source, which was not sufficiently intense to saturate the photovoltage. The 1.6 volt value was measured with a xenon lamp source, which provides a much more intense light than the mercury lamp. Therefore Φ_B lies between 0.63 and 1.7 volts, and most reasonably should be closer to 1.7 volts. However a large thermal activation energy (viz., 1.7 eV) has not been measured for the GaN LED's. In addition, inspection of the Schottky emission expression shows that the actual value of the

thermal activation energy is proportional to the square root of the applied voltage. The results for the GaN diodes do not give a voltage dependence for the thermal activation energy. Therefore the Schottky process does not apply. A similar argument can be given against the Frenkel-Poole mechanism, which has the same voltage and temperature dependencies.

The space-charge-limited-current process has little temperature dependence, so the argument given above against the Schottky process does not apply. The topic of space-charge-limited-currents in insulators has been discussed at length in a recent textbook [LAMPERT and MARK, 1970]. The discussions given in this book for single carrier space-charge-limited current may be very briefly summarized as follows. In all cases a power law of the form

$$I \alpha V^n \qquad (5.1.4)$$

is found. The value of n obtained depends on the assumptions made about traps in the insulator. The most commonly encountered cases are the trap-free insulator and the insulator with one or more kinds of traps each located at a precisely defined energy level. The "trap-free" case also applies to the situation where the injected charge greatly exceeds the number of traps, so that all the traps are full and do not affect the conduction process. For any of these cases, a value of the power law exponent n = 2 has been derived.

However, a set of traps located at a precise energy level is only a good approximation for single-crystalline materials of high chemical and structural purity. In a material with a large amount of either

chemical or structural disorder, each trap does not have a uniquely defined environment. The result will be a smearing out (in energy) of the level. Such a picture could well be applied to GaN for the following reasons: the insulating regions of the diodes were doped with more than 10^{20} atoms/cm^3; undoped GaN apparently contains a large number of nitrogen vacancies; and the material grows with a cellular structure rather than perfectly single-crystalline. The power law exponent for a trap distribution where the number of traps is exponentially distributed in the forbidden gap may be expressed as

$$n = \ell + 1, \tag{5.1.5}$$

where ℓ is a parameter characterizing the trap distribution and $\ell > 1$. Therefore the current-voltage dependence found for the GaN diodes, where $2 < n < 3$ in the electroluminescence range of voltage, and $n > 3$ at lower voltages, might be explained by single carrier space-charge-limited current in the presence of an exponential distribution of traps.

There are two major problems encountered by invoking such a model. The current at a given voltage should be inversely proportional to the thickness of the insulator raised to the $2\ell + 1$ power with this model. However, LED's have been prepared which have i-layers differing in thickness by one order of magnitude but which have identical electrical characteristics. If the model of space-charge-limited current were correct, the current should have been at least three orders of magnitude larger in the thin samples. These test samples were obtained as follows. The substrate is always placed perpendicular to the gas stream so that the entire specimen is at the same temperature and sees the same gas concentrations (Section 3.1). Some gas does get around to the back side

of the substrate and thin GaN layers grow there too. Ordinarily the back side of the wafer is sandblasted clean. However, a contact can simply be placed on this back side, as well as the front side. It was found that the diodes made on the two sides of various wafers were identical, even though the i-layers on the front sides were about 10 microns wide, and the back-side i-layers were about 1 micron wide. This is in obvious conflict with a space-charge-limited current model.

Furthermore, the potential distributions shown in Figure 4.41 and 4.42 are not the ones expected for single carrier space-charge-limited current. The electric potential and its derivative with distance should be both monotonically increasing across the insulator. Instead, the potential in the GaN i-layers was found to only increase at the two junctions, while remaining constant across the bulk of the layer. The first derivative of the potential changed from + to - to zero to + to minus. Therefore the proposition that the diode current is controlled by bulk space charge effects is inconsistent with the experimental results.

There remains the possibility of two carrier space-charge-limited current. This mechanism is more easily discussed in conjunction with the models for electroluminescence, and so has been reserved for Section 5.3. It will be shown in Section 5.3 that two carrier space-charge-limited current (double injection) also does not consistently explain the experimental results.

The final mechanism to be considered here is quantum mechanical tunnelling. This mechanism is also expected to show little or no temperature dependence. The GaN LED's have the proper potential distri-

bution for quantum mechanical tunnelling through an approximately triangular potential barrier at the cathode (negative electrode). The electrons could tunnel from the n-GaN conduction band through the barrier at the i-n junction into the conduction band of the i-GaN:Mg (or i-GaN:Zn) with forward bias, and from the metal contact into the insulating region with reverse bias. This type of behavior is governed by the Fowler-Nordheim Equation [FOWLER and NORDHEIM, 1928],

$$J \sim F^2 \exp\left[\frac{-8\pi(2m^*)^{1/2}(q\phi_B)^{3/2}}{3qhF}\right], \qquad (5.1.6)$$

where J is the current density, F is the electric field in the barrier region, m* is the electron effective mass, q is the electronic charge, h is Planck's constant, and ϕ_B is the barrier height in volts. This equation was originally derived for cold cathode field emission of electrons from metals, and a complete derivation and discussion of the equation and of the topic of field emission can be found elsewhere [GOMER, 1961].

Before the Fowler-Nordheim Equation can be used, it is necessary to obtain the relationship between the electric field F in the barrier region and the applied voltage V. This can be done to a first approximation as follows. Starting with Poission's Equation in the depletion region at the barrier,

$$\frac{dF}{dx} = \frac{4\pi}{\epsilon} Nq. \qquad (5.1.7)$$

Integrating,

$$F(x) = \left(\frac{4\pi Nq}{\varepsilon}\right)x + c, \tag{5.1.8}$$

where c is a constant. The boundary condition at x = w, where w is the width of the depletion region, is

$$F(w) = 0. \tag{5.1.9}$$

Therefore,

$$F(x) = \left(\frac{4\pi Nq}{\varepsilon}\right)(x - w). \tag{5.1.10}$$

Now, if an electron at the cathode is at a potential V with respect to the anode, then

$$V(x) = -\int_{x}^{w} F(x)dx, \tag{5.1.11}$$

and

$$V(x) = \left(\frac{2\pi Nq}{\varepsilon}\right)(w - x)^2. \tag{5.1.12}$$

Substituting for (w - x),

$$V(x) = \frac{1}{2}\left(\frac{4\pi Nq}{\varepsilon}\right)^{-1} F^2(x), \tag{5.1.13}$$

and

$$F(x) = \left(\frac{8\pi Nq}{\varepsilon}\right)^{1/2} V^{1/2}(x). \tag{5.1.14}$$

Thus the dependence,

$$F \sim V^{1/2}, \tag{5.1.15}$$

may be substituted in the Fowler-Nordheim Equation yielding

$$I \sim V \exp[-V_o/V)^{1/2}], \qquad (5.1.16)$$

where

$$V_o = \frac{16\pi m^* \epsilon \phi_B^3}{9h^2 N} . \qquad (5.1.17)$$

The application of Equation 5.1.16 to the I-V characteristics of GaN m-i-n diodes is duscussed in the next section.

5.2 Mechanism for GaN m-i-n Diode Electrical Characteristics

The forward bias (+) I-V characteristics of the Mg-doped GaN diodes have been plotted in the form of log(I/V) vs. $V^{-1/2}$ to see if they fit Equation 5.1.16. For example, the data presented in log I vs. log V form in Figure 4.11 is shown in Figure 5.1 plotted to the Fowler-Nordheim Equation. A straight line is obtained over three orders of magnitude of current, from 2.5 to 25 volts. As another example, the data presented in Figure 4.14 have been replotted as log (I/V) vs. $V^{-1/2}$ in Figure 5.2 and again good agreement is found at all temperatures studied. Therefore the forward bias current-voltage dependence of GaN:Mg m-i-n diodes indicates current control at the negative electrode by a tunnelling mechanism.

This same relationship should hold for Zn-doped as well as Mg-doped diodes. A typical log I - log V characteristic for Zn-doped GaN LED's [PANKOVE, 1972, Figure 8] is shown in Figure 5.3. These data are plotted using the Fowler-Nordheim Equation in Figure 5.4 and once again a straight line is obtained for three orders of magnitude of current, between 2.5 and 25 volts. Sample heating becomes apparent at

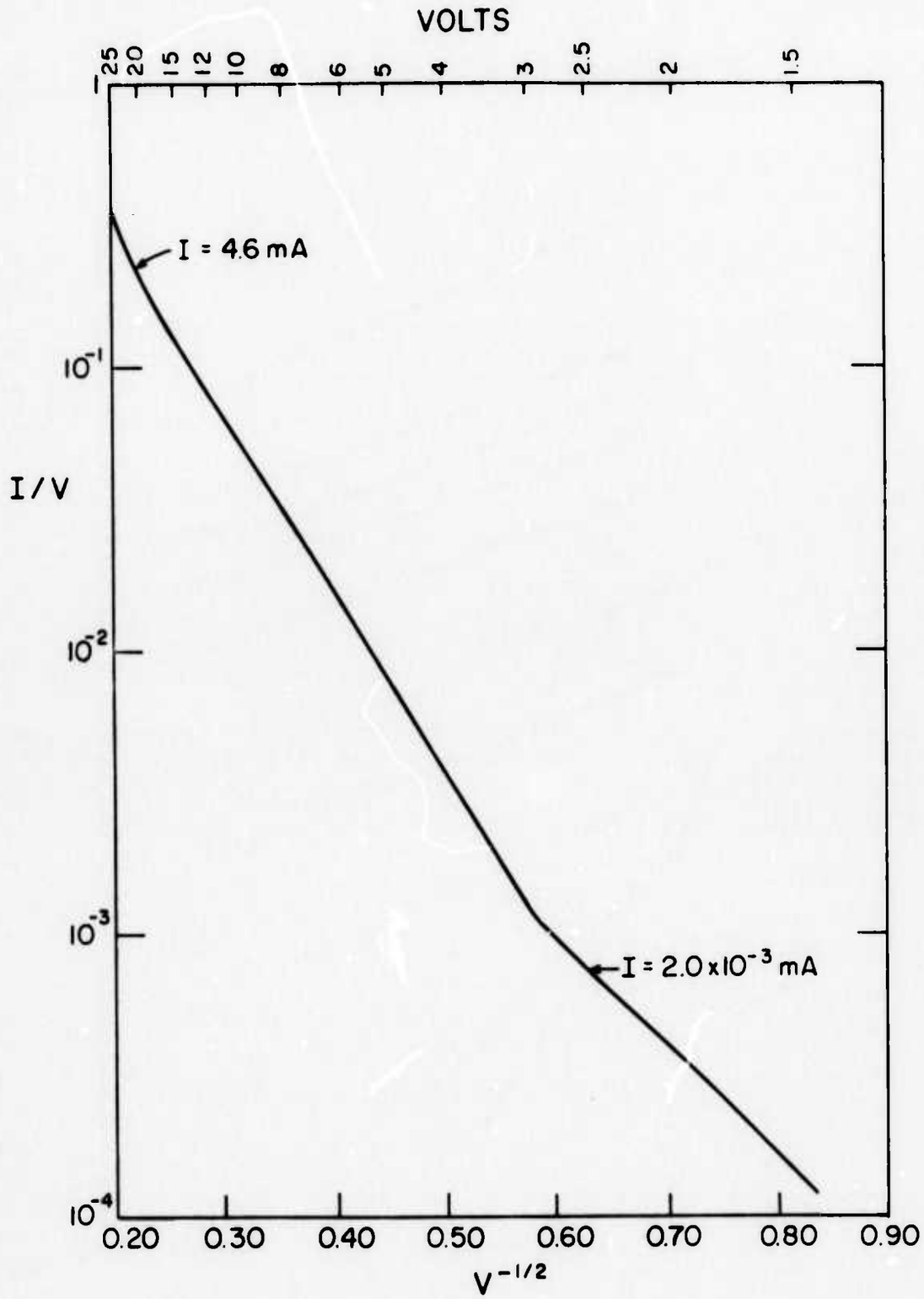

Figure 5.1 Fowler-Nordheim plot of GaN:Mg light-emitting diode current-voltage characteristic. Cf. Figure 4.11.

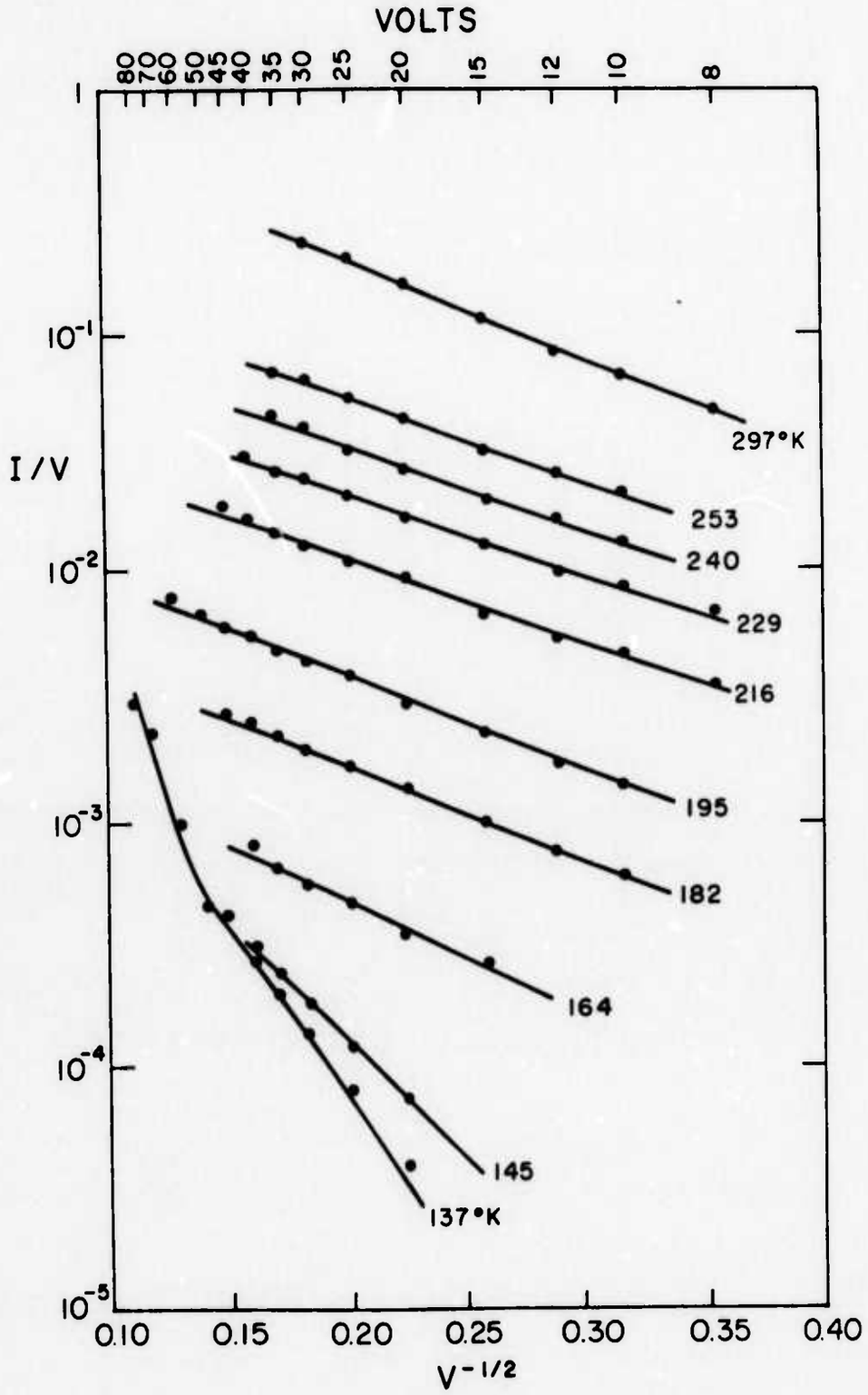

Figure 5.2 Fowler-Nordheim plot of GaN:Mg light-emitting diode current-voltage characteristics at various temperatures. Cf. Figure 4.14.

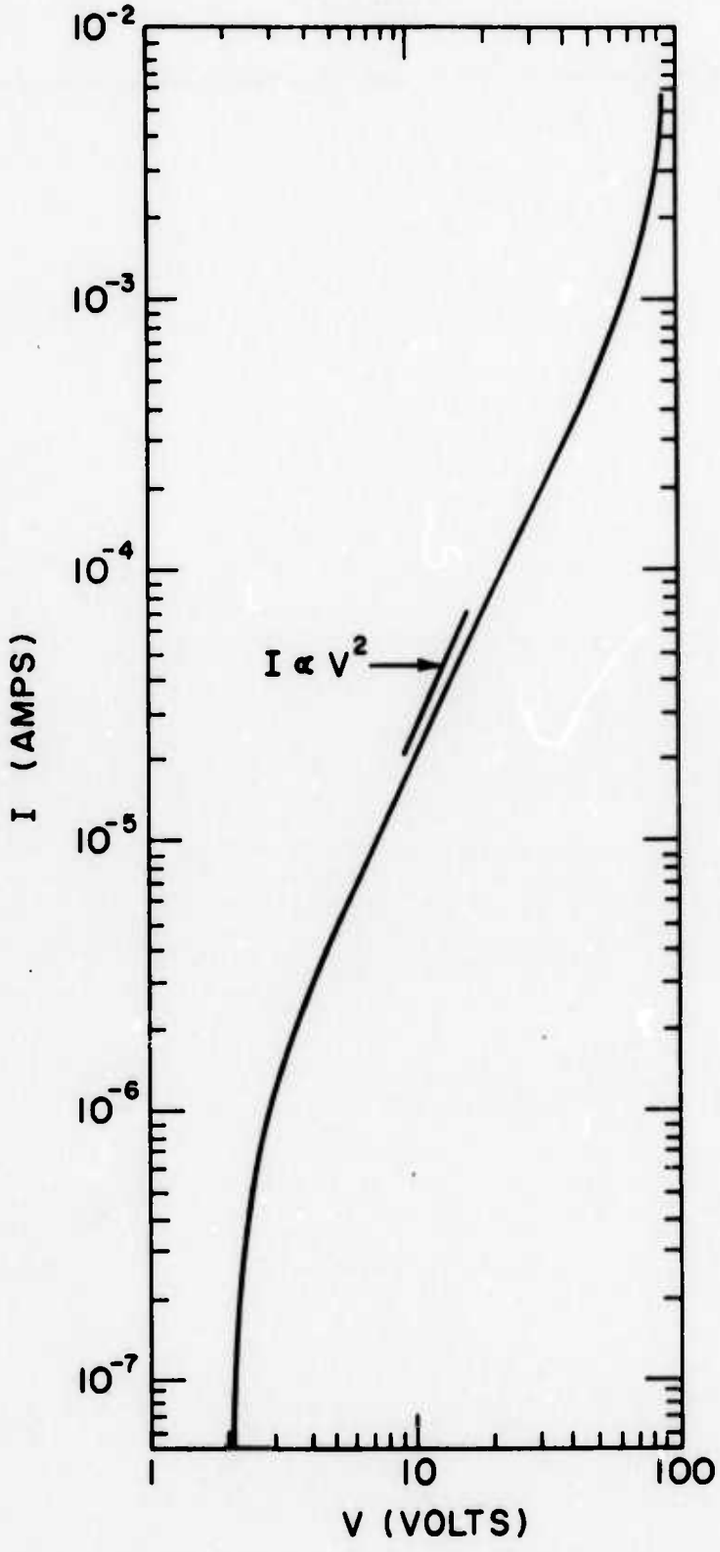

Figure 5.3 Plot of log I versus log V for GaN:Zn light-emitting diode (after PANKOVE, 1972, Figure 8).

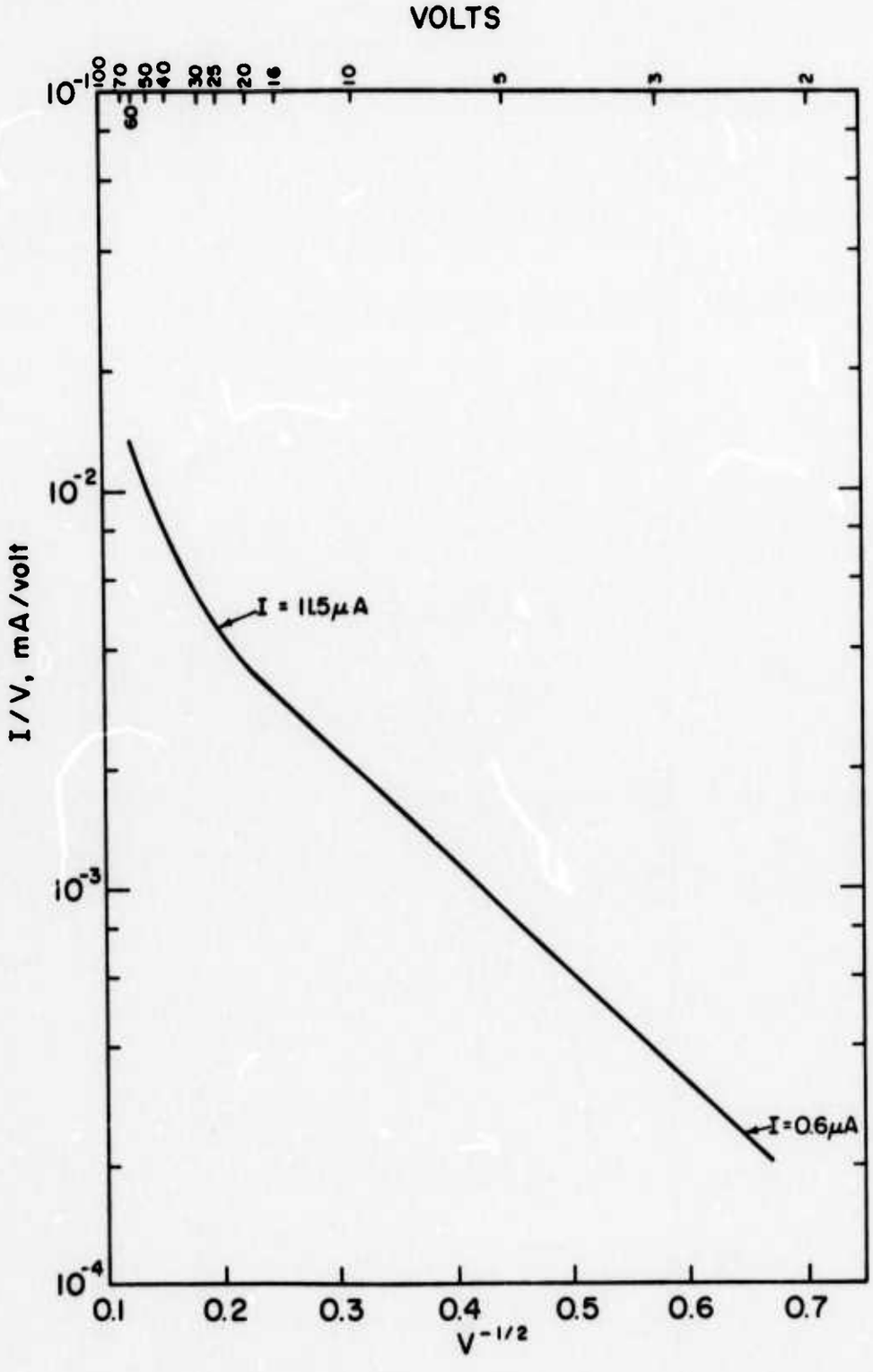

Figure 5.4 The I-V characteristic of the GaN:Zn light-emitting diode shown in Figure 5.3, replotted to the Fowler-Nordheim Equation.

higher voltages. It is interesting to note that an equation of the form $I = AV \exp[-(V_o/V)^{1/2}]$ can be approximated by power laws of the form $I \alpha V^n$ over short ranges of voltage.

It should be possible to obtain Φ_B by measuring V_o (see Equation 5.1.17), with $V_o^{1/2}$ taken from the slope of the Fowler-Nordheim plot. The value of $V_o^{1/2}$ is 14.5 for the diode of Figure 5.1 and 6.425 for the diode of Figure 5.4. Using $\varepsilon = 5.5$ and $m^* = 0.2$ m in Equation 5.1.16, then Φ is between 1.3 and 2.5 volts for the first diode and between 0.8 and 1.6 volts for the second diode, if it is assumed that $10^{18} \leq N \leq 10^{19}$ cm^{-3}. These are entirely reasonable values for the height of the potential barrier, which was shown to be about 1.7 volts in Section 5.1. An exact value of Φ_B cannot be obtained at this time because too many GaN parameters remain uncertain.

The reverse bias characteristics of the GaN diodes present a more formidable problem than the forward bias characteristics. The experimentally determined reverse bias current-voltage dependencies do not fit the Fowler-Nordheim Equation. The arguments given earlier in this chapter (Section 5.1) against the various other mechanisms for diode current flow are valid for the reverse as well as the forward characteristics. Evidently the m-i junction provides a more complicated barrier to current flow than the cases considered. Perhaps the complications arise due to the filling and emptying of surface state traps when a voltage is applied to the metal-insulator junction.

The model of diode current control by quantum mechanical tunnelling through a triangular potential barrier, governed by the Fowler-Nordheim Equation, has previously been proposed for ZnS electroluminescent diodes

[VECHT and WERRING, 1970; FISCHER, 1963]. There are in fact a number of other similarities between ZnS and GaN diodes. The ZnS diodes emit green and blue light, as do GaN diodes. Also, the same small value (~0.1 eV) for the thermal activation energy for the diode current has been reported for ZnS LED's [NEUMARK, 1956; THORNTON, 1961] as is reported for GaN LED's in the present study.

5.3 Mechanisms for Electroluminescence

Since p-type conductivity does not occur in ZnS and p-n junction formation is not possible, most workers concerned with LED's in that material have assumed that impact ionization is responsible for the observed electroluminescence [ZALM, 1956; PIPER and WILLIAMS, 1958]. They have concluded that the fields required for internal field emission of electrons from the luminescent centers to the conduction band are too high to be reasonable. For example, it was calculated [ZALM, 1956] that an electric field strength of 10^6 volts/cm would be necessary to achieve a rate of internal field emission of one excitation per second from an impurity level 2.4 eV below the conduction band in ZnS. For impact ionization a breakdown field of 6×10^5 volts/cm was calculated. An even higher field of 2×10^7 volts/cm for direct field ionization of ZnS luminescent centers (assumed in this case to be 3 eV below the conduction band) was calculated by Piper and Williams [PIPER and WILLIAMS, 1955]. Such calculations are not convincing because of the assumptions made in deriving the equations, and in addition many of the ZnS parameters used in the calculations were not known with any certainty. Performing calculations for GaN is even more difficult since less work has

been done with this material and fewer of the parameters are well-established. It appears from the ZnS calculations that perhaps the same magnitude of field strength is required for either process, and therefore they may both be occurring simultaneously, although as noted before, almost all ZnS studies have settled for the impact ionization mechanism, since it always involves the smaller required field. Calculations should be very similar for GaN, because the energy gap and depth of the luminescent centers for GaN and ZnS are almost the same. However, it should be noted from Figure 4.42 that the electric field at the GaN i-n junction is actually known: There is a drop of about 10 volts across 10^{-4} cm, giving a field of about 10^{5} volts/cm, a reasonable field for the impact ionization process.

The only clear, reliable evidence for the internal field emission process has been provided in reverse-biased p-n junctions in silicon [CHYNOWETH and McKAY, 1957]. Very abrupt junctions were fabricated in this small band gap (1.1 eV) semiconductor, in order to have a depletion region so narrow that impact avalanches could not form in it. The electroluminescence which was observed occurred uniformly throughout the samples. Reverse-biased silicon p-n junctions with a normal depletion region width exhibited pin-points of light, considered to be characteristic of impact ionization avalanches [CHYNOWETH and McKAY, 1956]. As another example, light that is emitted in the form of small distinct spots in ZnTe m-i-p diodes has recently been observed, and also ascribed to an impact ionization mechanism [DONNELLY, FOYT, LINDLEY and ISELER, 1970].

Most studies on ZnS electroluminescent diodes have shown that the

luminous intensity L is related to the applied voltage V by the expression,

$$L = L_o \exp(-b/V^{1/2}). \qquad (5.3.1)$$

The luminous intensity characteristics of the GaN LED's were plotted using this equation. For example, the results which were displayed on a linear scale in Figure 4.12 are shown in Figure 5.5 on a log L vs. $V^{-1/2}$ plot. Good agreement is found in the region above 10 volts. A definite threshold voltage of about 6 volts is apparent. In fact, this is the voltage at which the first light spots turn on, as observed in the microscope. This formulation of the luminous intensity equation holds for both forward and reverse bias, as shown in Figure 5.6. The luminous intensity data obtained at various temperatures which were displayed in Figure 4.14 have also been fitted to Equation 5.3.1 in Figure 5.7 and, again, good agreement is found at all temperatures. The threshold voltage (~8 volts) is again apparent.

The luminous intensity versus diode current is displayed in Figure 5.8 for the device whose characteristics were shown in Figure 4.14. In the current range above the luminescence threshold, the luminous intensity is approximately linearly proportional to the current. This indicates that a monomolecular process appears to be responsible for the luminescence. The intensity of light generated as a result of impact ionization is a linear function of the current [FISCHER, 1965, and MOREHEAD, 1967], whereas direct recombination of free electrons and holes following minority carrier injection is a bimolecular process yielding $L \alpha np$ and therefore a square law dependence of L on I [THORNTON, 1961; VECHT and

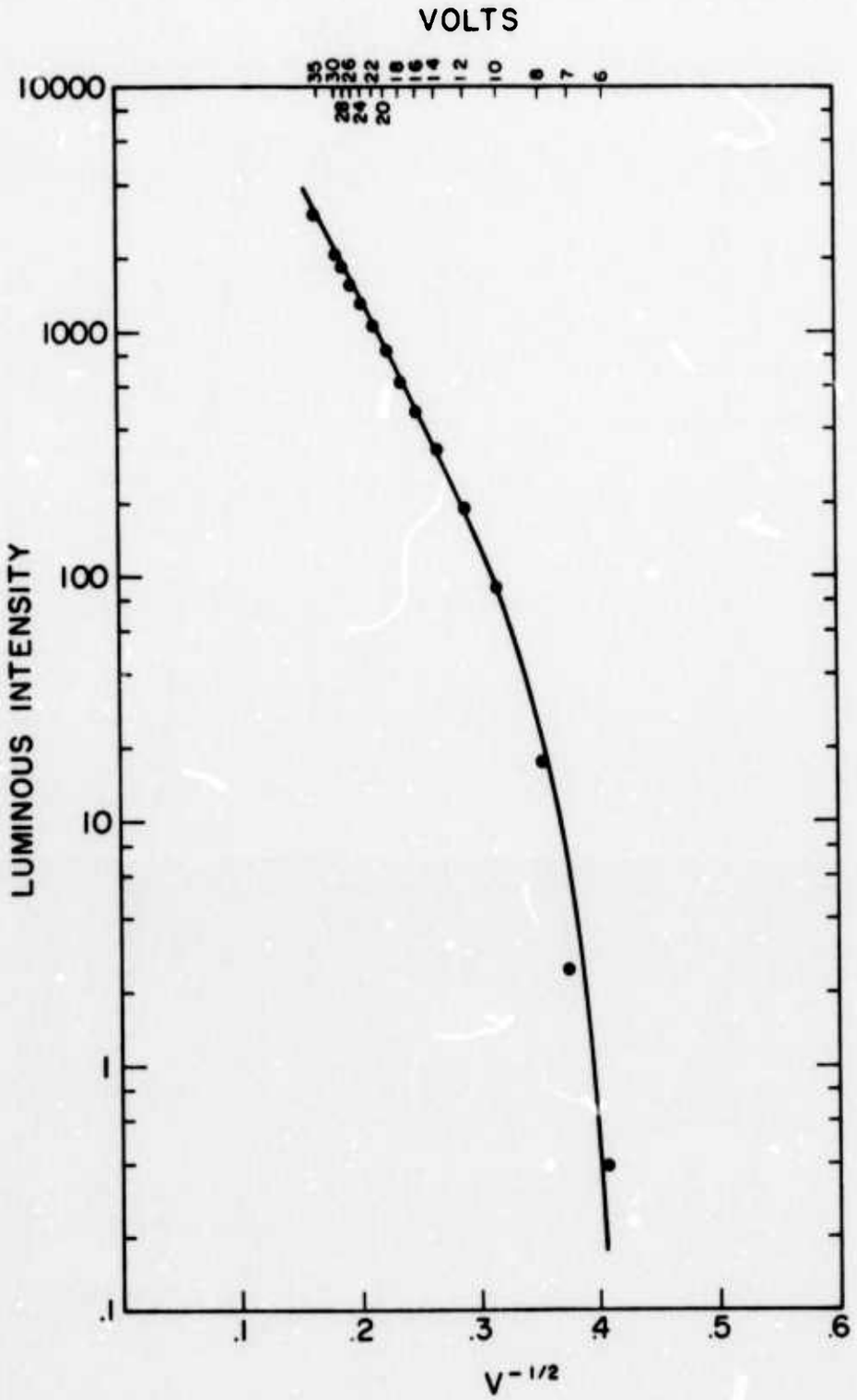

Figure 5.5 Log of electroluminescence intensity versus (voltage)$^{-1/2}$. Cf. Figure 4.12.

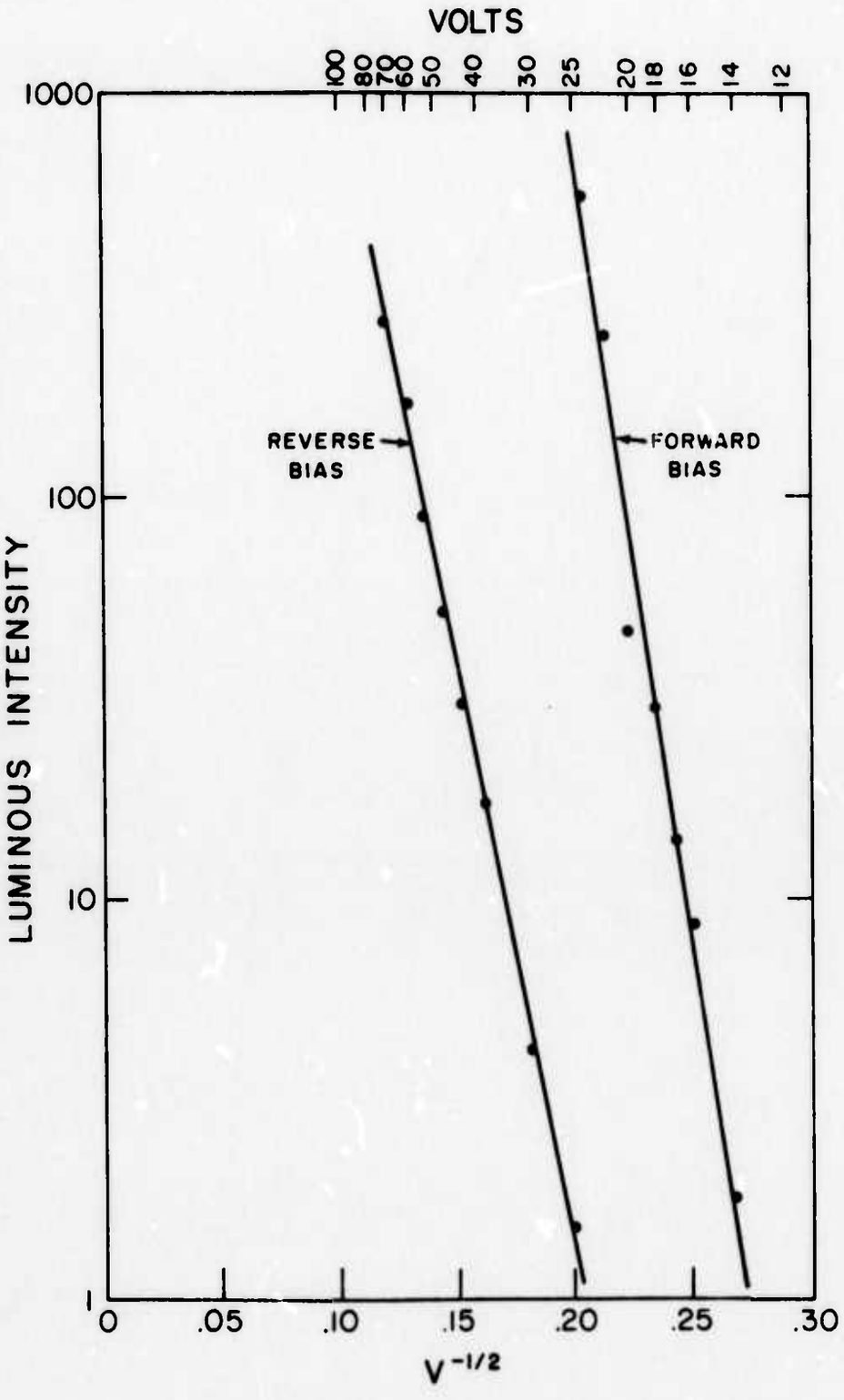

Figure 5.6 Log of forward and reverse bias electroluminescence intensity versus (voltage)$^{-1/2}$.

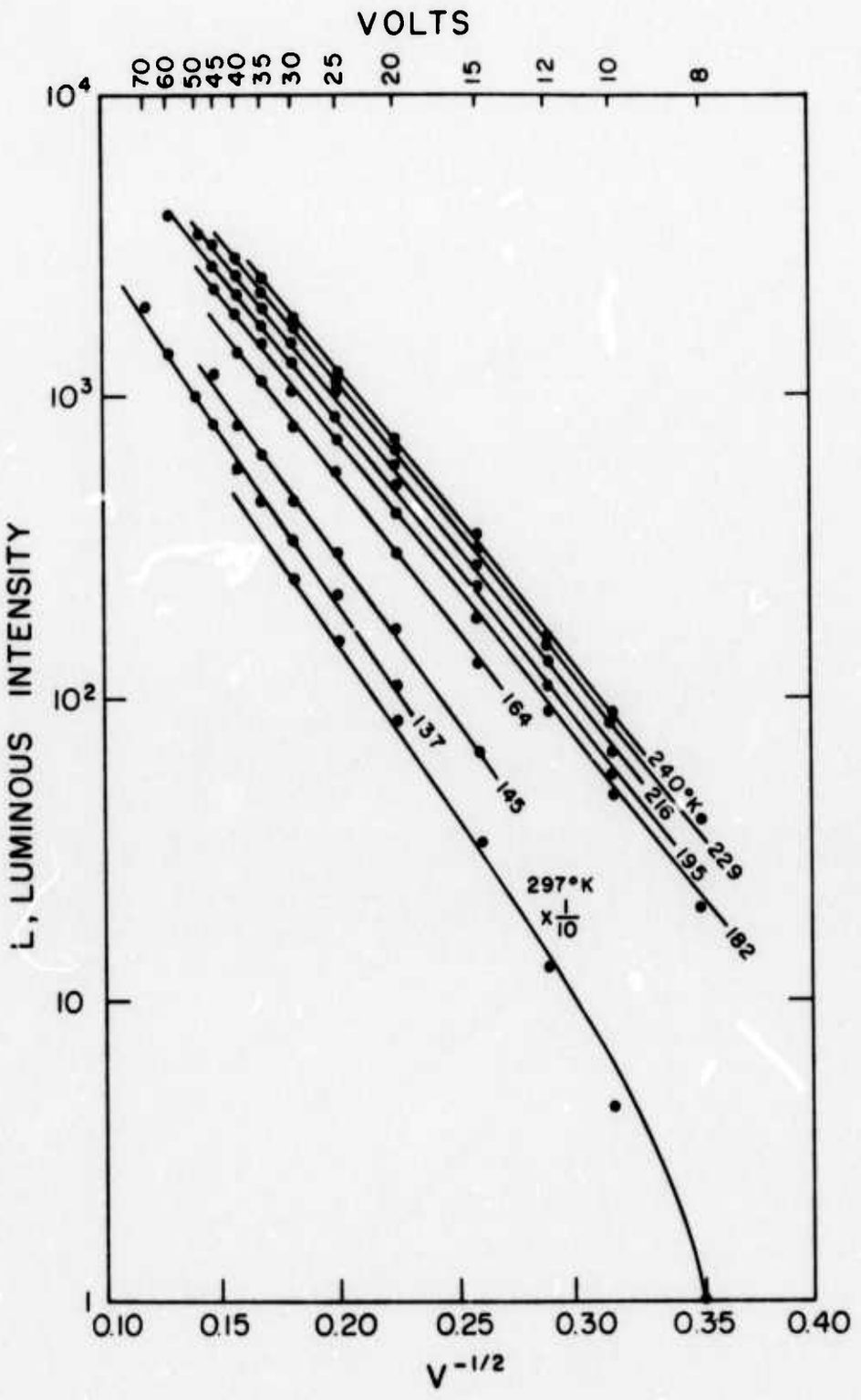

Figure 5.7 Log of electroluminescence intensity versus (voltage)$^{-1/2}$ at various temperatures. Cf. Figure 4.1

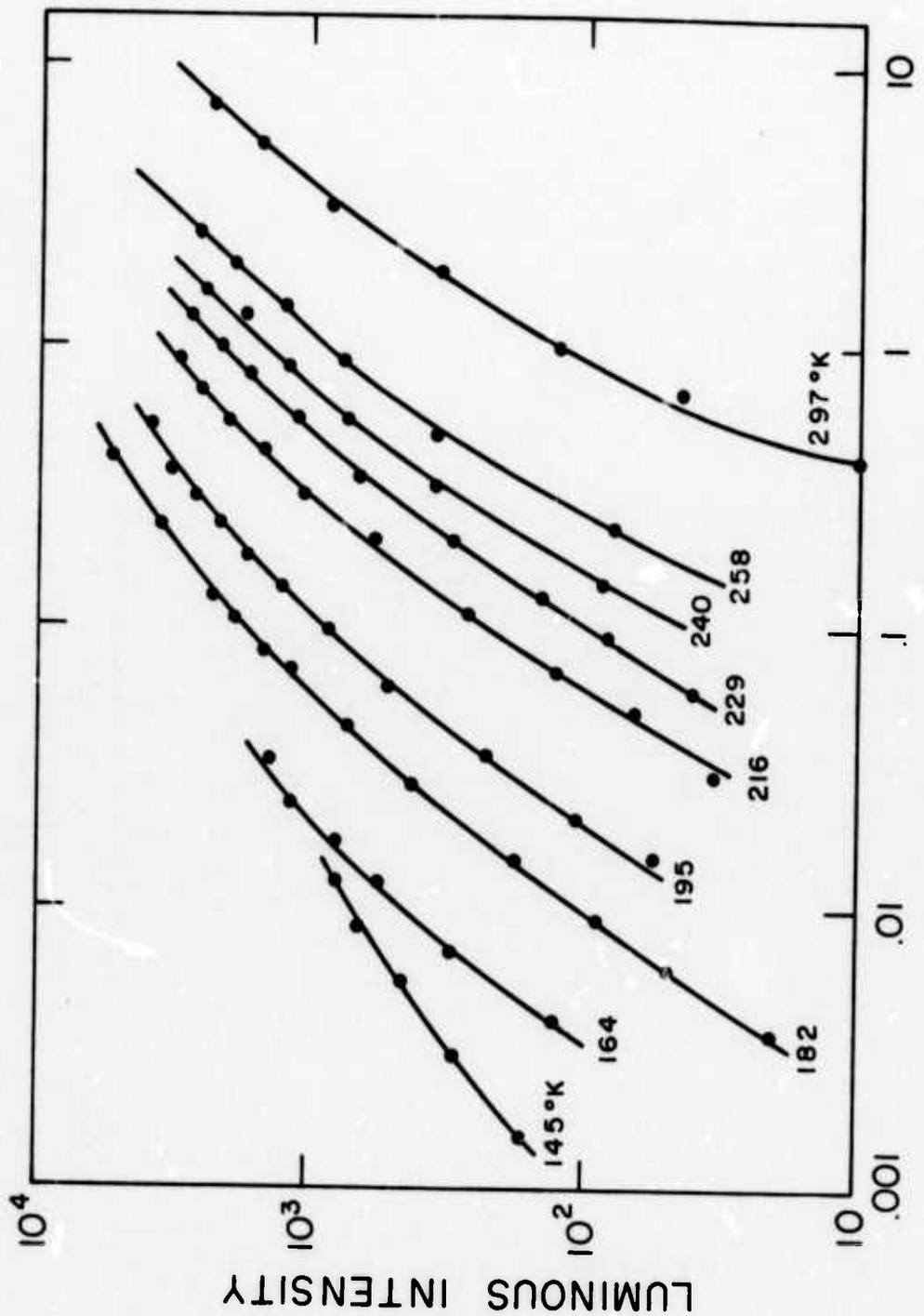

Figure 5.8 Log of luminous intensity versus log of diode current at various temperatures. Cf. Figure 4.14.

WERRING, 1970]. Unfortunately this is not an inviolable criterion for separating the processes of minority carrier injection and impact ionization, because high minority carrier injection levels give rise to a linear dependence of L on I [SMITH, 1957; LOEBNER and POOR, 1959; KEATING, 1963].

The possibility of double injection in GaN m-i-n diodes has recently been suggested to explain the electrical and electroluminescent characteristics of these devices [LOEBNER, 1973]. Specifically, this mechanism has been proposed [LOEBNER, 1973] to explain the properties of certain high-efficiency (~1% quantum efficiency at room temperature) green-light-emitting Zn-doped GaN diodes of Pankove and co-workers [PANKOVE, 1973]. These highly efficient GaN diodes apparently exhibit uniform light emission (generated at the cathode) over the entire sample [LOEBNER, 1973], in contradistinction to the present study where only spotty emission patterns (with light generated at the cathode) were observed.

The theories of the double injection phenomenon, which involves the simultaneous injection into an insulator or semiconductor of holes at the anode and electrons at the cathode, have been discussed at length by Lampert and Mark [LAMPERT and MARK, 1970]. Let us consider the case of double injection into a material with a single set of recombination centers and without thermal free carriers, a case particularly applicable to the insulating region of the GaN m-i-n diodes investigated throughout the present study. In the simplest case of this type discussed by Lampert and Mark, there is a single set of defect states (the recombination centers) lying well below the Fermi level and therefore completely occupied by electrons in thermal equilibrium. These recombi-

nation centers would correspond to the Mg levels in GaN. The assumption is made that the recombination centers are acceptor-like (consistent with our proposal for the Mg states in GaN), that is, negatively charged when occupied by electrons, so that the capture cross section for holes, σ_p, is much greater than the capture cross section for electrons, σ_n. Lampert and Mark point out that local electrical neutrality can be maintained for this situation through compensation of the acceptor-like recombination centers by shallow donors (again consistent with the GaN case proposed in the present study) which play no further role in the electrical behavior of the insulator.

At very low levels of injection, where the occupancy of the recombination centers remains undisturbed, the electron lifetime τ_n is essentially infinite since there are no empty traps to capture the electrons. On the other hand, the hole lifetime τ_p will be quite short and the injected current will essentially be a trap-free space charge limited electron current (as described in Section 5.1) which recombines with injected holes approximately within a diffusion length of the anode. Therefore under these low level injection conditions electroluminescence would be observed at the anode.

When the applied voltage is increased, the situation changes because holes are driven appreciable distances in the crystal. Because $\sigma_p >> \sigma_n$ the recombination centers quickly fill up with holes, and as this happens, the hole lifetime increases. At high injection levels both holes and electrons are injected into the insulator and it will become largely neutral, $n \approx p$. Under these conditions the steady state requires that $\tau_n \approx \tau_p$, and therefore the hole lifetime has greatly increased, perhaps

by many orders of magnitude. The "recombination barrier" to the passage of holes decreases with increasing injection level: the more holes injected, the easier it is for them to traverse the insulator. In fact it becomes so much easier that the voltage required will actually decrease as the current increases, leading to a region of current-controlled negative resistance in the device I-V characteristics. This negative resistance has been observed in numerous studies of double injection [for example, ASHLEY, 1963; BARNETT and MILNES, 1966; TYLER, 1954; HOLONYAK, 1962]. A generalization of the preceding model considers that the recombination centers may be only partially occupied at the outset, but the current-voltage characteristic for this case is very similar to the previous derivation, except for some changes in details [LAMPERT and MARK, 1970].

It is of interest to discuss one of the papers on double injection in insulating CdS [SMITH, 1957]. The CdS crystals used in the study were pure, undoped, high-resistivity (insulating) n-type. Gallium electrodes were spaced about 1 mm apart on the face of a crystal, and a potential difference of several hundred volts was applied across the electrodes. As the voltage was increased, electroluminescence was observed, first as a few bright spots at the anode. As the voltage was further increased, green beams of light were observed to originate from the bright spots at the anode and then to extend across the crystal, so that eventually the entire crystal was filled with green light. These observations were interpreted in terms of the injection of electrons and holes into the crystal from the contacts, followed by band to band recombination.

Let us return now to the GaN m-i-n diodes. It must be agreed that double injection cannot occur with reverse bias: there are no holes in the n-GaN to be injected. Now consider Figures 4.26 and 4.27. The light spots shown in the two figures are quite similar, although the forward bias spots (Figure 4.26) do not appear at the same positions as the reverse bias spots (Figure 4.27). If it is agreed that reverse bias spots were created by impact ionization, then it should be noted that the forward bias light spots have a very similar appearance. Recall also that with double injection in the presence of recombination centers, the light should move from the anode towards the cathode with increasing bias voltage, with the brightest light eventually appearing where the pn product is maximum. This position might be at the cathode, but no experimental evidence for movement of the light spots through the i-layer with increasing voltage has been observed in the present study. Furthermore, no negative resistance region in the I-V characteristics has been found, and the current at a fixed voltage was shown to be essentially independent of the thickness d of the insulating region, while for the double-injection mechanism it is expected that $I \alpha d^{-3}$ [LAMPERT and MARK, 1970]. In addition, one might expect to see some small evidence of band to band recombination of electrons and holes with double injection, but none has ever been reported in the GaN literature, and none was observed in this study.

The lack of observation of any of the phenomena discussed above in GaN m-i-n diodes certainly does not catagorically rule out the possibility of double injection electroluminescence. However, if any of them should be identified in the GaN devices in the future it will certainly

make a double injection model more plausible. It should be pointed out that the present observations which give support to the double injection theory are: a) the potential distribution, with high field regions at the electrodes, is consistent with the model [see LAMPERT and MARK, 1970]; b) the efficiency of some GaN diodes, especially the 1% efficiency for green Zn-doped diodes, appears too high for an impact ionization process; c) the diodes exhibit $I \alpha V^2$ electrical characteristics, consistent with the double injection theory [LAMPERT and MARK, 1970]. From our observations in the present study, we cannot quarrel with a) and b). However, as far as c) is concerned, I is apparently only always proportional to V^2 for the Zn-doped diodes of Pankove, while we have observed powers of between 2 and 3 for the Mg-doped diodes. In addition, powers of 4 and 5 have been found at lower voltages (both for Mg- and Zn-doped diodes) while the double injection model predicts a linear dependence of I on V at small voltages. Therefore it is thought that double injection may well be an attractive model for explaining the characteristics of highly efficient, uniformly emitting, green Zn-doped GaN m-i-n diodes, but we have reservations about applying it to the particular Mg-doped GaN diodes employed in the present study.

5.4 Impact Ionization in GaN m-i-n Diodes

Experimental evidences such as cathodic origin of the light emission, linear dependence of brightness on current, threshold voltage for light emission at above band gap voltage, and high field strength in the depletion region suggest impact ionization as a possible excitation mechanism for electroluminescence [PARK, GEESNER, and SHIN,

1972]. The impact ionization process is described in this section.

When an electrical conduction process obeys Ohm's Law, the free charge carriers involved in the conduction have thermal energies which are much greater than the energy corresponding to the drift velocity under the applied field. The electron energy distribution is governed by the lattice temperature, and electron interactions with acoustical phonons maintain equilibrium. Departures from thermal equilibrium occur when very high fields are applied. An effective electron temperature T_e can be defined, which is greater than the lattice temperature. Low energy electrons lose the energy they gain from the field through elastic collisions with phonons. Very high energy electrons retain some of their energy after collisions, and their average energy increases as a result of this cumulative process. On this basis it can be calculated [GOFFAUX, 1956 and 1957] that the average electron temperature T_e is related to the lattice temperature T and the applied field F by

$$\frac{1}{kT_e} = \frac{1}{kT} - \frac{cF^2}{h\nu_L}, \qquad (5.4.1)$$

where c is approximately constant and ν_L is the frequency of lattice vibrations.

In order to establish a relationship between the luminous intensity and the applied voltage, we may consider a very simple classical model for the impact ionization process. There is necessarily a minimum energy E_m required for the removal of an electron from a luminescent center into the conduction band through a collision process. It is possible to estimate the probability of an electron in the conduction

band actually attaining such an energy from the electric field [HENISCH, 1962]. Suppose an electron has a free path ℓ between collisions. Then in this path of length ℓ it will gain an energy $q\ell F$. If $\bar{\ell}$ is the mean free path for electrons and a Boltzmann distribution is assumed, then the number of electrons having free paths of length ℓ or greater can be expressed as

$$n = n_o \exp(-\ell/\bar{\ell}) \tag{5.4.2}$$

$$= n_o \exp(-E_m/q\bar{\ell}F). \tag{5.4.3}$$

The same field dependence for the ionization probability, $P = \exp(-\text{const.}/F)$, has been found by considering statistical fluctuations [SEITZ, 1949].

Now, the light emission intensity should depend partly on the ionization probability and partly on the number of carriers available for acceleration by the field. If the ionization probability is the governing term, then Equation 5.2.3 should give the field dependence of the luminous intensity. Using the dependence of the field on the applied voltage derived earlier, viz., $F \sim V^{1/2}$, then

$$L = L_o \exp(-b/V^{1/2}), \tag{5.4.4}$$

which is, indeed, the observed relationship between L and V for the GaN LED's. Notice that if the supply of primary electrons is the governing term, then the same type of L-V dependence is predicted from Equation 5.1.15.

The argument give above is not very convincing [HENISCH, 1962].

It assumes that the energy distribution of free electrons is independent of the applied field, whereas the discussion at the beginning of the section indicated that the electron distribution can be strongly affected by the presence of a high field. One may assume that the emission intensity is proportional to the number of electrons having energies in excess of E_m at an electron temperature of T_e. Then

$$L = L_o \exp\left[-\frac{E_m}{kT}\left(\frac{T}{T_e}\right)\right], \tag{5.4.5}$$

and substituting for T_e from Equation 5.4.1,

$$L = L_o \exp\left(-\frac{E_m}{kT}\right)\exp\left(\frac{E_m cF^2}{h\nu_L}\right). \tag{5.4.6}$$

Now, E_m must be at least 2.9 eV for the GaN LED's. However, the activation energy for the temperature dependence of L was found to be about 0.05 eV. In addition, Equation 5.4.6 does not predict the field dependence that has been found.

One therefore may assume that either the supply of primary electrons determines L, that the electron temperature hardly deviates from the lattice temperature, or else that the situation is perhaps more complicated. It is interesting to note that the emission intensity falls off rapidly to zero beyond about 3 eV, giving no indication of hot electrons recombining with the luminescent centers. This fact indicates that most of the electrons in the conduction band are not at high energies but are in thermal equilibrium at the bottom of the band. This would certainly explain the low efficiency of the diodes: most of the electrons merely

pass through the i-layer without contributing to the electroluminescence. A shift in the position of the luminescence peak to shorter wavelengths with increased bias voltage, and hence electric field, was shown in Figures 4.4 and 4.6. This can be explained by noting that the luminescence centers are not at a discrete energy level but are spread out into a narrow band, as shown by photoluminescence, and therefore increasing the field allows the emptying of the deeper lying levels by impact ionization.

Actual evidence of impact ionization (avalanche multiplication) has been found in the GaN LED's. Carrier multiplication can be measured by studying the diode photocurrent as a function of applied bias voltage, the process of photomultiplication [LIVINGSTONE and ALLEN, 1970]. When band gap light is focussed on a semiconductor junction, the hole-electron pairs which are created are separated by the junction field. These carriers then comprise the photocurrent. This excess current will not be influenced by the applied bias unless impact ionization is taking place. If it is, then at some voltage level the photocurrent will begin to increase with applied bias. The carrier multiplication factor M is the ratio of the photocurrent at a high bias voltage to the (constant) value of the photocurrent at low levels of bias. The carrier multiplication factor observed for the GaN diodes studied is shown in Figure 5.9. This helps to confirm the impact ionization mechanism.

The catastrophic consequences of dielectric breakdown can be avoided by an inhomogeneous field distribution in the crystal during the operation of the acceleration mechanism of excitation of electroluminescence. That is, since this mechanism operates at field strengths approaching or even

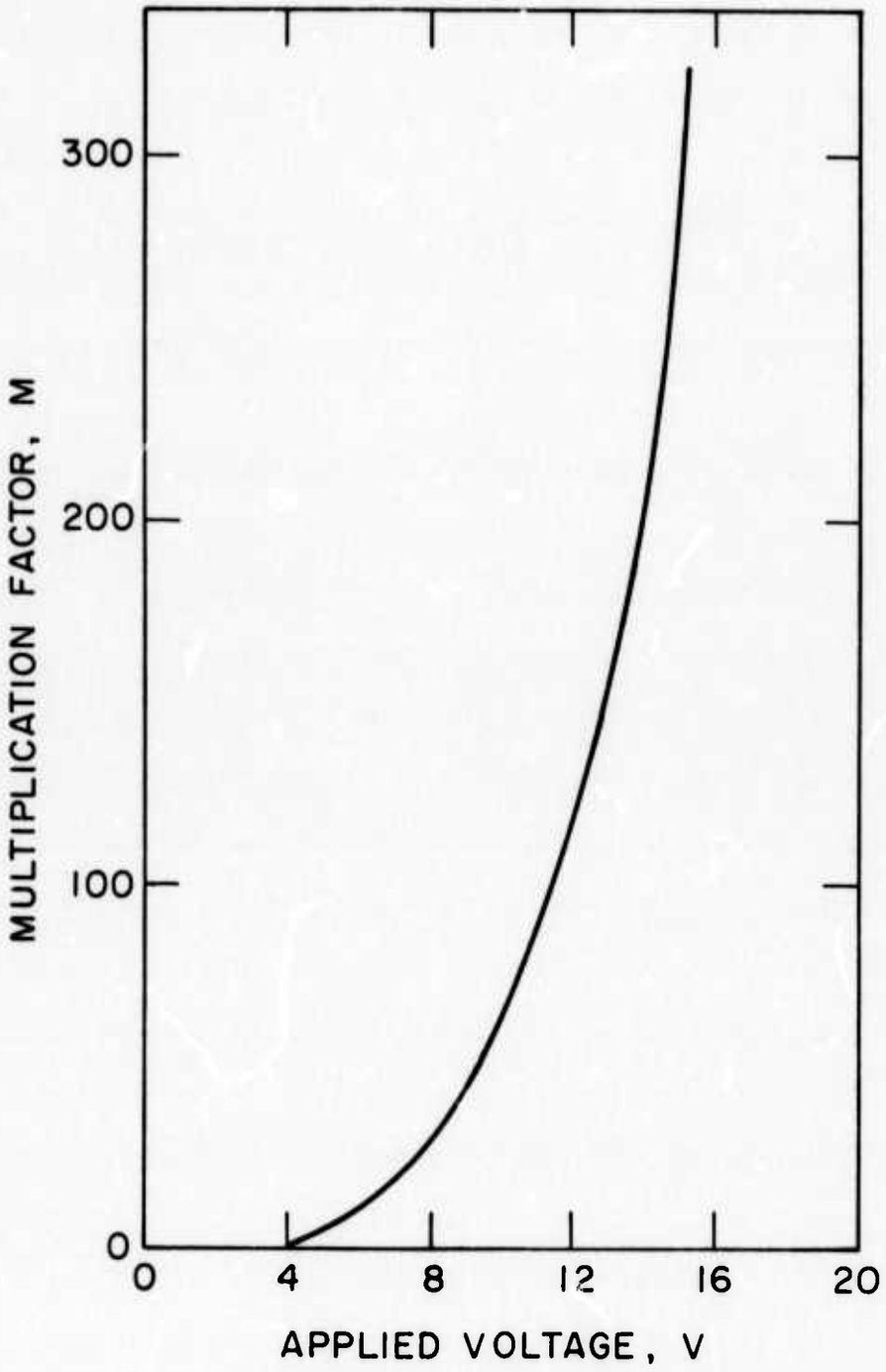

Figure 5.9 Carrier multiplication factor M as a function of applied voltage for a GaN light-emitting diode.

equallying the field strengths which are ordinarily responsible for dielectric breakdown, field configurations yielding stability against breakdown are necessary. For example, a narrow high-field region in series with an extensive low-field region permits operation over a broad range of applied voltages without creation of an unstable breakdown condition. The electron multiplication in the high-field is terminated in the low-field region before avalanches sufficiently great for breakdown can develop. The potential and field distribution proposed for the GaN LED's in Section 5.5 is particularly stable against dielectric breakdown because, in addition to the required inhomogeneous field distribution involved, the width of the depletion region broadens while the fields in the barrier increase as the square root of the applied voltage. However, it has been noted earlier (Section 4.6) that a continuous increase in the voltage applied to a diode results in the burn-up of the brightest light spot and a short-circuited diode. At the position of the brightest light spot a tiny black dot, burnt through the insulating region, remains. It is possible that this catastrophic burn-up of a diode at a single point is due to dielectric breakdown from the avalanche multiplication occurring in the light spot at that point.

It is possible to derive the dependence of the external quantum efficiency on the applied voltage with an impact ionization mechanism. Suppose again that the number of luminescent centers which are ionized at any given time is small and may be neglected compared to the total number of such centers N_L. When an electron crosses the depletion region of width w, it interacts with $\sigma w N_L$ of the centers, where σ is the cross-section for impact ionization. Then the quantum efficiency

of the electroluminescence, η_q, is the product of the number of centers ionized and the radiative efficiency of recombination, η_{rad}, so that

$$\eta_q = \sigma w N_L \eta_{rad}. \tag{5.4.7}$$

The cross-section for impact ionization may be expressed as

$$\sigma = \sigma_o \exp[-(F_o/F)], \tag{5.4.8}$$

if the excitation process has a sharp energy threshold and if the mean electron energy is much less than the threshold energy [THORNTON, 1967]. Now assuming that

$$w = V/F, \tag{5.4.9}$$

and

$$F \sim V^{1/2}, \tag{5.4.10}$$

then

$$\eta_q = \sigma_o w N_L \eta_{rad} \exp[-(F_o/F)] \tag{5.4.11}$$

$$= \sigma_o N_L \eta_{rad} \frac{V}{F} \exp[-(F_o/F)], \tag{5.4.12}$$

or

$$\eta_q \sim V^{1/2} \exp[-(V_o/V)^{1/2}]. \tag{5.4.13}$$

The results shown in Figure 4.9 have been plotted as $\eta_q/V^{1/2}$ vs. $V^{-1/2}$ in Figure 5.10. Excellent agreement is found at applied voltages below

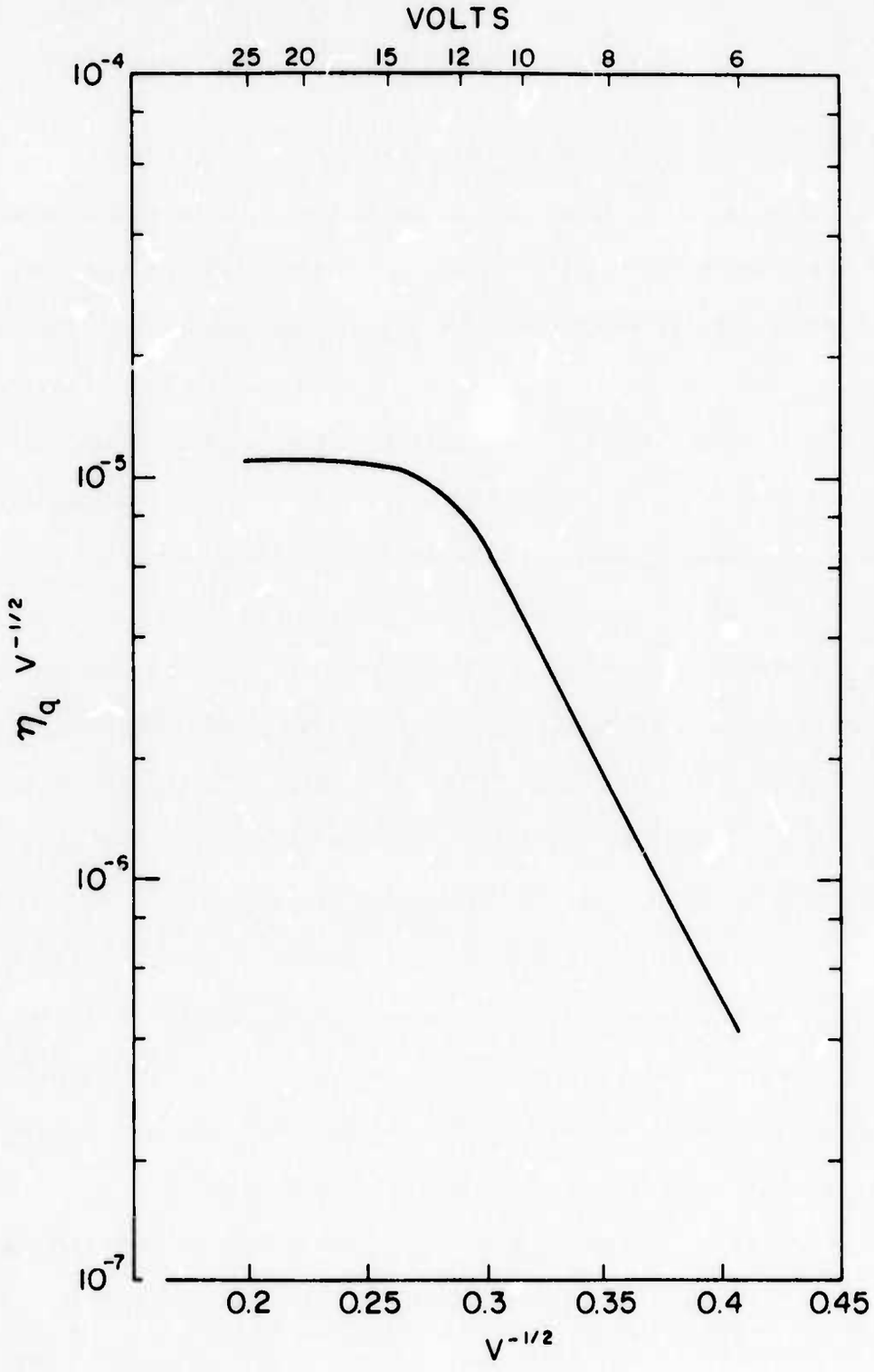

Figure 5.10 Plot of (external quantum efficiency) x (voltage)$^{-1/2}$ versus (voltage)$^{-1/2}$.

about 14 volts. This gives further support to the model.

5.5 Nature of the Potential Barrier

There can be no doubt that potential barriers exist in the m-i-n structure GaN light-emitting diodes. (If there were no barriers, then the device current would simply be directly proportional to the applied voltage, and this is not the case.) The two regions in the devices which have steep potential gradients have been clearly identified in the SEM (Section 4.8). These two areas are the transition region between the metal contact and the doped insulating GaN layer (the m-i junction), and the transition region between the doped insulating GaN and the undoped n-type GaN (i-n junction). In addition, the i-n junction has been unambiguously identified as source area for the forward-bias electroluminescence, while the m-i junction is apparently responsible for the reverse-bias electroluminescence. A gradient in potential gives rise to an electric field, which is the force seen by a charged particle. Electroluminescence is light created due to the action of an electric field, so there must definitely be an electric field and consequently a potential barrier at the i-n junction. It is expected that the same applies to the m-i junction, especially since the potential drop at this junction was actually seen in the SEM.

A potential barrier is set up by a region of uncompensated charge. Consider for example an ordinary p-n junction in a semiconductor material. The portion of the material which is n-type contains donor impurities. These donor impurities each have an extra electron in excess of the number necessary for the bonding requirements of the host

semiconductor. The p-type portion contains acceptor impurities which each lack one bonding electron. The donors and acceptors are thermally ionized so that the excess electrons are placed in the conduction band in the n-type portion while electrons from the valence band move to the acceptor impurities in the p-type portion, leaving holes in the valence band. At the junction between the n- and p-type regions, there are concentration gradients of mobile electrons and holes. Therefore holes diffuse from the p to the n side, while electrons diffuse from n to p. The electrons and holes which have diffused across the junction in opposite direction each encounter carriers of the opposite type in the region into which they have diffused. Thus, for example, electrons which diffuse into the p-type region are then situated in a region with a large concentration of holes, and the two types of carriers recombine and so are removed. However, for every electron which has diffused from the n- to the p-type region, an uncompensated positively charged donor ion is left behind in the n-type material. In the same way uncompensated negatively charged acceptor ions remain in the p region. An electrical double-layer of positive and negative charges is thereby formed. An electric field is associated with this double-layer of charge, and it is so directed as to oppose further diffusion of mobile electrons and holes. It is in this way that the potential barrier at a p-n junction is formed. The situation is depicted graphically in Figure 5.11.

The application of a forward bias to the p-n junction serves to decrease the potential barrier and to allow the carriers to again diffuse. The carriers which diffuse across the junction are minority

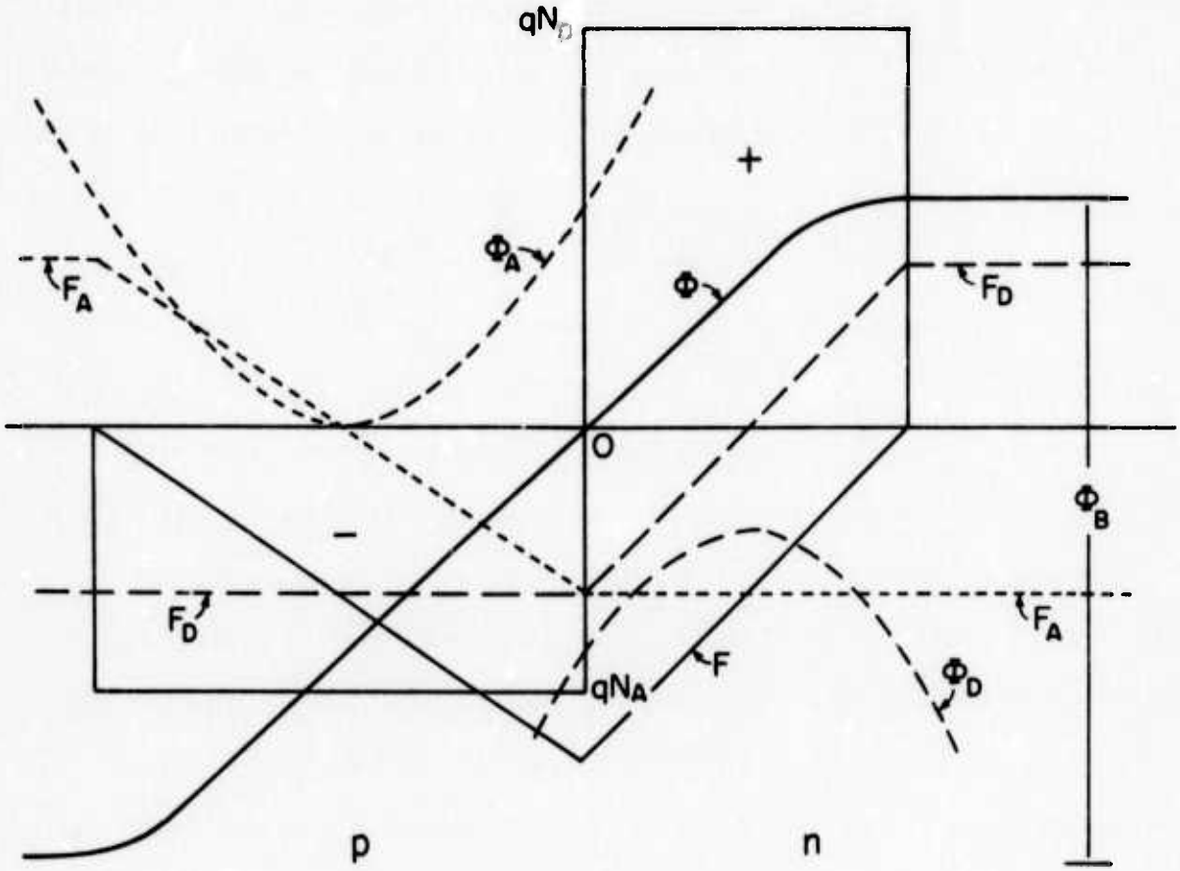

Figure 5.11 Charge concentrations, electric fields, and electric potentials at a p-n junction. N_A, N_D are respectively the concentrations of acceptors and donors; F_A, F_D, and F are respectively the electric field due to the ionized acceptors, electric field due to the ionized donors, and total electric field; Φ_A, Φ_D, and Φ are respectively the potential due to the ionized acceptors, potential due to the ionized donors, and total potential; and Φ_B is the barrier potential.

carriers in the region in which they have diffused, and may radiatively recombine with majority carriers present there to produce electroluminescence. Application of a forward bias does not reduce the junction potential barrier in the GaN m-i-n diodes. The junction in question is not a p-n junction, but an i-n junction. Suppose the i-region is considered to be high resistance p-type. If this really were a "p"-n junction which could be forward biased so that the barrier is reduced, then the current-voltage characteristics should follow the standard p-n junction equation

$$I = I_o[\exp(qV/kT)-1]; \qquad (5.5.1)$$

however, this dependence was not found. Furthermore, band gap light should be emitted and the devices should show high luminous efficiencies, but neither of these is true. Another model for the potential barrier is obviously required.

Consider the model for the potential barrier proposed for ZnS [ZALM, 1956]. A ZnS crystal was assumed to be in contact with two metal electrodes, one at each end. ZnS is insulating, with donor impurity levels 0.4 eV below the conduction band, plus a set of deep luminescent centers. Electrons from the donors in the ZnS nearest to the electrodes escape to the electrodes, resulting in a positive space charge in the ZnS and an equal negative charge in the electrodes.

Now suppose a potential difference is applied across the electrodes, making one negative and one positive. The barrier at the cathode (negative electrode) increases and a greater part of the voltage drop is found at the barrier than would correspond to a linear potential distri-

bution. The increased barrier requires increased positive space charge at the cathode. This cannot be formed by thermal excitation in ZnS, because the donors are much too deep. Instead the model assumes that these 0.4 eV deep donors can be emptied by internal field emission, or else that the impact ionization process which empties the luminescent centers serves to provide the positive charge simply by emptying these centers of their electrons.

In either case, the electric field is strongest at the metal-ZnS interface and electrons from the metal penetrate the cathode barrier by tunnelling and are accelerated in the high field surface region until they have sufficient energy to carry on the excitation of the luminescent centers.

The situation in the GaN m-i-n diodes is analogous but with important differences. The donor levels in undoped GaN show no thermal activation energy at all and are apparently right at the bottom of the conduction band. Thus GaN is an excellent n-type conductor. The addition of Zn or Mg makes the GaN insulating; apparently these impurities form deep acceptors which compensate the donors. There must be significantly more acceptors than donors, or else the GaN would still appear n-type and the Fermi level would be close to the conduction band rather than at the center of the energy gap. Therefore the i-region must contain uncompensated acceptors. An estimate of their number, made from capacitance measurements, is approximately 10^{16} cm^{-3}; however the interpretation of capacitance measurements on such a complicated system as the GaN m-i-n diodes is difficult and this calculated number may not be reliable. At the i-n junction, the potential barrier is

formed by electrons diffusing from the n-region into the i-region, where they become trapped on the acceptors. A forward bias causes electrons to penetrate the barrier by tunnelling. These electrons also become trapped and therefore increase the barrier until all the traps are filled. In this way most of the potential drop occurs across this junction, as was demonstrated in the SEM studies.

There is one difficulty with this model. If the traps were uniformly distributed throughout the i-region, then the whole i-region should become negatively charged as all the traps fill. It is therefore necessary to assume that there are excess traps just in the region of the junction. This is reasonable, since the lattice parameters of undoped and Mg-doped GaN are sufficiently different to cause strains and therefore defects such as dislocations at the junction. A similar model may be applied to the reverse-bias situation.

5.6 Model for GaN Light-Emitting Diodes

Based on the foregoing discussion of experimental results and theory, the following model is proposed to explain the operation of GaN light-emitting diodes. The diodes consist of a highly conducting region of n-type GaN with a large number of shallow, fully ionized donors, an insulating region of GaN which is heavily doped with deep acceptors (luminescent centers), and a non-ohmic metal contact to the insulating region. When the metal contact is biased positive with respect to the n-GaN region, electrons tunnel from the conduction band of the n-GaN into the conduction band of the i-GaN. Here a region of high field is encountered, and some of the electrons are accelerated to high energies.

Electrons having sufficiently high energies can impact ionize the filled luminescence centers in this i-GaN region. Most electrons are in thermal equilibrium in the i-GaN conduction band, and it is the recombination of these electrons with the empty luminescent centers that is responsible for the electroluminescence. These processes are shown schematically in Figure 5.12.

The same explanation, viz., quantum mechanical tunnelling, may also be applicable to the reverse bias current-voltage characteristics. An impact-ionization mechanism is probably also responsible for the reverse bias electroluminescence. However, the reason for the appearance of the reverse bias electroluminescence peaks at wavelengths which are not the same as the forward bias electroluminescence and the photoluminescence peak remains unclear.

A further insight into this picture is presented by diodes where the insulating layer is formed by proton bombardment. These devices exhibit non-ohmic diode electrical characteristics and electroluminescence when reverse bias is applied, but have an ohmic character with a complete lack of light generation with forward bias. The reverse-bias characteristics are controlled by the m-i junction, and this interface has the same abrupt form in the proton bombarded diodes as it does in the doped-during-growth diodes. It is simply a barrier between a metal and an insulating semiconductor with different work functions. However, the i-n junction controls the forward-bias diode characteristics, and this interface is not expected to be th same for the two types of devices. In fact, it is reasonable to expect that the transition from n-type GaN to a disordered i-type GaN produced by proton bombardment

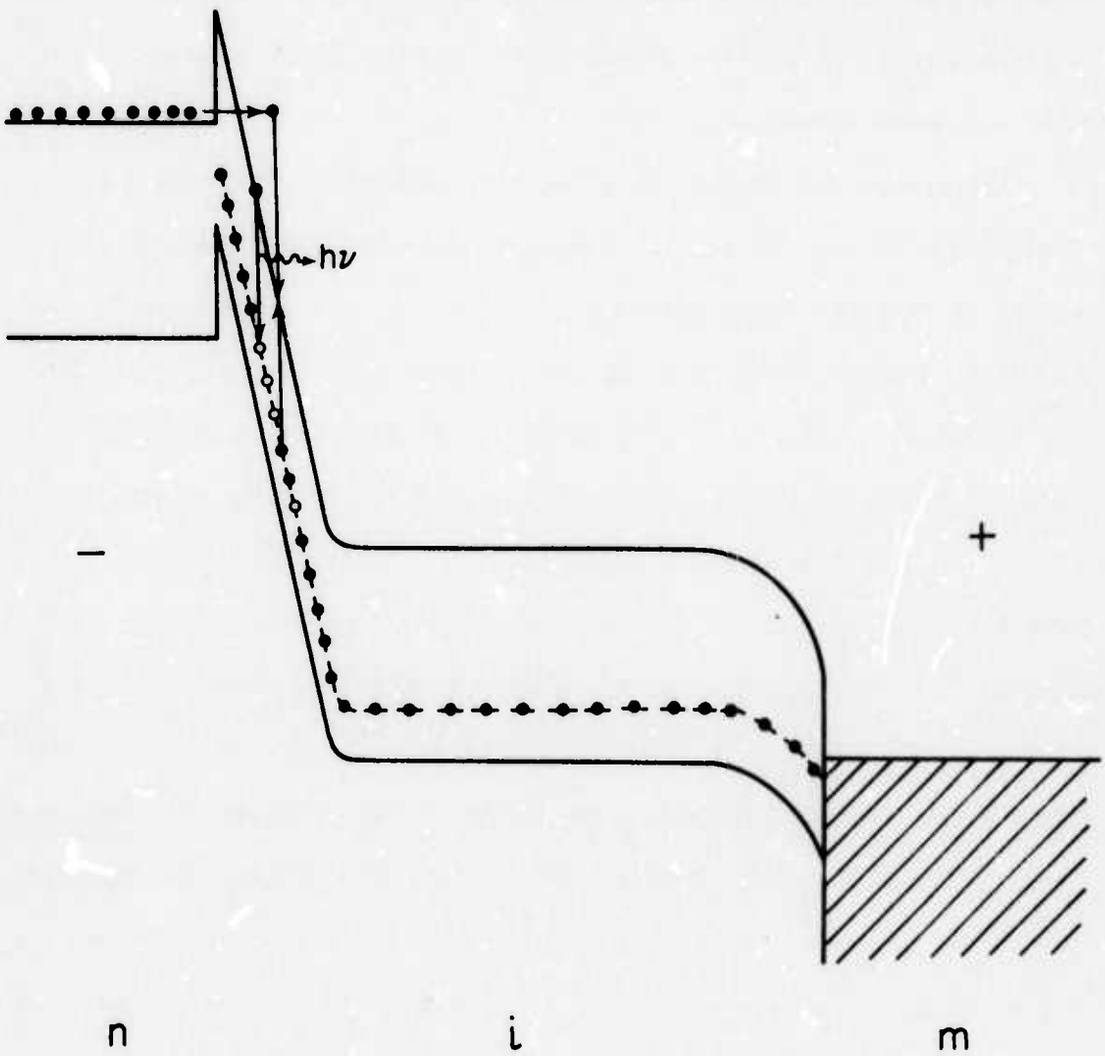

Figure 5.12 Schematic of processes responsible for electroluminescence in GaN m-i-n diodes. The situation for forward bias is illustrated.

will be quite gradual, rather than abrupt, and therefore that such an interface will not provide a barrier to current flow. This is exactly what was found experimentally.

The growth and device operation of a GaN LED may therefore be described with the aid of the idealized, two-dimensional sketch presented in Figure 5.13 (angles and distances in this sketch should not be taken literally; they are approximations). The nucleation of the GaN island on a $(1\bar{1}02)$ sapphire substrate is depicted in part (a). These islands grow, most rapidly in the direction of the c-axis, and eventually meet, forming a continuous film in part (b). Continued growth of the layer leads to the formation of subgrain boundaries between the crystal cells, as shown in part (c). The deep-acceptor doping is next begun. The i-layer forms, with a junction between the two regions that has the same shape as the facetted surface. This is shown in part (d). The wafer is removed from the furnace and the metal contact is attached. Forward bias (metal positive) is applied, and light spots form at the cathode. It is reasonable to expect that the avalanches which are responsible for the light occur at the subgrain boundaries. No evidence for precipitates or dislocations within the cells has been found. A definite correlation between the site of light spots due to an impact ionization process and crystal imperfections has been shown for silicon diodes [CHYNOWETH and PEARSON, 1958]. In these diodes it was seen that the avalanches occurred at points where dislocations passed through the junction. Three reasons for this correlation were proposed. (1) A dislocation may produce a singularity in the space charge distribution if it is a preferential area for

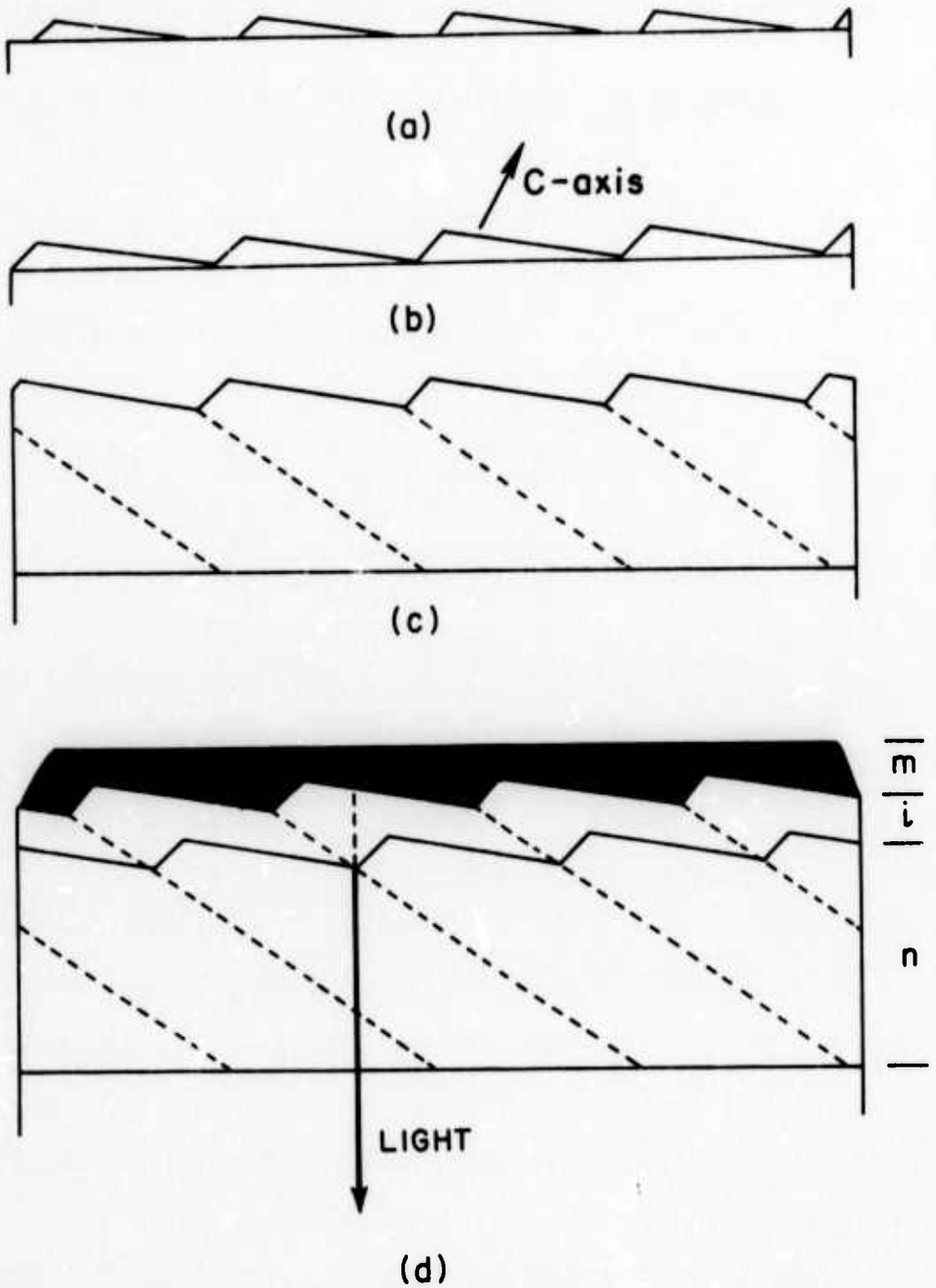

Figure 5.13 Growth and device operation of a gallium nitride light-emitting diode: (a) Nucleation of GaN islands on a (1102) sapphire substrate; (b) Growth of GaN islands, until they meet; (c) Growth of continuous GaN film after the islands have met, indicating the position of the sub-grain boundaries; (d) Complete GaN m-i-n diode, showing the structural origin of the electroluminescence with forward bias.

impurities to reside in. This in turn can result in a local enhancement of the electric field. (2) The electrical characteristics of the dislocations may cause a channeling of carriers and distortions of the field. If a dislocation were charged, the field would be enhanced. (3) In the immediate vicinity of the dislocation some of the crystal lattice is compressed and some is expanded. In the compressed area, the reduced band gap can result in a higher impact ionization rate. It is interesting to note that electroluminescence was first observed in SiC and ZnS, materials which are particularly prone to the formation of stacking faults. Although disorder is not a necessary condition for electroluminescence, boundaries between ordered regions can provide conditions particularly favorable for electroluminescence [STROCK, 1960].

The subgrain boundaries are the important crystal imperfection in GaN. The geometry of Figure 5.13 (d) indicates the position of the apparent source of the light when the electroluminescence is viewed through the n-layer (as it always is), and the actual source position where a subgrain boundary crosses the i-n junction. This may be compared to Figure 4.24 which shows the actual position of the light spots that a viewer sees through the n-layer. The construction in Figure 5.13 (d) indicates why the light spots appear to occur in the center of the cells.

From this description it is to be expected that diodes with the smallest cell size would have the most light spots and therefore would be the brightest. This is indeed the case, as recent growth runs have shown: diodes grown under conditions where more islands nucleate, which means several inches downstream from the ammonia inlet tube, are the

brightest. Further work needs to be done to maximize these conditions. A continuing research program should be aimed at finding the exact growth conditions which lead to the largest concentration of luminescent spots in samples, and hence the brightest GaN light-emitting diodes. Such a program would involve a systematic variation of growth conditions, such as temperatures, flowrates, and substrate position, in order to obtain the optimum structure of GaN films.

Chapter 6

CONCLUSIONS

This study describes the synthesis and behavior of electrical junctions in GaN films, and particularly the observation of violet electroluminescence from Mg-doped GaN. If a structure consisting of a layer of undoped n-type GaN, a layer of Mg-doped insulating GaN, and a metal contact to the insulating layer is formed, then it is possible to fabricate light-emitting diodes from this material which exhibit an emission peak at about 2.9 eV in the violet portion of the visible spectrum. Such m-i-n diodes are biased so that the metal contact is positive with respect to the n-GaN, and about 20 volts is required for the light to be visible in a well-lit room. Reverse bias results is emission peaks at other wavelengths.

The electroluminescence in the GaN diodes is generated in the form of discrete, microscopic spots less than 10 microns in diameter. The positions of these spots are related to the facetted structure of the GaN layers, which were epitaxially grown on sapphire substrates by the open flow vapor growth technique of chemical vapor deposition. The diodes contain two electrical junctions (metal-insulator and insulator-semiconductor) and the light is created by impact ionization at the junction which is the cathode. The impact ionization produces electron avalanches at the subgrain boundaries in the GaN, and these avalanches serve to empty the luminescent centers. High electrical fields required for electron acceleration to the energies necessary for the impact ionization process are only found in the vicinities of the junctions

Preceding page blank

and not uniformly across the insulating layer. Such a potential distribution (sharp potential gradient at the cathode) is consistent with a model of diode current control by tunnelling through a triangular potential barrier. The diode electrical characteristics follow the Fowler-Nordheim Equation which governs this process. These explanations are valid for Zn- as well as Mg-doped GaN diodes.

At this time the efficiencies of the Mg-doped diodes are still rather low. The highest value of external quantum efficiency obtained was only 0.005%. There is good reason to believe that the efficiency can be greatly improved, because values as high as 1% have been found elsewhere for green Zn-doped GaN LED's, and there is nothing to indicate that Mg should make any worse a luminescent center than Zn in this material. A more careful control of the GaN growth conditions with special attention to the creation of more sites favorable for the formation of light-producing avalanches is a desirable area for further study in order to improve the characteristics of gallium nitride light-emitting diodes.

REFERENCES

Addamiano, A., 1961, J. Electrochem. Soc. 108, 1072.

Allen, J. W., A. W. Livingstone, and K. Turvey, 1972, Solid-State Electron. 15, 1363.

Ashley, K. L., 1963, Ph.D. Thesis, Carnegie Institute of Technology.

Aven, M., 1965, Appl. Phys. Lett. 7, 146.

Aven, M., and W. Garwacki, 1964, Applied Phys. Lett. 5, 160.

Ban, V. S., J. Electrochem. Soc. 119, 761.

Barker, Jr., A. S., and M. Ilegems, 1973, Phys. Rev. B 7, 743.

Barnett, A. M., and A. G. Milnes, 1966, J. Appl. Phys. 37, 4215.

Bergh, A. A., and P. J. Dean, 1972, Proc. IEEE 60, 156.

Biter, W., J. Indradev, and F. Williams, 1969, J. Phys. Chem. Solids 30, 503.

Bloom, S., 1971, J. Phys. Chem. Solids, 32, 2027.

Borfeld, D. P., and H. P. Kleinknecht, 1968, J. Appl. Phys. 39, 6014.

Bourne, J., and R. L. Jacobs, 1972, J. Phys. C: Solid St. Phys. 5, 3462.

Chin, T. N., and L. A. Boyer, 1973, Solid-State Electron. 16, 143.

Chu, T. L., 1971, J. Electrochem. Soc. 118, 1200.

Chynoweth, A. G., and K. G. McKay, 1956, Phys. Rev. 102, 369.

Chynoweth, A. G., and K. G. McKay, 1957, Phys. Rev. 106, 418.

Chynoweth, A. G., and G. L. Pearson, 1958, J. Appl. Phys. 29, 1103.

Dingle, R., D. D. Sell, S. E. Stokowski, P. J. Dean, R. B. Zetterstrom, 1971, Phys. Rev. B 3, 497.

Dingle, R., and M. Ilegems, 1971, Solid State Commun. 9, 175.

Dingle, R., K. L. Shaklee, R. F. Leheny, and R. B. Zetterstrom, 1971, Appl. Phys. Lett. 19, 5.

Dingle, R., D. D. Sell, S. E. Stokowski, and M. Ilegems, 1971, Phys. Rev. B 4, 1211.

Donnelly, J. P., A. G. Foyt, W. T. Lindley, and G. W. Iseler, 1970, Solid-State Electron. 13, 755.

Eastman, P. C., R. R. Haering, and P. A. Barnes, 1964, Solid-State Electron. 7, 879.

Ejder, E., 1971, Phys. Status Solid. (a) 6, 445.

Fahrenbruch, A. L., 1973, Ph.D. Thesis, Stanford University.

Faulkner, K. R., B. J. Isherwood, B. P. Richards, and I. H. Scoby, 1970, J. Mater. Sci. 5, 308.

Fischer, A. G., 1963, J. Electrochem. Soc. 110, 733.

Fischer, A. G., 1965, Proc. of 7th International Conf. on the Physics of Semiconductors, Dumond, Paris, Vol. 4, 259.

Fischer, A. G., 1966, in Luminescence of Inorganic Solids, Ed. P. Goldberg, Academic Press, Chap. 10.

Fowler, R. H., and L. W. Nordheim, 1928, Proc. Roy. Soc. (London) 119, 173.

Galginaitis, S. V., 1971, Met. Trans. 2, 757.

Goffaux, R., 1956, J. Phys. Radium 17, 763.

Goffaux, R., 1957, J. Phys. Radium 18, 1.

Gomer, R., 1961, Field Emission and Field Ionization, Harvard University Press, Cambridge, Mass.

Grimmeiss, H. G., and H. Koelmans, 1959, Z. Naturforsch. 14a, 264.

Grimmeiss, H. G., R. Groth, and J. Maak, 1960, Z. Naturforsch 15a, 799.

Grimmeiss, H. G., and B. Monemar, 1970, J. Appl. Phys. 41, 4054.

Hahn, H., and R. Juza, 1940, Z. anorg. u. all. Chem. 244, 111.

Hakki, B. W., 1971, J. Electrochem. Soc. 118, 1469.

Heiland, G. E. Mollwo, and F. Stockman, 1959, Solid State Phys. 8, 190.

Henisch, H. K., 1962, Electroluminescence, Pergamon Press, Oxford.

Hill, D. E., 1965, J. Appl. Phys. 36, 3405.

Holonyak, Jr., N., 1962, Proc. IRE 50, 2421.

Hovel, H. J., and J. J. Cuomo, 1972, Appl. Phys. Lett. 20, 71.

Hsieh, J. J., 1971, Ph.D. Thesis, University of Southern California.

Ilegems, M., 1972, J. Cryst. Growth 13/14, 360.

Ilegems, M., R. Dingle, and R. A. Logan, 1972, J. Appl. Phys. 43, 3797.

Ilegems, M., and H. C. Montgomery, 1973, J. Phys. Chem. Solids 34, 885.

Johnson, L. F., H. J. Guggenheim, T. C. Rich, and F. W. Ostermayer, 1972, J. Appl. Phys. 43, 1125.

Johnson, W. C., J. B. Parsons, and M. C. Crew, 1932, J. Phys. Chem. 36, 2651.

Jones, D., and A. H. Lettington, 1972, Solid State Commun. 11, 701.

Juza, R., and F. Hund, 1948, Z. anorg. u. allg. Chem. 257, 13.

Kauer, E., and A. Rabenau, 1957, Z. Naturforsch. 12a, 942.

Keating, P. N., 1963, J. Phys. Chem. Solids 24, 1101.

Kennedy, D. I., and M. J. Russ, 1967, J. Appl. Phys. 38, 4387.

Kosicki, B. B., and D. Kahng, 1969, J. Vac. Sci. and Tech. 6, 593.

Kosicki, B. B., R. J. Powell, and J. C. Burgiel, 1970, Phys. Rev. Letters, 24, 1421.

Lampert, M. A., and P. Mark, 1970, Current Injection in Solids, Academic Press, New York.

Lehmann, W., 1958, J. Electrochem. Soc. 105, 585.

Leverenz, H. W., 1950, Luminescence of Solids, Dover Publications, New York.

Livingstone, A. W., and J. W. Allen, 1970, J. Phys. C: Solid St. Phys. 3, 2468.

Livingstone, A. W., K. Turvey, and J. W. Allen, 1973, Solid-State Electron. 16, 351.

Loebner, E. E., 1973, private communication.

Loebner, E. E., and E. W. Poor, Jr., 1959, Phys. Rev. Lett. 3, 23.

Logan, R. A., H. C. White, and W. Wiegmann, 1971, Solid-State Electron. 14, 55.

Logan, R. A., and C. D. Thurmond, 1972, J. Electrochem. Soc. 119, 1727.

Lorenz, M. R., and B. B. Binkowski, 1962, J. Electrochem. Soc. 109, 24.

Lossev, O. W., 1923, Telegrafia i Telefonia, 18, 61.

MacChesney, J. B., P. M. Bridenbaugh, and P. B. O'Conner, 1970, Mat. Res. Bull. 5, 783.

MacDonald, N. C., and T. E. Everhart, 1965, Appl. Phys. Lett. 7, 267.

Manasevit, H. M., F. M. Erdmann, and W. J. Simpson, 1971, J. Electrochem. Soc. 118, 1864.

Manchon, Jr., D. D., A. S. Barker, Jr., P. J. Dean, and R. B. Zetterstrom, 1970, Solid State Commun. 8, 1227.

Mandel, G., 1964, Phys. Rev. 134, A1073.

Mandel, G., F. F. Morehead, and P. R. Wagner, 1964, Phys. Rev. 136, A826.

Maruska, H. P., and J. I. Pankove, 1967, Solid-State Electron. 10, 917.

Maruska, H. P., and J. J. Tietjen, 1969, Appl. Phys. Lett. 15, 327.

Morehead, F. F., 1967, in Physics and Chemistry of II-VI Compounds, North-Holland Publishing, Amsterdam, Chap. 12.

Neumark, G. F., 1956, Phys. Rev. 103, 41.

Nuese, C. J., and F. Z. Hawrylo, 1970, unpublished results.

Pankove, J. I., 1972, J. Lumin. 7, 114.

Pankove, J. I., 1973, RCA Review, 34, 336.

Pankove, J. I., J. E. Berkeyheiser, H. P. Maruska, and J. Wittke, 1970, Solid State Commun. 8, 1051.

Pankove, J. I., H. P. Maruska, and J. E. Berkeyheiser, 1970, Appl. Phys. Lett. 17, 197.

Pankove, J. I., E. A. Miller, and J. E. Berkeyheiser, 1971, RCA Review 32, 383.

Pankove, J. I., E. A. Miller, and J. E. Berkeyheiser, 1972, J. Lumin. 5, 84.

Pankove, J. I., E. A. Miller, and J. E. Berkeyheiser, 1973, J. Lumin. 6, 54.

Park, Y. S., C. R. Geesner, and B. K. Shin, 1972, Appl. Phys. Lett. 21, 567.

Pastrnak, J., and L. Souckova, 1963, Phys. Status Solids 3, K71.

Patrick, L., 1957, J. Appl. Phys. 28, 765.

Piper, W. W., and F. E. Williams, 1955, Brit. J. Appl. Phys. 6, Suppl. 4, S39.

Piper, W. W., and F. E. Williams, 1958, Solid State Phys. 6, 95.

Potter, R. M., J. M. Blank, and A. Addamiano, 1969, J. Appl. Phys. 40, 2253.

Rabenau, A., 1962, in Compound Semiconductors, Vol. 1, Reinhold, New York, Chap. 19.

Renner, Th., 1959, Z. anorg. u. allg. Chem. 298, 22.

Rhines, W. C., 1972, Ph.D. Thesis, Stanford University.

Rosenzweig, W., R. A. Logan, and W. Wiegmann, 1971, Solid-State Electron. 14, 655.

Saul, R. H., J. Armstrong, and W. H. Hacket, Jr., 1969, Appl. Phys. Lett. 15, 229.

Seitz, F., 1949, Phys. Rev. 76, 1376.

Smith, R. W., 1957, Phys. Rev. 105, 900.

Strock, L. W., 1960, Illum. Eng. 55, 24.

Stull, D. R., 1967, JANAF Thermochemical Tables.

Sze, S. M., 1969, Physics of Semiconductor Devices, Wiley-Interscience, New York.

Thornton, P. R., 1967, The Physics of Electroluminescent Devices, E. & F. N. Spon, Ltd., London.

Thornton, P. R., 1968, Scanning Electron Microscopy, Chapman and Hall, Ltd., London.

Thornton, W. A., 1961, J. Electrochem. Soc. 108, 636.

Thurmond, C. D., and R. A. Logan, 1972, J. Electrochem. Soc. 119, 622.

Tietjen, J. J., and J. A. Amick, 1966, J. Electrochem. Soc. 113, 724.

Title, R. S., G. Mandel, and F. F. Morehead, 1964, Phys. Rev. 136, A300.

Tyler, W. W., 1954, Phys. Rev. 96, 226.

Vecht, A., N. J. Werring, R. Ellis, and P. J. F. Smith, 1969, J. Phys. D: Appl. Phys. 2, 953.

Vecht, A., and N. J. Werring, 1970, J. Phys. D: Appl. Phys. 3, 105.

Violin, E. E., A. A. Kalnin, V. V. Pasynkov, Yu. M. Tairov, and D. A. Yaskov, 1969, in Silicon Carbide -- 1968 Eds. H. K. Henisch and R. Roy, Pergamon Press, pp. 231-241.

Wachtman, J. B., and L. H. Maxwell, 1962, J. Amer. Ceram. Soc. 45, 319.

Woodall, J. M., R. Lynch, and D. Shang, 1970, Extended Abstracts, Spring Meeting of the Electrochemical Society, Los Angeles, Calif., pp. 208-209.

Wright, W. D., 1964, The Measurement of Color, Van Nostrand, Princeton, N.J.

Zalm, P., 1956, Philips Res. Rep. 11, 353.